AD-A189 706 INCOHERENT MULTIPLE APERTURE OPTICAL IMAGING SYSTEMS: ANALYSIS AND DESIGN(U) AIR FORCE INST OF TECH WRIGHT-PATTERSON AFB OH SCHOOL OF ENGI.. R T REILANDER 1/2

UNCLASSIFIED DEC 87 AFIT/GSO/ENP/87D-2 F/G 17/5 NL

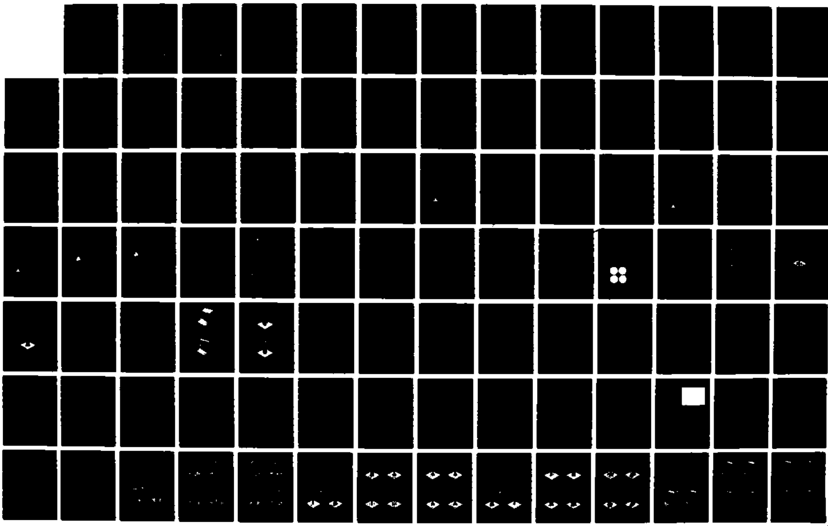

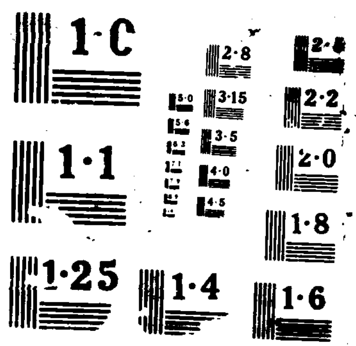
1·1
1·25
1·4
1·6
1·8
2·0
2·2
2·8
3·15
3·5
4·0
4·5

DEPARTMENT OF THE AIR FORCE

AIR UNIVERSITY

AIR FORCE INSTITUTE OF TECHNOLOGY

Wright-Patterson Air Force Base, Ohio

(1)

AFIT/GSO/ENP/87D-2

INCOHERENT MULTIPLE APERTURE OPTICAL IMAGING SYSTEMS: ANALYSIS AND DESIGN

THESIS

Robert T. Reilander
Major, Canadian Armed Forces

AFIT/GSO/ENP/87D-2

AFIT/GSO/ENP/87D-2

INCOHERENT MULTIPLE APERTURE OPTICAL IMAGING SYSTEMS: ANALYSIS AND DESIGN

THESIS

Presented to the Faculty of the School of Engineering

of the Air Force Institute of Technology

Air University

In Partial Fulfillment of the

Requirements for the Degree of

Master of Science in Space Operations

Robert T. Reilander, B.Eng.

Major, Canadian Armed Forces

December 1987

Approved for pubic release; distribution unlimited

Preface

Due to the size and weight restrictions on optical elements both on the ground and especially in space, optical detection must employ multiple aperture techniques in order to gain improved image resolution. The Air Force Weapons Laboratory (AFWL) is planning such a system, composed of four collecting mirrors arranged in a square pattern. This thesis studies the AFWL proposal, and compares it with other possible mirror arrangements of up to four elements. Each combination is assessed in its ability to image edges, slits, rectangles and circles. A comparison of the results yields which arrangements offer the best resolution.

I would like to thank Lt Col Jim Mills for his proposal of this topic, and for his endless guidance as my advisor throughout it. I owe great thanks to Lt Dana Bergey for his help in getting me started with the computer analysis, and also to Ron Gabriel for his direction and assistance in the lab. Most importantly, I am eternally grateful to my wife Joanne and young son Daniel, whose encouragement, patience, and concern, put my work into perspective.

Robert T. Reilander

Table of Contents

List of Figures

Figure page

Figure		page

Figure		page
F-1.	Aperture 1 Rectangle	86
F-2.	Aperture 2 Rectangle	86
F-3.	Aperture 3 Rectangle	87
F-4.	Aperture 4 Rectangle	87
F-5.	Aperture 5 Rectangle	87
F-6.	Aperture 6 Rectangle	87
F-7.	Aperture 7 Rectangle	88
F-8.	Aperture 8 Rectangle	88
F-9.	Aperture 9 Rectangle	88
F-10.	Aperture 10 Rectangle	88
G-1.	Aperture 1 Circle	89
G-2.	Aperture 2 Circle	89
G-3.	Aperture 3 Circle	90
G-4.	Aperture 4 Circle	90
G-5.	Aperture 5 Circle	90
G-6.	Aperture 6 Circle	90
G-7.	Aperture 7 Circle	91
G-8.	Aperture 8 Circle	91
G-9.	Aperture 9 Circle	91
G-10.	Aperture 10 Circle	91
H-1.	Aperture 1 Best Edge	92
H-2.	Aperture 1 Worst Edge	92
H-3.	Aperture 2 Best Edge	93
H-4.	Aperture 2 Worst Edge	93
H-5.	Aperture 3 Best Edge	93

Figure page

Figure	page

List of Tables

AFIT/GSO/ENP/87D-2

Abstract

The purpose of this thesis was to evaluate and compare the resolution capability of various multiple aperture systems. Performance was to be assessed while they imaged objects using incoherent light. Ten aperture configurations, containing from one to four sub-apertures, were compared. Both symmetric and asymmetric (Golay) configurations were studied. Included was a tight square array, planned for development by the Air Force Weapons Lab (AFWL).

A computer program simulated the imaging of edges, slits, rectangles and circles for each array. This theoretical analysis was verified by actual experimentation in a laboratory. A mathematical examination of the data provided a ranking of each aperture's performance relative to the others. The AFWL proposal proved to be the best multiple aperture design. These results were based upon the author's own design of resolution criteria.

This study concluded with an analysis of the design criteria for optimum performance for multiple apertures of up to four elements. Maximum sub-aperture size, minimum sub-aperture spacing, maximum number of elements, and a symmetric arrangement were all determined to be desirable in order to obtain the best incoherent imaging resolution.

INCOHERENT MULTIPLE APERTURE OPTICAL IMAGING SYSTEMS: ANALYSIS AND DESIGN

I. Introduction

Brief Introduction of Terms

An aperture is an opening through which an object may be viewed. A lens, a mirror, and a hole in a piece of paper are all examples of apertures. A multiple aperture combines several smaller apertures (sub-apertures) in parallel to simulate one large one. An optical system that contains a multiple aperture is known as a Multiple Aperture Optical System (MAOS).

There are several yardsticks with which to measure a given multiple aperture. The first is its "equivalent collecting diameter". This is the diameter a single aperture would have to have in order to equal the same collecting area of the sum of all individual sub-apertures (1:85). A second term is the "resolution diameter". This is the diameter a single aperture would have to have in order to be capable of the same angular resolution as the multiple aperture system. It is therefore equal to the linear distance between the outside edges of the two furthest separated sub-apertures (1:85). This "resolution diameter" is sometimes simply referred to as the "equivalent diameter". This diameter is the smallest one capable of

enclosing the complete multiple aperture array. (Note; all sub-apertures must be located in the same plane.)

In order to compare one aperture with another, it is necessary to discuss each system's effectiveness. As is common in optical systems, this effectiveness can be measured in terms of optical resolution. Resolution is usually defined as the ability to distinguish between two independently visible adjacent parts (19). A further explanation of resolution is defined in the experimental analysis section. Essentially, it is the ability to discern an edge in a given image. In other words, the clearer and sharper the edges of the image, the better the resolution.

Problem Statement

The purpose of this thesis was to evaluate and compare the resolution capability of various multiple aperture configurations. Particular attention was devoted to a four element aperture. A series of objects was illuminated with incoherent light and then imaged by this array of apertures. The objects of interest were edges, slits, rectangles, and circles, since these are the basic building blocks from which any larger object may be built. Each multiple aperture design was studied to determine how the number, size, and geometric arrangement of sub-apertures affected each image. All tests were computer simulated. The accuracy of the computer simulation was then verified through actual experimentation in the optics laboratory.

Justification of Thesis

This thesis was proposed by Lieutenant Colonel J. Mills (11), who had been previously contacted by the Air Force Weapons Laboratory (AFWL). AFWL is building a multiple aperture telescope in support of the Strategic Defense Initiative (SDI) and has proposed construction of a particular four-aperture system. To this end, this thesis concentrates on four-aperture systems, assessing the AFWL proposal and then comparing several other possible configurations.

This thesis also compliments an earlier thesis entitled "COHERENT MULTIPLE APERTURE OPTICAL IMAGING SYSTEMS: ANALYSIS AND DESIGN" produced by Second Lieutenant D. Bergey in March 1987 (2). It was one of Bergey's recommendations that his study of optical imaging systems be continued into the realm of incoherent light.

Scope of the Thesis

This thesis concentrates on four-element multiple aperture systems. Several single-element apertures are studied as references. Simple two- and three-element systems are also included for comparison.

The objects of study are limited to edges and slits (for one-dimensional analysis) and rectangles and circles (for two-dimensional analysis). All objects are illuminated with incoherent light only.

All imaging is performed for the "ideal" case. It assumes all aperture elements are co-planar, and that there are no phase or alignment errors in combining the images produced by each element. This thesis does not address such alignment errors, nor does it attempt to study the consequences of any other real-world defect or aberration.

Method of Treatment and Organization

This thesis contains a literature search and review which begins by identifying the reasons why multiple aperture technology was developed. Included is an explanation of the various mirror types which resulted. The history of MAOS architecture follows. This literature search and review ends with an overview of some MAOS architectures currently in existence.

This thesis next contains the theoretical development of incoherent imaging. A Fortran computer simulation of this theory was run for each aperture/object combination. Computer simulation outputs were recorded in a variety of two- and three-dimensional plots.

After the simulation runs were complete, some scenarios were physically reconstructed in the Optics Laboratory to reveal the real world response. Through an iterative process, the simulation and real-world results were correlated and confirmed.

Once all the results were in, a record of findings was tabulated. This thesis concludes with a summary of the

findings, and a recommendation of certain preferred aperture configurations.

II. Historical Development

Reasons for Larger Telescopes

Carleton and Hoffman (3:30) explain that there are two major reasons for creating larger telescopes. The first has to do with light-gathering power. As the dimensions of the aperture increase, so too does the number of photons that can be collected. "With modern detectors, many observations are limited by photon-counting statistics, and require impractically long integration times with present telescopes" (3:30).

The second reason relates to the physical laws of the diffraction of light. The resolution limit of light for a single circular aperture is defined by the following formula:

$$R = 1.22\ \lambda / D \tag{1}$$

where R is the resolution or minimum separation of two incoherent point sources in radians, λ is the wavelength in meters of light being observed, and D is the diameter in meters of the receiving aperture (3:30). Clearly, as the diameter increases in size, the value of R decreases. In other words, the resolution improves.

Mirror Types

Traditionally, the primary mirror of a reflecting telescope has been monolithic (a single element). As mirror diameters grew, the complexity of building them rose exponentially. Mirror weight also ballooned since larger diameters implied thicker bases for support. For most of this century, a maximum diameter limit was reached at about 5 meters. Schwartzchild explains that with larger mirrors, the sheer weight of the mirror causes surface deformations resulting in degraded performance (15:18). "To preserve image quality, one cannot tolerate surface deformations much greater than a tenth of a micron" (15:18). Therefore, heavy mirrors are useless.

The solution to this problem is to build lighter mirrors. Today, multiple mirror technology allows the primary mirror of a telescope to be handled in manageable pieces. There are two main methods of doing this. The first is the segmented mirror concept. A large mirror is constructed from a mosaic of smaller mirrors, all fitting together like a jigsaw puzzle. Unfortunately, each piece has to be machined uniquely. According to Waldrop, the complexities of such an undertaking make the segmented mirror concept largely undesirable. Even using the latest technology, the grinding and polishing of individual skewed surfaces to the required tolerances remains a formidable task (18:281).

The second option is the multiple mirror concept. Here, several identical mirrors are configured in parallel to function as a single mirror (18:280). "The light gathered by the separate mirrors is merged into a single image" (5:23). The technology has long been available to produce ordinary small circular mirrors. Now the challenge is to combine the images into one single output. This remaining task is now technically feasible, not physically impossible.

History of Multiple Aperture Optical Systems

For centuries, mankind has realized that as apertures increase in size, performance improves. The trend has therefore been to build bigger and bigger telescopes. In 1928, plans were made to create the now famous 200 inch (5.08 meters) Mount Palomar reflector. This was the largest mirror ever attempted.

> "The great technical difficulties that had to be surmounted in the construction of the 200 inch, and its enormous cost, gave many people the feeling that a limit had been reached in the march towards bigger telescopes" (10:100).

Consequently, any attempt to build larger apertures would require some new thinking.

In 1932, Italian Guido Horn-d'Auturo asked the question:

> "If it became impossible to cast larger mirrors, would it not be feasible to assemble smaller mirrors to form a reflecting surface of great size" (10:100)?

In later years, he was able to place 61 small hexagonal mirrored tiles together to form a single 1.8 meter

reflecting surface. This was the "first serious application" of multiple mirrors (3:30). It marked the beginning of a new era in optical design. In the 1960's, two 22 foot (6.71 meters) mirrors were constructed in similar fashion at Narrabri, Australia. In Arizona, a 10 meter collector was built for gamma-ray research. These designs were only for light collection, "and laid no claim to optical precision" (10:101). Certainly, these were multiple mirror aperture systems, but they were no rival for conventional monolithic mirrors.

Jacchia states that as early as 1949, a different type of multiple aperture telescope was being proposed by Vaisala of Finland. Vaisala arranged six circular mirrors (each 32 cm diameter) in a hexagonal pattern, adding a seventh mirror at the center of the hexagon (10:102). This configuration demonstrated greater optical precision than that of the segmented mirrors described above. The true multiple mirror concept was born.

It would still take several decades before a large MAOS would be properly engineered and employed. Until the middle 1970's, astronomers were coping with existing limited aperture sizes by employing more and more sensitive detectors with which to count photons. (Detectors count the photons that are gathered by the aperture). In the quest for targets that were further away and weaker in intensity than any others sought before, photons became harder to detect.

Eventually, the theoretical limit of the detector sensitivities was reached. Astronomers were therefore "turning once again to the quest for larger telescope mirrors to gather more light for their detectors" (15:30). A MAOS was a necessity now.

The first and most famous multiple aperture telescope was the Multiple Mirror Telescope of the University of Arizona. Completed in 1978, this synthetic aperture has proved its worth. It was much cheaper than trying to build a monolithic aperture of the same size (4:47). Further, this telescope had the added bonus of allowing its mirrors to operate independently for simultaneous studies of the same object (at different wavelengths for example) (14:23). The successes of this aperture allowed others to follow.

Multiple Mirror Applications

At present, there are many MAOS that either already exist or are in final development. Each employs a unique architectural mirror arrangement. The variety of these arrangements suggests that there is no consensus over which mirror pattern is best. Here are three famous current examples of MAOS.

The Multiple Mirror Telescope (MMT). In the early 1970's, the University of Arizona, in conjunction with the Smithsonian Astronomical Observatory, was considering designs for a new telescope. Both the segmented mirror and

multiple mirror designs were considered. In December 1971, the multiple mirror concept was selected (3:30).

"The MMT uses six 72-inch (1.8 meter) co-planar mirrors in concert to create the light-gathering equivalent of a single 176 inch (4.5 meter) mirror" (5:23). The six mirrors are arranged symmetrically on a single mount about a central axis (in a hexagon shape).

National New Technology Telescope (NNTT). This new telescope is still under construction. Similar to the MMT, it will also employ an array of mirrors on a single mount. The NNTT will use only four mirrors, each one 7.5 meters in diameter. They will be arranged in a square co-planar pattern, symmetric about a central axis. "Together the four mirrors would simulate a single mirror 15 meters across, for imaging purposes. For interferometric work they would be the equivalent of a 21 meter baseline" (17:55).

European Very Large Telescope (VLT). "The European answer to the NNTT is the VLT, which will combine four 8 meter mirrors to achieve the light-gathering power of a single 16 meter dish. Unlike the NNTT, the mirrors will be carried on separate mountings" (14:23). The VLT will position its mirrors in a linear array. The VLT will form a synthetic aperture 150 meters long. "For imaging operations in visible or infrared light, the performance of the VLT will not differ dramatically from that of the NNTT" (14:24). When used as as interferometer the VLT will be able to

employ the 150 meter baseline to give resolution seven times better than that possible with the NNTT (14:24). The VLT is particularly interesting in that its four mirrors, when looking at a common object, will rarely be co-planar. Nor will the spacing between mirrors remain fixed. This class of MAOS therefore represents a whole new dimension to the complexity of combining the images gathered by the different elements. Such arrangements are beyond the scope of this thesis.

The Future of Multiple Mirror Applications

The employment of high resolution optical devices in the future will most certainly continue to involve Multiple Aperture Optics. The size and weight of the collecting elements will continue to be restricted by technology, cost, and the limitations of boosting large objects into space. The need for continuing research into Multiple Aperture Optical Systems is reinforced.

III. Theoretical Development

Geometric Imaging

A basic imaging equation for geometric optics using thin lenses is the Gaussian form of the Thin Lens Law (16:575):

$$\frac{1}{o} + \frac{1}{i} = \frac{1}{f} \tag{2}$$

where o is the distance from the lens to the object, i is the distance from the lens to the image, and f is the focal length of the lens as illustrated in Figure 1.

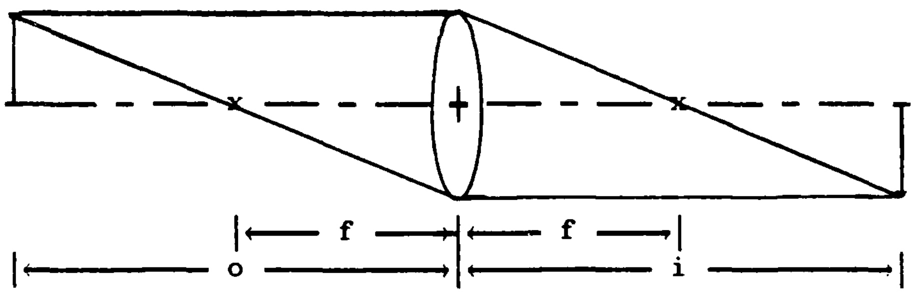

Figure 1. Simple Thin Lens Imaging

Lenses produce magnification, or image scaling. For the system described in Figure 1, an image is produced that is M times as big as the original object. M is the magnification factor, and is defined as (16:576):

$$M = -\frac{i}{o} \tag{3}$$

where the negative sign indicates that the image is inverted.

Although the above description was limited to thin lenses, the basic equation also applies to more complicated systems as long as f is replaced by the effective focal length of the complete system. Further, the distances o and i need to be measured from the appropriate principle planes of the optical system.

Entrance and Exit Pupils

The pupil function of an optical system is determined by the limiting aperture. In the single lens system of Figure 1, the pupil is the entire lens. In more complex systems however, such as in Figure 2, the limiting aperture is not one of the lenses. In this case, the limiting factor is called the aperture stop. An aperture stop limits the amount of light that may pass through a system. O'Shea explains that it limits the amount of light collecting ability of any system (13:68).

In Figure 2, a complex optical system is constructed from two lenses of different focal lengths, separated by an aperture stop. The space to the left of the first lens is called object space. The space to the right of the right lens is called image

space. O'Shea explains (13:68) that the image of the aperture stop as seen from object space is called the Entrance Pupil (Figure 2.a). Similarly, the image of the aperture stop when viewed from image space is called the Exit Pupil (Figure 2.b). Both the Entrance and Exit Pupils are seen (in this case) to be virtual images.

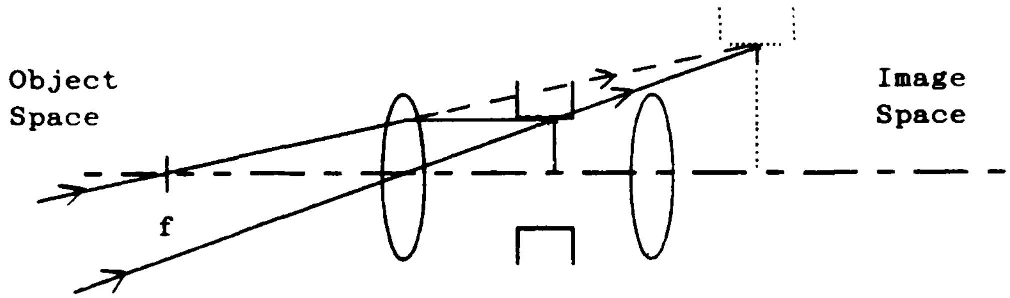

Figure 2 a. Entrance pupil

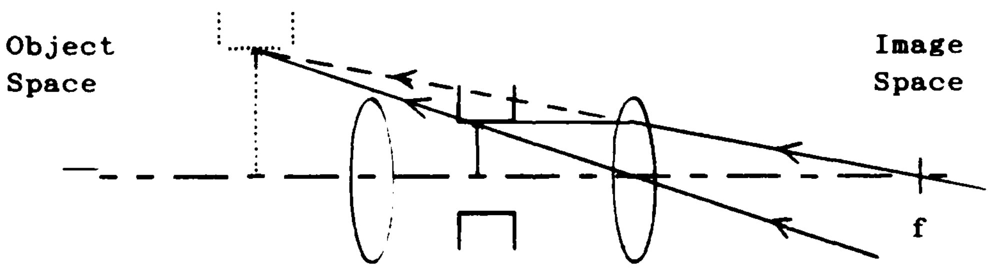

Figure 2 b. Exit Pupil

<u>Impulse Response</u>

For incoherent light cases, the Point Spread Function $|\mathbf{h}|^2$ of an optical system is simply the system response to a point

source of light located in the object plane some distance away. In other words, it is the irradiance pattern that will result when this point source is imaged. Diffraction effects within any optical system will prevent the point source from being imaged back into another point. Rather, some irradiance distribution will result. (Figure 3) (7:335) In a Fourier optics analysis, this infinite point source object is best represented by the Dirac Delta Function δ.

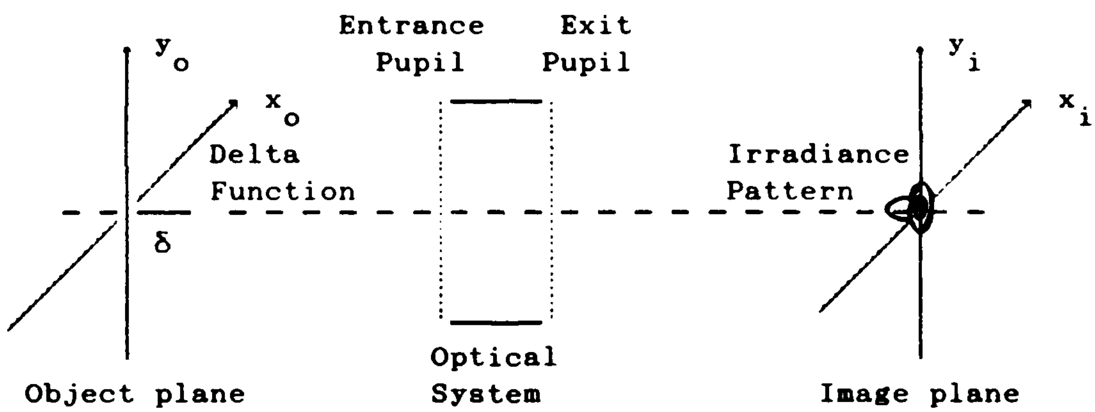

Figure 3. Imaging model of Delta function

Goodman (9:18) defines the coherent impulse response $\mathbf{h}$ as:

$$\mathbf{h}(x_i, y_i; \zeta, \eta) = S\{\delta(x_o - \zeta,\ y_o - \eta)\} \qquad (4)$$

where $\mathbf{h}$ is the response of the system at a point (x_i, y_i) of the

output space to the delta function (δ) input at coordinates (ζ,η) of the input space. S is representative of the system operator.

The true picture of the impulse response is not complete without also tying in geometric optics. An impulse response, like any other image, is subject to some magnification. Goodman defines the true scaled coherent impulse response $\tilde{h}$ as (9:96):

$$\tilde{h} = \frac{1}{M}\, h \qquad (5)$$

Goodman elaborates on the definition of the scaled coherent impulse response $\tilde{h}$ (9:105):

$$\tilde{h}(x_i,y_i) = \iint_{-\infty}^{\infty} P(\lambda d_i\tilde{x},\lambda d_i\tilde{y})\; e^{[-j2\pi(x_i\tilde{x} + y_i\tilde{y})]}\, d\tilde{x}\, d\tilde{y} \qquad (6)$$

where P is the Pupil function (or aperture function defined by the area of transmittance of the exit aperture), λ is the wavelength of light used, d_i is the distance from the exit pupil to the image, $\tilde{x} = \frac{x}{\lambda d_i}$, $\tilde{y} = \frac{y}{\lambda d_i}$, the xy plane defines the location of the Exit Pupil, and the $x_i y_i$ plane defines the image screen. Since the above formula is simply a Fourier transform integral, it is clear that the impulse response of a system is the transform of that system's exit pupil function. (ie; $\tilde{h} = F\{P\}$)

Point Spread Function

For incoherent light, the system response (in the image plane) to an object point source of light is called the Point Spread Function (PSF). It follows that an optical system's Impulse Response and PSF are related.

Gaskill explains (7:485) that the PSF is "proportional to the squared modulus of the system's coherent impulse response". PSFs for the various apertures assessed in this thesis are illustrated in Appendix B.

Optical Transfer Function

The Optical Transfer Function (OTF) of a system is a measure of system performance that indicates the effect of the system in the frequency domain (9:20). Basically, it is a weighting function in frequency space that acts upon input waves, altering amplitude and phase components according to the system's properties. The OTF is not only a function of the size and shape of the exit pupil, but also of aberrations within the system.

Fourier Optics provide an effective description of the OTF. To be a proper weighting function, it is normalized so that its maximum value is equal to "1". Since this is in the frequency domain, this maximum occurs on the optical axis, along the zero

frequency component. Goodman defines $\mathcal{H}$ (the normalized OTF) as (9:114):

$$\mathcal{H}(f_x, f_y) = \frac{\displaystyle\iint_{-\infty}^{\infty} |\tilde{\mathbf{h}}(x_i, y_i)|^2 \, e^{[-j2\pi(f_x x_i + f_y y_i)]} \, dx_i \, dy_i}{\displaystyle\iint_{-\infty}^{\infty} |\tilde{\mathbf{h}}(x_i, y_i)|^2 \, dx_i \, dy_i} \qquad (7)$$

where $f_x = \frac{\zeta}{\lambda di}$ and $f_y = \frac{\eta}{\lambda di}$. The variables f_x and f_y represent the spatial frequency plane located at the exit pupil. The numerator of this equation is a Fourier transform of the square of the magnitude of the Impulse Response. The denominator is an identical equation, except it represents the maximum value of the OTF, occurring at $f_x = 0$ and $f_y = 0$. For this reason, there is no exponential in the denominator.

The OTF of any optical system is one of the most important system descriptors. A complete list of apertures and their corresponding OTFs as assessed in this thesis is included in Appendix C.

Incoherent Imaging

The basic premise of incoherent imaging systems is that

they obey the irradiance convolution integral (9:113):

$$I_i(x_i,y_i) = K \iint_{-\infty}^{\infty} |\tilde{h}(x_i - \tilde{x}_o, y_i - \tilde{y}_o)|^2 \, I_g(\tilde{x}_o,\tilde{y}_o) d\tilde{x}_o \, d\tilde{y}_o \qquad (8)$$

where I_i is the resulting irradiance in the image plane, and I_g is the geometrically scaled object irradiance. (Scaling results from geometric imaging). The integral takes place over the scaled object space. The convolution occurs between the resulting geometric image and the point spread function (ie- the squared magnitude of the impulse response) for that system performing the imaging. The constant K is a proportionality constant. Figure 4 illustrates this convolution in one dimension:

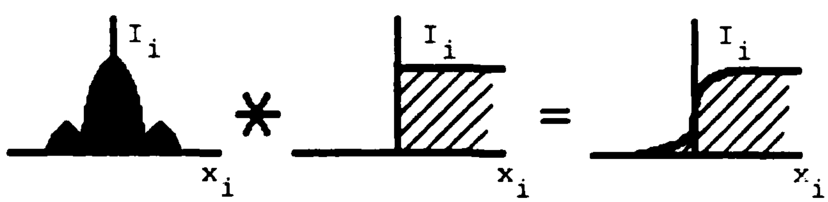

Point Spread Function   Scaled Object   Image Irradiance

Figure 4 . Incoherent Imaging Convolution

In order to do away with proportionality constants and allow resolution comparisons between systems, it is beneficial to normalize all the quantities involved, the same as was performed for the OTF. Two new variables are therefore defined (9:113):

$$G_g(f_x,f_y) = \frac{\displaystyle\iint_{-\infty}^{\infty} I_g(\tilde{x}_o,\tilde{y}_o)\, e^{[-j2\pi(f_x\tilde{x}_o + f_y\tilde{y}_o)]}\, d\tilde{x}_o\, d\tilde{y}_o}{\displaystyle\iint_{-\infty}^{\infty} I_g(\tilde{x}_o,\tilde{y}_o)\, d\tilde{x}_o\, d\tilde{y}_o} \qquad (9)$$

and

$$G_i(f_x,f_y) = \frac{\displaystyle\iint_{-\infty}^{\infty} I_i(x_i,y_i)\, e^{[-j2\pi(f_x x_i + f_y y_i)]}\, dx_i\, dy_i}{\displaystyle\iint_{-\infty}^{\infty} I_i(x_i,y_i)\, dx_i\, dy_i} \qquad (10)$$

where G_g and G_i are the normalized frequency spectra of the scaled object and resultant image respectively. Like the OTF, these are normalized over the maximum component located at the zero frequency. Both of these equations contain Fourier transforms from real space to frequency space.

The irradiance convolution integral (Equation 8) can be rewritten as:

$$I_i(x_i,y_i) = K\left[\,|\tilde{h}(x_i,y_i)|^2 * I_g(\tilde{x}_o,\tilde{y}_o)\,\right] \qquad (11)$$

where * denotes convolution. Taking the Fourier of both sides and applying the convolution theorem to this equation produces:

$$\mathcal{F}\left[\,I_i(x_i,y_i)\right] = K\,\mathcal{F}\left[\,|\tilde{h}(x_i,y_i)|^2\right]\mathcal{F}\left[\,I_g(\tilde{x}_o,\tilde{y}_o)\,\right] \qquad (12)$$

By substitution, and utilizing the normalized definitions for these Fourier transforms already defined, the result is:

$$\mathcal{G}_i(f_x,f_y) = \mathcal{H}(f_x,f_y)\,\mathcal{G}_g(f_x,f_y) \qquad (13)$$

where the constant K is no longer a factor due to normalization.

In this way, Fourier Optics provide a tool for analysis of the output spectra without having to suffer through difficult convolutions. Since $\mathcal{G}_i$ is the frequency spectra of our image in the f_x f_y plane, to uncover the actual image it is necessary to take the inverse Fourier transform:

$$I(x_i, y_i) = F^{-1} \left[G_i(f_x, f_x) \right] \qquad (14)$$

Here, I is the actual irradiance observed in real space at the image plane.

IV. Theoretical Imaging Of Objects

Predicted Image Of An Edge

In the previous Chapter, the irradiance convolution integral (Equation 8) was rewritten in its simpler form:

$$I_i(x_i,y_i) = K\left[\,|\tilde{h}(x_i,y_i)|^2 * I_g(\tilde{x}_o,\tilde{y}_o)\,\right] \qquad (15)$$

The square of the magnitude of the scaled impulse response has already been defined as the Point Spread Function (PSF). The PSF is convolved with the geometric image to produce the actual image. The constant K may be discarded since all image intensities will be normalized in order to compare resolution between apertures.

In one dimension, Figure 5 shows how the PSF, when convolved with a normal edge, results in a rounding of the corners in the output image.

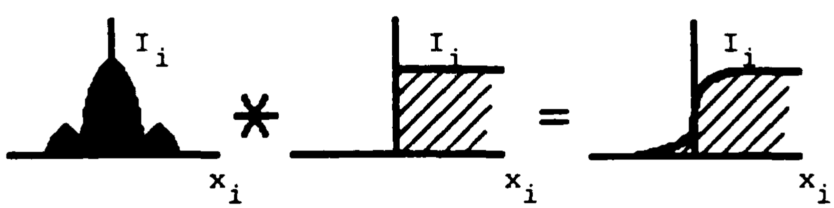

Figure 5. A PSF convolved with one-dimensional edge.

The resulting irradiance pattern approximates the shape of an edge but is "fuzzy" on the edges. The fuzziness is directly attributable to the width of the optical system's PSF. A narrow PSF will yield a sharper edge, while a wide PSF produces more blur.

Figure 6 (12:119) illustrates more clearly just what is taking place at the edge image. A comparison is also shown with the results of Bergey's (2) coherent light analysis of the same object. If it were not for the PSF, the geometric image of the edge would result. Bergey found that with coherent light, the upper irradiance varied as per a SINC function, with peaks of relative irradiance exceeding the absolute value of 1 even though normalized. For incoherent light, the transition is much smoother, and never exceeds the value of 1. There is a rapid increase in intensity as you near the edge, and then a rapid decrease as you leave the edge. The relative irradiance reaches a 50 % value (for the case of incoherent imaging) at the spot where the geometric edge would normally form.

Predicted Image of a Slit

The next step after investigating a single edge is to study two edges, or a slit. The first edge turns the object on, and the second edge turns it off. A slit can be thought of as a narrow

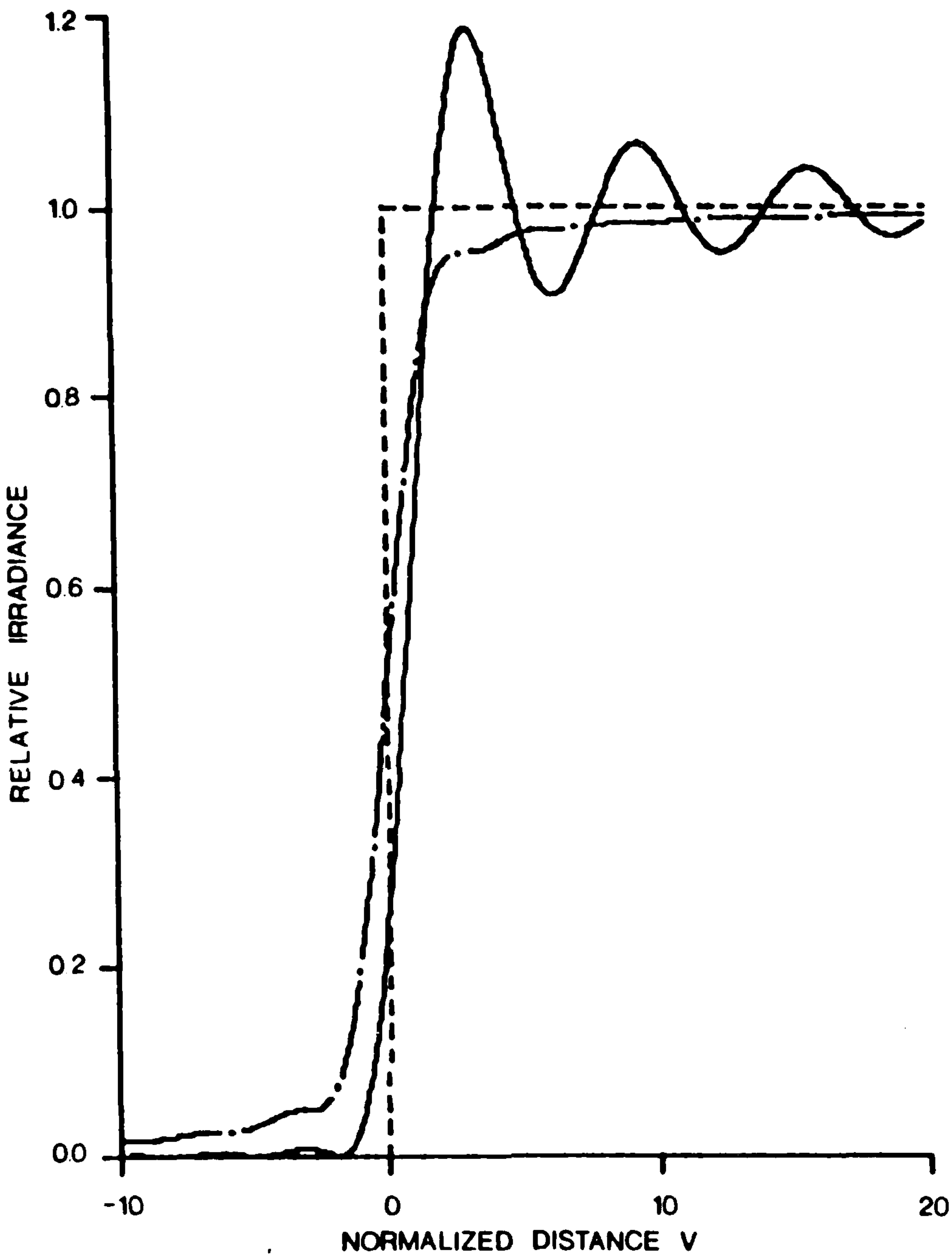

Figure 6. The coherent and incoherent images of an edge are plotted relative to the geometrical image of the edge. (_____ coherent, ___.___.___ incoherent, - - - - - geometrical) (12:119)

rectangle of infinite length in one direction, although the analysis is strictly one dimensional. Figure 7 illustrates a PSF convolved with a slit. The process is exactly as for the previous edge, with a second edge being a "mirror image" of the first.

If the slit is relatively wide compared to the PSF (at least five to ten times wider), there will be an area at the center of the image where a plateau of maximum irradiance has been reached (as shown in Figure 7). If the PSF is too wide relative to the slit however, no plateau forms and it is not be possible to resolve the image and discern the target. In other words, the blur from the first edge overlaps the blur from the second edge.

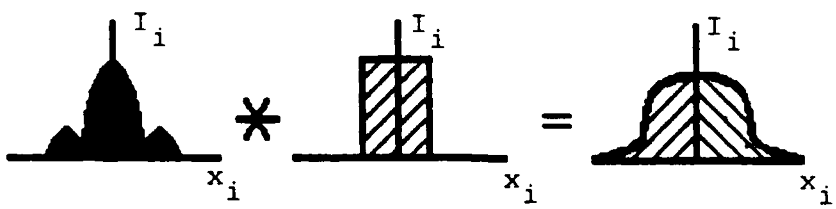

Figure 7. A PSF convolved with one-dimensional slit.

Predicted Image of a Rectangle

The rectangle is the first of the objects requiring a two-dimensional analysis. It can be thought of as a box consisting

of four edges, or two sets of overlapping slits at right angles to one another. Providing the rectangle is large compared to the PSF, the four edges act independantly except in the corners, where the blurring is enhanced. When the PSF is large and the rectangle small, all edges can have overlapping blurring to the point that the target may not be discernable. Figure 8 illustrates the case where the rectangle is not several times bigger than the PSF.

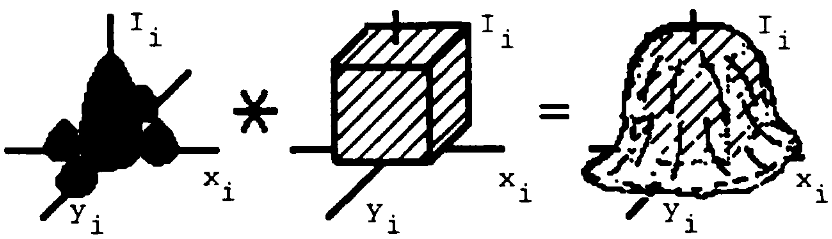

Figure 8. A PSF convolved with two-dimensional rectangle.

Predicted Image of a Circle

The last object of study is the circle, another two-dimensional target. Unlike the previous objects, there is no straight edge, unless the circle is massive enough that any small arc may be approximated by a straight line. The limiting case deals with much smaller targets however. Even when the PSF is small compared to the circle, the blurring is intensified around the circumference because the edge curves towards the center.

Therefore, sharpness is worse than that with just an ordinary straight edge. Further, when the PSF is large compared to the circle, it is easier than with the rectangle to have the blurring obscure the target. Figure 9 illustrates a relatively large PSF convolved with a two dimensional circle.

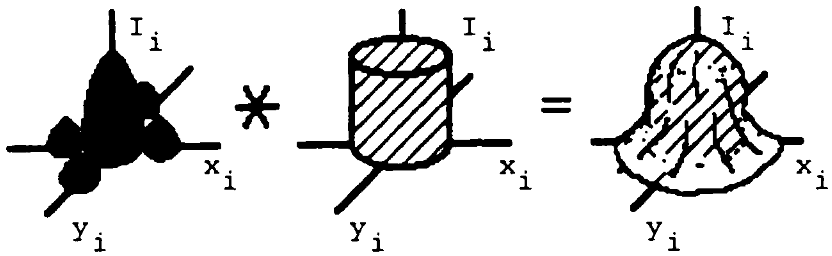

Figure 9. A PSF convolved with two-dimensional circle.

V. Aperture Configurations For Analysis

Design Constraints

A total of ten different aperture configurations was studied in this thesis. These are diagramed in Figure 10. These ten were arrived at through analysis of all possible combinations of sub-apertures, given several constraints.

The first constraint was that all sub-aperture diameters had to be of equal diameter. An arbitrary choice of .125 inches was used as a sub-aperture diameter. A four element array of this size represented an aperture system with an effective collecting diameter of .25 inches. Aperture 1 is the only exception to the first constraint, and contains only a single .25 inch hole (a model of this base case). Aperture number 2 represents the base case for a single aperture of the smaller size. All remaining apertures were constructed from variations in patterns of this sub-aperture.

A second constraint was that no two sub-apertures could be any closer together than they were for the closest elements of the AFWL proposal. This arbitrary overhead concession would allow for mounting and alignment gear to be positioned around and between each mirror as necessary.

The final constraint was that sub-apertures couldn't be so far apart that "zeros" occur within the interior of their Optical Transfer Function (see Appendix C). If they were, valuable frequency components of the image would be lost.

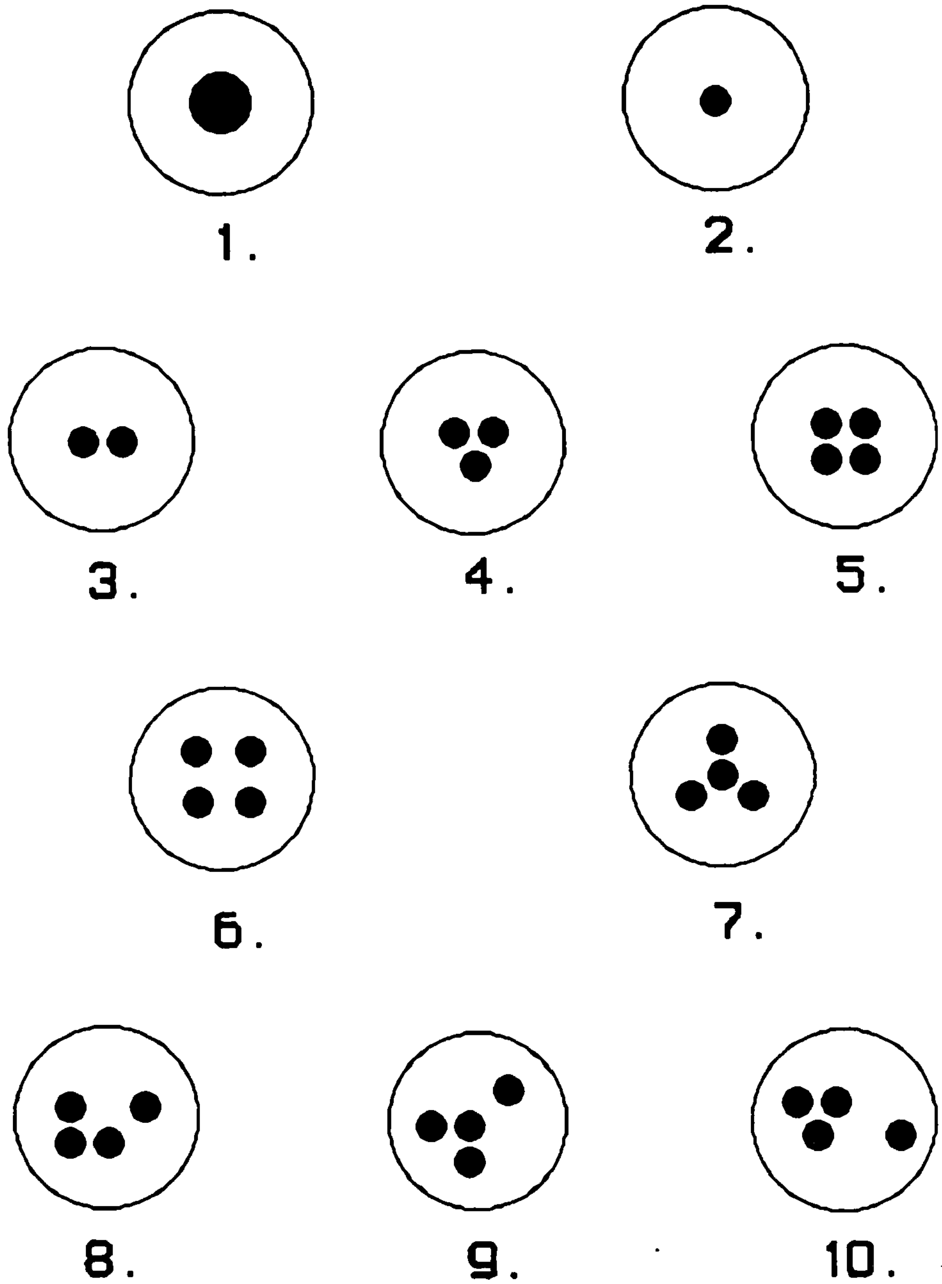

Figure 10. Aperture Shapes

Aperture Configurations

The approach in selecting the aperture configurations was based upon the following question: "If you could put up to four mirrors in space in whatever pattern you wanted (assuming the mission is incoherent optical imaging), which arrangement would you chose?"

As already stated, Aperture 1 represents the maximum collecting power of four elements embodied in a single element as a yardstick for reference. Aperture 2 is a simple one element system. Aperture 3 contains two elements. Aperture 4 contains 3 elements in a traditional triangle. Aperture 5 is the first of the four element patterns. It is the AFWL proposal: a tight square at a scale of 1/63 full size. Aperture 6 expands the square, while apertures 7 through 10 are Golay (8) apertures.

The Golay apertures are of particular interest because of their nonredundant Optical Transfer Function (OTF) properties. Each is based on either a square or triangular matrix in which some pieces are missing. The resulting OTFs are completely nonredundant: there is no overlap except at the central spike. The theory here is that improved resolution can be obtained with a thinned set of elements, removing those that are redundant. The beauty of this is that the resulting OTFs are uniform out to very large spatial frequencies. See Appendix C for examples.

Table 1 describes the basic shape of each test aperture, while Table 2 details their dimensions.

TABLE 1. Aperture Shapes

APERTURE ARRANGEMENT	SHAPE
1	1 element large circle
2	1 element small circle
3	2 element figure 8
4	3 element triangle
5	4 element square (AFWL 1/63 scale)
6	4 element larger square
7	4 element Golay (non-redundant)
8	4 element Golay (non-redundant)
9	4 element Golay (non-redundant)
10	4 element Golay (non-redundant)

TABLE 2. Aperture Specifications

APERTURE ARRANGEMENT NUMBER	EFFECTIVE COLLECTING DIAMETER	EFFECTIVE RESOLUTION DIAMETER	SUB APERTURE DIAMETER	NUMBER OF APERTURES
1	.25 inch	.25 inch	.25 inch	1
2	.125 inch	.125 inch	.125 inch	1
3	.177 inch	.266 inch	.125 inch	2
4	.217 inch	.287 inch	.125 inch	3
5	.25 inch	.324 inch	.125 inch	4
6	.25 inch	.375 inch	.125 inch	4
7	.25 inch	.406 inch	.125 inch	4
8	.25 inch	.439 inch	.125 inch	4
9	.25 inch	.457 inch	.125 inch	4
10	.25 inch	.497 inch	.125 inch	4

VI. Computer Simulation Procedure

General Procedure

For each aperture arrangement, a computer simulation was performed to determine the Point Spread Function and the Optical Transfer Function for that configuration. The results of these are located in Appendices B and C respectively. Further, for each object to be imaged, a three-dimensional image was output as seen through each of the apertures. The results of imaging edges are found in Appendix D, slits in Appendix E, rectangles in Appendix F and circles in Appendix G.

The three-dimensional images give a good subjective feel for each scenario, but for more accurate mathematical comparison, a two-dimensional slice through the heart of some images was also produced. These would allow direct comparison between various apertures, as well as allow correlation with the similar two-dimensional experimental output from the lab.

As an additional double-check, each computer run was also programmed to reproduce the input object and aperture forms, just to be sure no input errors were made.

Description of Computer Code

This computer simulation was performed in Fortran on the VAX 11/780 Electrical Engineering Computer. The main program (IMAGE.FOR) is listed in Appendix L. Extensive use

was made of the IMSL Routine "Fast Fourier Transform (FFT) 3D" to manipulate the data.

In order to facilitate the many different runs of the IMAGE program, a driver file was created called "DO.COM". This driver file contained the specifications for each aperture and object configuration. In this way, all the input parameters could be fed to the main program without having to recompile each run.

The main program utilized two 256 by 256 arrays. Array A contained the aperture, while Array B originally contained the object. At various stages of execution, the contents of the two arrays were sampled and their data was stored in independent data files for later analysis. The final output was retained in Array B.

The 256 by 256 array (or sample) size was chosen for mathematical convenience. It was as large an array as possible without requiring huge execution times by the computer. Within this coordinate framework, all objects, apertures and images were sized. Objects were scaled such that their resulting images did not exceed the sample space. A sub-aperture radius of 10 was chosen through trial and error. This sub-aperture, when employed in some of the "wider" aperture configurations, was as large as possible without causing its OTF to overflow the sample space.

There were several three-dimensional output files. "OTF.DAT" saved the Optical Transfer Function. "APER.DAT"

held the shape of the aperture that was input. "PSF.DAT" was the Point Spread Function data. "OBJ.DAT" reproduced the object that was being imaged. Finally, "INT.DAT" stored the intensity distribution of the resulting image. Each of these files contained data in a singular columnar format, 2304 numbers in length. This could then be translated by MATRIX-X (a graphics utility program) into a three-dimensional picture. The resulting images were 48 by 48.

The only other output data file was "INT2.DAT". This contained a simple 48 element column array with the intensity values of any desired slice through the three-dimensional image. This data could the be redisplayed, through MATRIX-X, into a two-dimensional line graph.

Since MATRIX-X had limited resolution capability, all data files were transferred to a Sun Work Station where they were properly graphed using "DISSPLA".

For the math analysis of each two-dimensional graph's slope, another short Fortran routine was written. This new routine accepted as input the "INT2.DAT" files from above, and output a description of each slope along with the area under each curve. It is from these numerical values that the images were objectively compared.

VII. Analysis of AFWL Aperture Proposal

Specifications

The AFWL aperture proposal involves four elements arranged in a tight square. None of the elements touches any other, since room is needed for mounting and alignment equipment. Free space for radiant cooling is another factor that makes it undesirable for adjacent collectors to physically touch. Figure 11 shows the shape and dimensions of this system. Table 3 gives the technical specifications of the geometry involved.

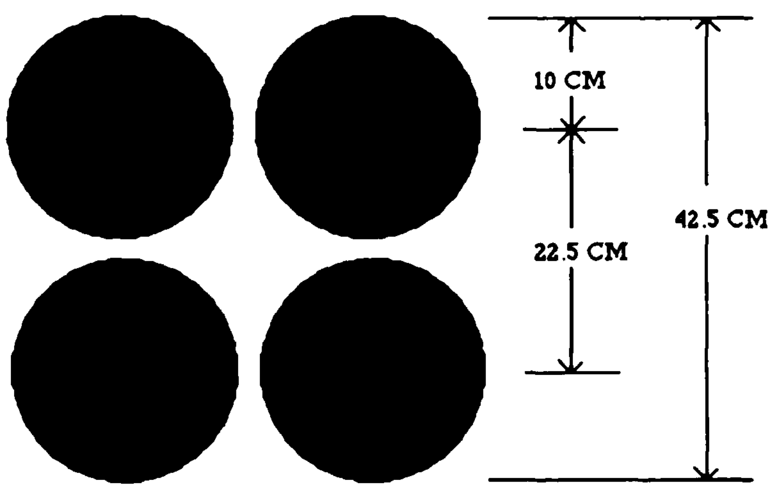

Figure 11. AFWL Aperture Proposal

Table 3. AFWL Aperture Dimensions

Proposed Aperture Characteristic	Size
Sub-aperture radius	10 cm
Sub-aperture diameter	20 cm
Closest distance between centers	22.5 cm
Effective collecting diameter	40 cm
Max effective resolution diameter	51.8 cm
Min effective resolution diameter	42.5 cm

Note that the effective resolution diameter is not constant. Maximum resolution is defined as the sharpest image possible for a given array. Minimum resolution is the worst image possible for a given array. These definitions are based on the author's resolution criteria, (to be detailed later) and are functions of the orientation of the array relative to the object. When the aperture array is aligned so that the X and Xo axes are parallel to one another, the resolution is maximized (Figure 12.a). When the aperture array is turned 45 degrees so that the X axis is now 45 degrees to the Xo axis, minimum resolution results (Figure 12.b).

At first glance, one expects the resolution to be better for Figure 12.b. The PSF for this orientation, however, has more irradiance front and back of the central spike (see Appendix B, aperture 5), than when rotated 45

degrees (relative to an edge aligned with the right hand edge of this paper). Thus, during convolution, the image is dragged out to a less sharp result than for Figure 12.a.

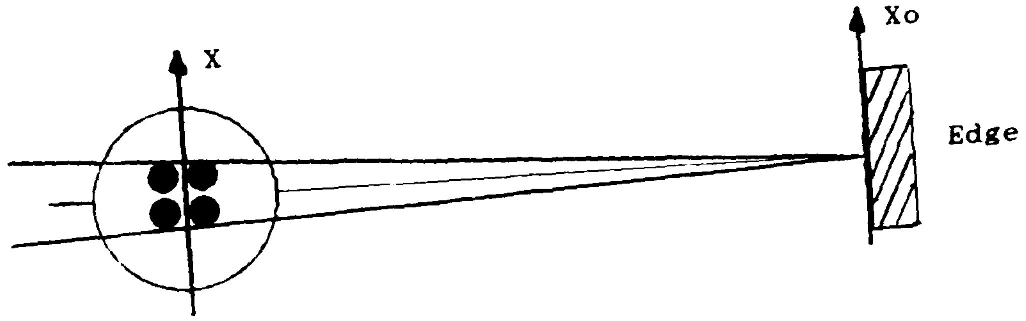

Figure 12.a. Maximum resolution orientation

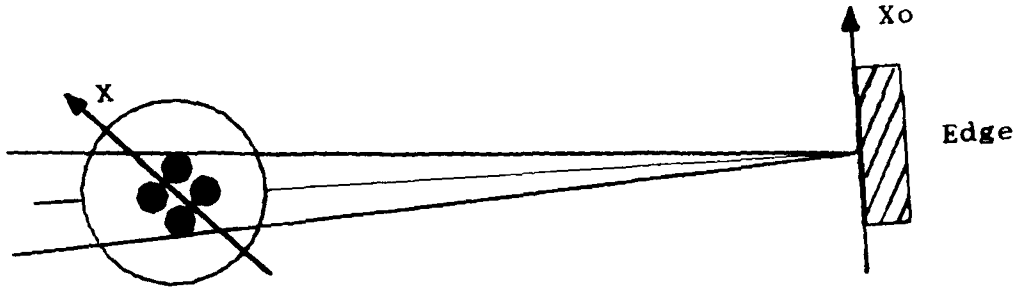

Figure 12.b. Minimum resolution orientation

Point Spread Function

Figure 13 shows the computer representation of this aperture's PSF. The irradiance pattern is compact with a large central spike surrounded by four much smaller spikes. This entire pattern subtends the same area as resulted from the PSF of one single sub-aperture element. The difference now is that the central spike has narrowed significantly, so

the bulk of the irradiance has been driven towards the center. The resulting images will be much sharper than if just one sub-aperture of this size is used.

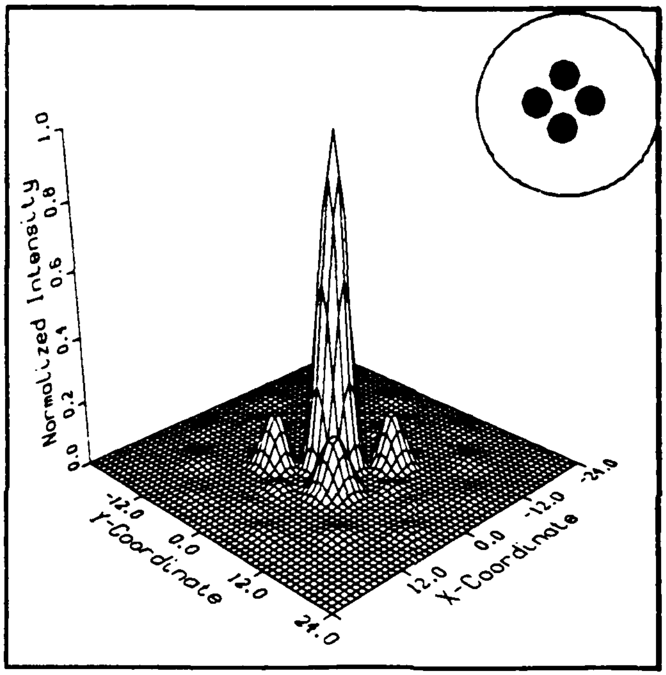

Figure 13. PSF for AFWL proposed aperture

Optical Transfer Function

In Figure 14, the OTF can be seen to have a large central peak and four sub-peaks. These sub-peaks are not completely independent of the main peak but rather contribute to it. It is almost as if the sub-peaks are not there. This is the mark of a good OTF. The weighting

function it represents should be continuous from its center to the edges. There should be no nulls in the process, and any valleys should be kept to a minimum. In short, the more unified the pattern, the better the OTF. This aperture proposal therefore has a very good OTF. It could be improved upon only if the space between sub-apertures was reduced to zero. As already stated, that may not be possible or desirable, from an engineering point of view.

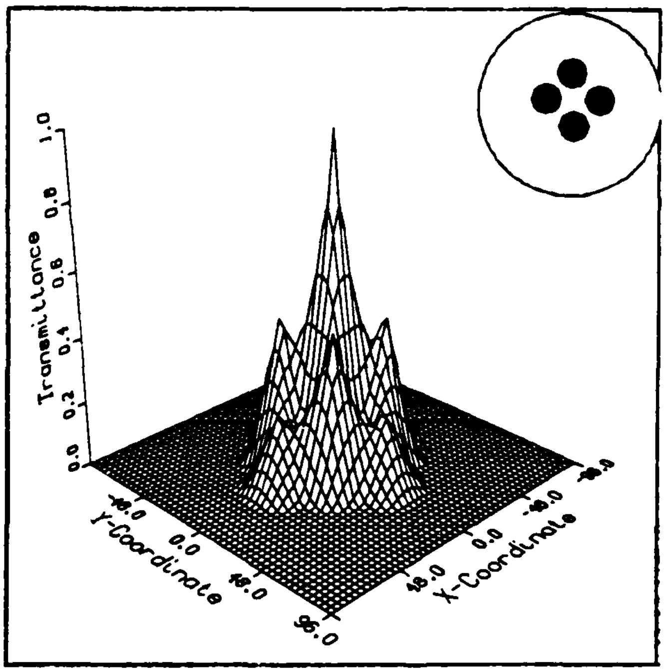

Figure 14. OTF for AFWL proposed aperture

Two-Dimensional Edge Resolution

The cross section of the image of an edge produced with this aperture shows what may be described as very good resolution. The slope of the transition line marking the irradiance of light across the edge is very steep; the steeper the better. The corners at the top and bottom of the transition line are not smooth. This is a function of the separation and positioning of the sub-apertures. The tighter these corners, the better. Figure 15 shows the max resolution case, while Figure 16 shows the min. Note the differences in the two curves. The result shows that the aperture array is marginally susceptible to variations in orientation. This problem is insignificant compared to the differences detected for some of the other aperture arrangements assessed in the following chapter, and hence is not considered to be of concern.

Three-Dimensional Image Resolution

Figures 17 through 20 illustrate the three-dimensional computer predictions for imaging an edge, slit, rectangle and circle through the AFWL proposal. In each case, the object is easily discernible. The actual dimensions of each object and image are unimportant. What is significant is the comparison to the same objects being imaged through different aperture arrays. The AFWL design does very well compared to other possible designs as discussed in the next chapter.

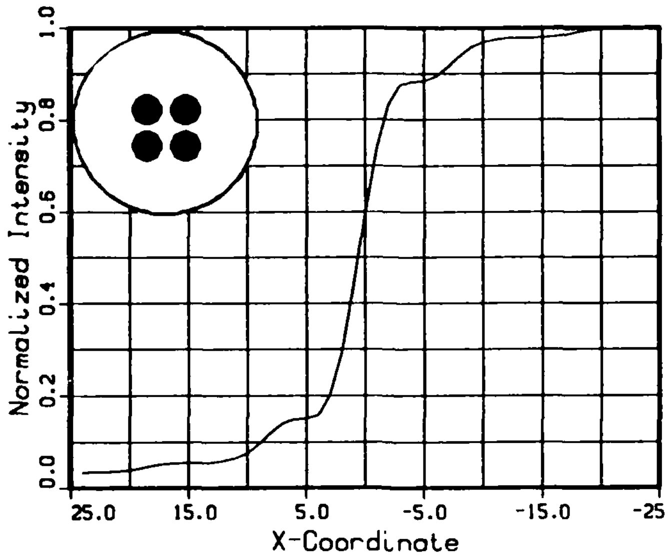

Figure 15. Irradiance of the image of an edge as seen through the AFWL proposed aperture while oriented for maximum resolution.

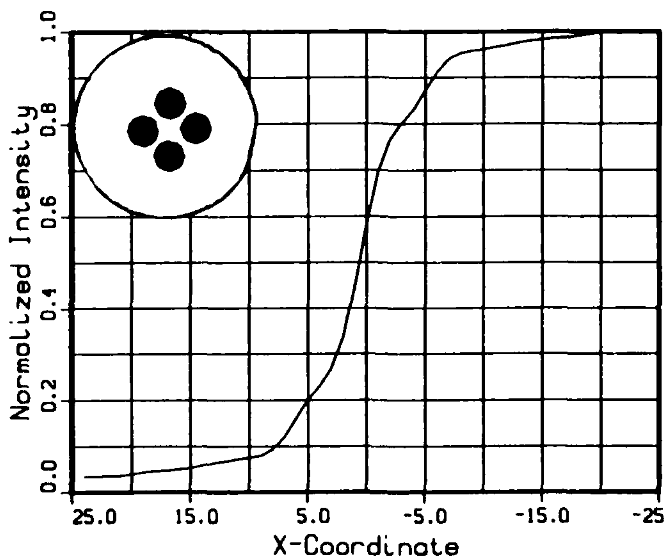

Figure 16. Irradiance of the image of an edge as seen through the AFWL proposed aperture while oriented for minimum resolution.

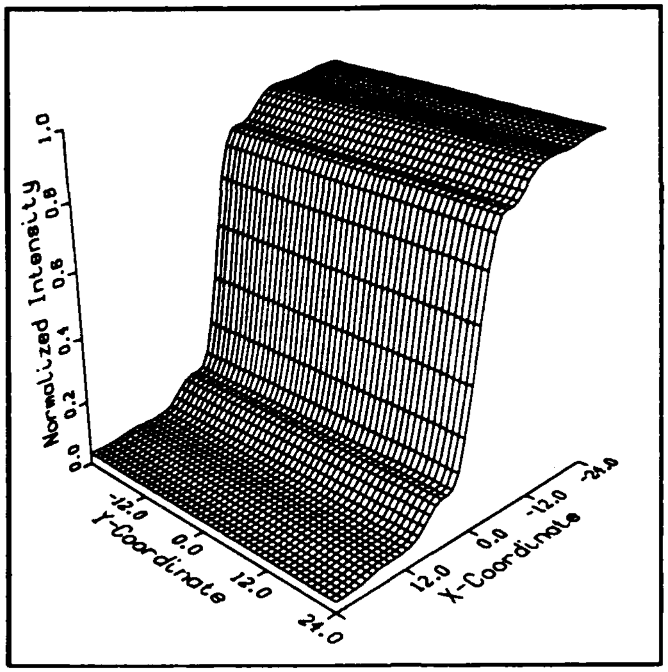

Figure 17. 3-D computer prediction of the irradiance of the image of an edge as seen through the AFWL proposed aperture while oriented for maximum resolution.

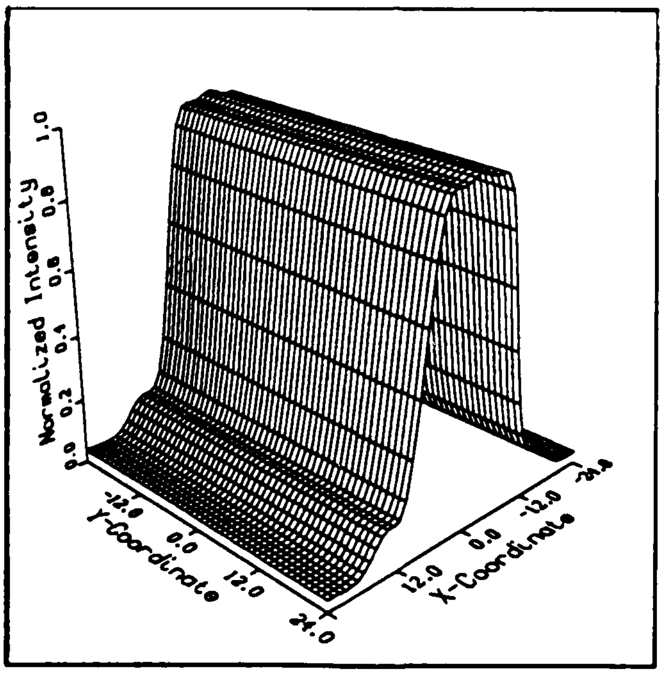

Figure 18. 3-D computer prediction of the irradiance of the image of a slit as seen through the AFWL proposed aperture while oriented for maximum resolution.

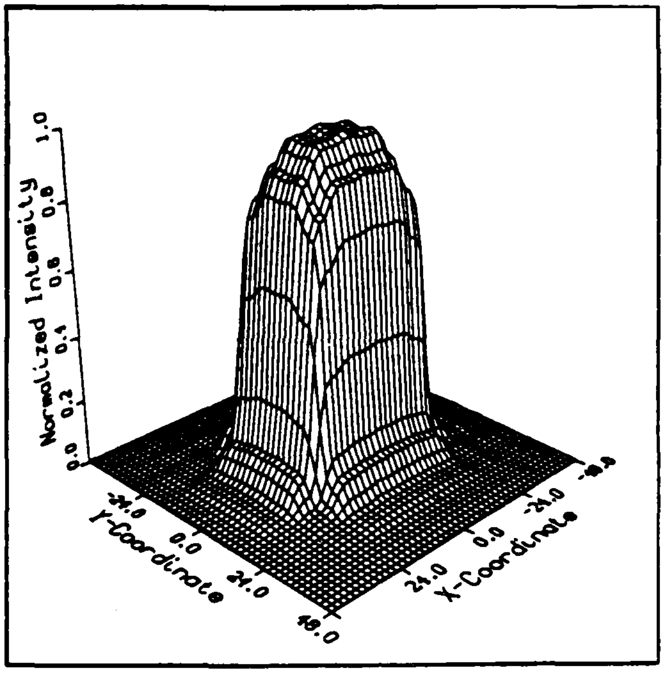

Figure 19. 3-D computer prediction of the irradiance of the image of a rectangle as seen through the AFWL proposed aperture.

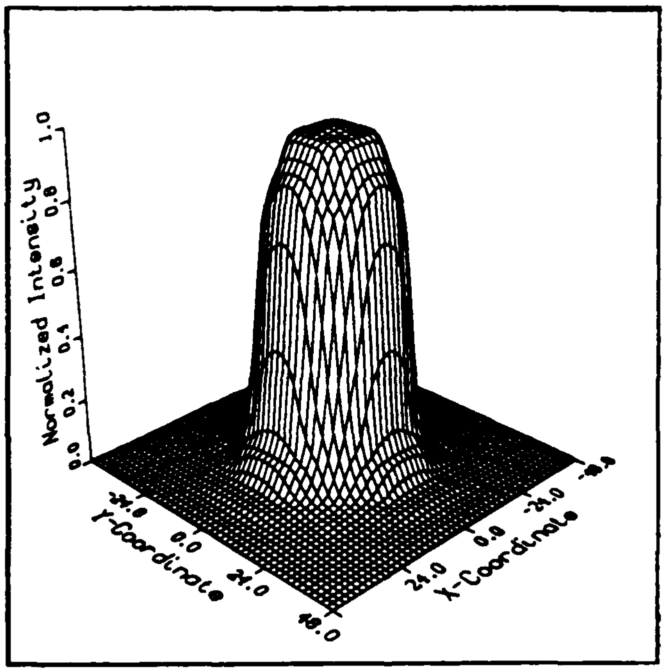

Figure 20. 3-D computer prediction of the irradiance of the image of a circle as seen through the AFWL proposed aperture.

VIII. Comparative Analysis Of Aperture Arrays

Comparison of Aperture Performance

The Appendices to this thesis offer a variety of figures showing each aperture's performance under different imaging conditions. It is difficult to just look at those graphical results and draw any sound conclusions.

Perhaps the best indicator of system performance is the edge analysis. A single slice of each edge image offers a meaningful glance at how each system performs. Figure 21 shows one such slice. There are several ways to describe the shape of the transitional curve it displays. The curve begins at near zero irradiance on the left and rises to a maximum of "1" on the right. The slope of the curve at a series of test points will be the first yardstick. In each case, the steeper the slope, the quicker the transition from dark to light is taking place, and hence the better defined is the image of an edge. These slopes are calculated on sections of the curve whose center is at the .5 irradiance mark (see Figure 21). In this analysis, three slopes are compared. Slope 1 is the maximum slope of the line, always located around the .5 irradiance point for each graph. Slope 2 is measured between "x" coordinates five units apart straddling the middle of the graph. Slope 3 is for "x" coordinates eleven units apart at the center of the graph. These three intervals were arbitrarily chosen to cover the

region where at least 80% and sometimes 95% of the edge transition takes place.

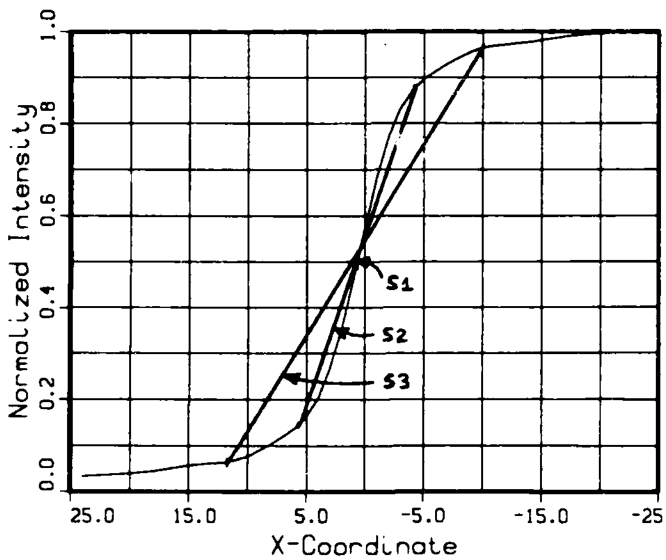

Figure 21. Image of Edge showing slopes to be studied.

A second yardstick is also available to help interpret those curves that are not smooth but have considerable variation. By integrating the area under the curve between certain limits, one can compare different aperture performances in those ranges. The analysis used here is to compare five overlapping regions, each starting at the center of the graph, and moving progressively further to the left hand side. The object is to minimize the area under the curve in each region. The aperture system that does this will show the sharpest edge. Figure 22 illustrates these

regions. Region 1 is the smallest, while region 5 is the largest. On the other side of the edge, a similar analysis can be performed for Region 6, except this time the data is maximized.

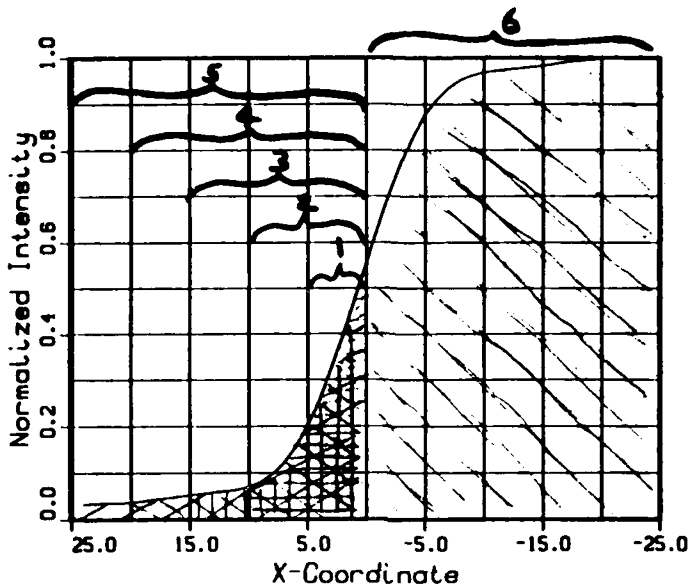

Figure 22. Five regions to be integrated and minimized. Region 6 to be maximized.

Theoretical Aperture Performance

The following evaluation is based on the theoretical performance of the 10 apertures studied. As previously stated, each aperture had a best and worst orientation relative to a fixed object (the edge). Appendix H shows the graphical results for each orientation. Figure 23 illustrates which orientation was best for each aperture. Apertures were aligned as illustrated, relative to an edge that is parallel to the right edge of the paper.

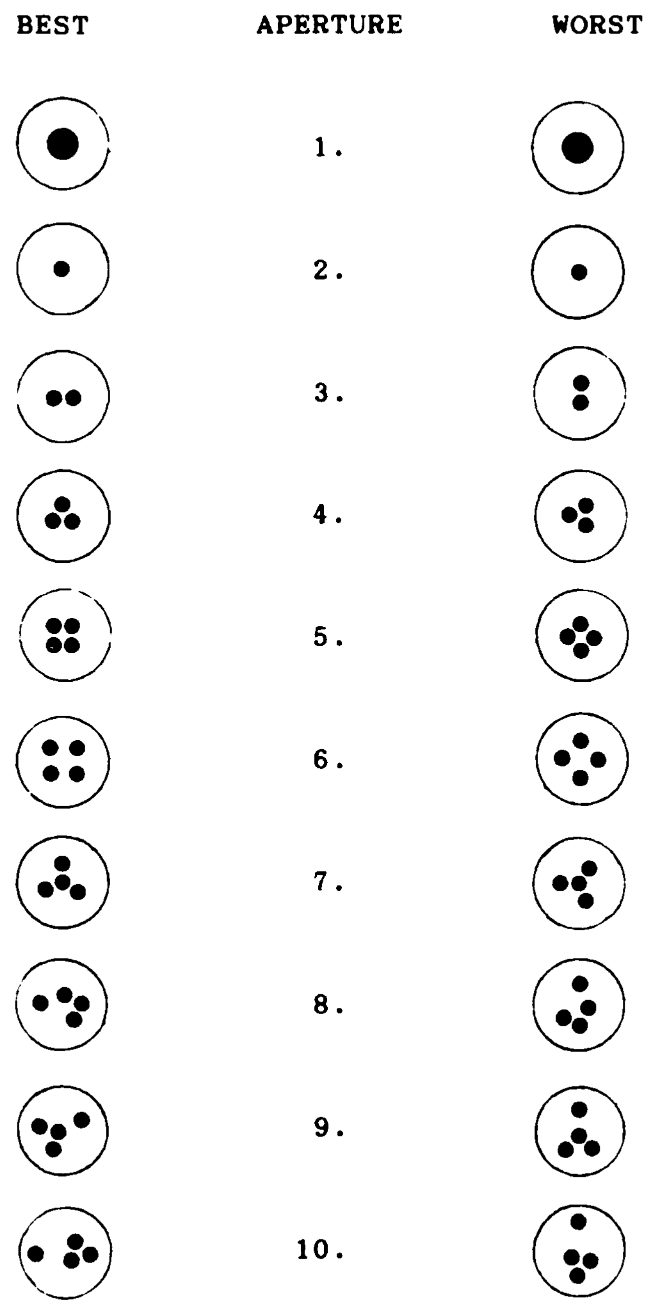

Figure 23. Aperture orientations resulting in "best" and "worst" resolution relative to an edge aligned with the right hand side of this page.

Table 4 records the line slope performance values for each orientation (best and worst) of each aperture.

Table 4. Comparison of Image Slopes by Aperture

Aperture	Slope 1	Slope 2	Slope 3
1 best	.161	.135	.081
1 worst	.161	.135	.081
average	.161	.135	.081
2 best	.081	.077	.066
2 worst	.081	.077	.066
average	.081	.077	.066
3 best	.161	.125	.066
3 worst	.081	.077	.066
average	.121	.101	.066
4 best	.135	.112	.069
4 worst	.124	.108	.071
average	.130	.110	.070
5 best	.162	.127	.068
5 worst	.134	.100	.065
average	.148	.113	.066
6 best	.161	.115	.058
6 worst	.116	.094	.062
average	.138	.105	.060
7 best	.153	.108	.068
7 worst	.122	.103	.067
average	.137	.105	.067
8 best	.156	.091	.068
8 worst	.116	.096	.065
average	.136	.094	.067
9 best	.135	.096	.064
9 worst	.128	.096	.063
average	.132	.096	.064
10 best	.180	.092	.067
10 worst	.117	.099	.066
average	.149	.096	.067

Table 5 contains the integration values of the areas under the curves in all six regions.

<u>Table 5. Image Regional Sizes for each Aperture</u>

Array	Area 1	Area 2	Area 3	Area 4	Area 5	Area 6
1 best	1.57	1.85	2.00	2.11	2.20	22.78
1 worst	1.57	1.85	2.00	2.11	2.20	22.78
average	1.57	1.85	2.00	2.11	2.20	22.78
2 best	2.01	2.66	2.97	3.20	3.38	21.97
2 worst	2.01	2.66	2.97	3.20	3.38	21.97
average	2.01	2.66	2.97	3.20	3.38	21.97
3 best	1.70	2.37	2.68	2.94	3.12	22.30
3 worst	2.01	2.67	2.97	3.20	3.38	21.97
average	1.85	2.52	2.83	3.07	3.25	22.13
4 best	1.78	2.38	2.69	2.92	3.09	22.31
4 worst	1.81	2.38	2.70	2.94	3.12	22.28
average	1.80	2.38	2.70	2.93	3.11	22.30
5 best	1.69	2.34	2.65	2.91	3.09	22.32
5 worst	1.87	2.52	2.86	3.10	3.27	22.11
average	1.78	2.43	2.76	3.00	3.18	22.22
6 best	1.78	2.54	2.85	3.07	3.24	22.13
6 worst	1.91	2.62	2.92	3.15	3.32	22.05
average	1.84	2.58	2.88	3.11	3.28	22.09
7 best	1.81	2.41	2.72	2.96	3.14	22.27
7 worst	1.84	2.48	2.79	3.03	3.21	22.17
average	1.83	2.45	2.76	3.00	3.18	22.22
8 best	1.90	2.56	2.87	3.10	3.28	22.12
8 worst	1.89	2.56	2.87	3.11	3.29	22.09
average	1.90	2.56	2.87	3.11	3.29	22.11
9 best	1.89	2.57	2.89	3.12	3.29	22.08
9 worst	1.90	2.57	2.89	3.13	3.30	22.07
average	1.90	2.57	2.89	3.13	3.30	22.07
10 best	1.87	2.49	2.83	3.06	3.24	22.18
10worst	1.87	2.52	2.84	3.08	3.26	22.12
average	1.87	2.51	2.84	3.07	3.25	22.15

Discussion of Resolution

There are many ways of ranking the apertures based on the data tabulated above. Clearly, the central slope (Slope 1) is the most significant indicator of how sharp an edge image is. The higher the slope, the better. Slopes 2 and 3 extend the process as indicators of how crisp the image is. Again, the higher the numbers, the better the resolution. A quick analysis of Table 4 shows a general trend. Big Slope 1s are usually associated with big Slope 2s. Comparing the average values of Slope 1 will adequately rank the aperture's performance. The other slopes may be needed in case of a tie-breaker. Table 6 records the aperture ranking from best to worst as judged from Slope 1 values.

Table 6. Average aperture performance, best to worst, based upon Slope 1 values

Ranking	Aperture configuration	Slope 1 average
1	1	.161
2	10	.149
3	5	.148
4	6	.138
5	7	.137
6	8	.136
7	9	.132
8	4	.130
9	3	.121
10	2	.081

Perhaps of equal importance to the average slopes listed in Table 6 is the stability of each slope based upon

aperture orientation with the object. To assess this sensitivity for each aperture, the worst slope value is divided by the best slope value, thereby producing a "stability" figure. The larger the value of the figure, the more stable is the resolution. It is desirable to have stable optics that give identical resolution regardless of aperture orientation. Table 7 ranks the apertures from best to worst based upon orientation stability. Best means it is most stable. Worst means it is least stable.

Table 7. Resolution stability, best to worst, based on the aperture orientation with respect to a fixed edge.

Ranking	Aperture configuration	Stability
1	1	1.00
2	2	1.00
3	9	0.95
4	4	0.92
5	5	0.83
6	7	0.80
7	8	0.74
8	6	0.72
9	10	0.65
10	3	0.50

The area integration results produce different ranking orders. It should be noted that this integration technique was performed on both sides of the edge. Because the curves appear symmetric about their middles, minimizing the left side is roughly the same as maximizing the right, although

it was the author's conclusion that the left side was more descriptive because the tail didn't always go to zero. In comparing Region values, it was noted that those areas with the smallest Region 1 usually had the smallest Region 2 through 5. Table 8 ranks the aperture configurations based on Region 1. A smaller area means better resolution in that less "misplaced" light was found.

Table 8. Average aperture performance, best to worst, based upon Region 1 integrated areas.

Ranking	Aperture configuration	Region 1 average
1	1	1.57
2	5	1.78
3	4	1.80
4	7	1.83
5	6	1.84
6	3	1.85
7	10	1.87
8	8	1.90
9	9	1.90
10	2	2.01

For purposes of comparison, Table 9 performs a similar ranking based on the values calculated for Region 5. There is a very slight alteration in the ranking, but the change is no consequence. The basic ranking remains intact.

Table 9. Average aperture performance, best to worst, based upon Region 5 integrated areas.

Ranking	Aperture configuration	Region 5 average
1	1	2.20
2	4	3.11
3	5	3.18
4	7	3.18
5	10	3.25
6	3	3.25
7	6	3.28
8	8	3.29
9	9	3.30
10	2	3.37

The ranking from the "area integration" hypothesis differs significantly from the "maximum slope" analysis. There are several reasons for this. The first is that the aperture designs are generally all quite good, and therefore the differences between them shouldn't be that significant. Further, a couple of sharp ridges in the irradiance pattern (as for coherent light, for example), providing they were finite, would offset the integral radically, yet might well be products of an excellent image. Another factor is that both ranking schemes are really measuring different things. One look at the graphs shows that an integration of the area under the curve may prove fruitful in comparing one Region with another, but to compare the total performance, the true integral would have to go to infinity. Meanwhile, on the high side of the edge, all curves maximize to "1", so this

may offer a more valid comparison. Maximizing the area under the curve, the new ranking scheme is shown in Table 10. The area of concern, Region 6, is shown in Figure 23.

Table 10. Average aperture performance, best to worst, based upon Region 6 integrated areas.

Ranking	Aperture configuration	Region 1 average
1	1	22.78
2	4	22.30
3	5	22.22
4	7	22.22
5	10	22.15
6	3	22.13
7	8	22.11
8	6	22.09
9	9	22.07
10	2	21.97

With the many ranking schemes just listed, there is no consensus over how the apertures compare overall, best to worst. Further, none of the above ranking schemes can be said to be more important than any other. Each is valid in its own way, for its own reasons.

The question of "what is the ultimate ranking?" still remains. Fortunately, there is a way to tie together the results of the previous five tables and arrive at an overall ranking. A numerical value can be assigned to each aperture representative of its placement in each table. For example, the aperture that came first in Table 6 would score 1 point,

while the aperture that came last would score 10. A similar scoring could take place for the other tables as well. In this way, each aperture configuration would acquire one score per table, and the sum of these five scores would be that aperture's overall score, or relative performance. Finally, these relative performance values could be ranked, offering a global picture of each aperture's relative performance. Table 11 shows the calculation of each aperture's performance score. Table 12 contains the final ranking.

Table 11. Calculation of aperture scoring based upon placement in Tables 6 through 10.

Aperture	Score 6	Score 7	Score 8	Score 9	Score10	Total
1	1	1	1	1	1	5
2	10	2	10	10	10	42
3	9	10	6	6	6	37
4	8	4	3	2	2	19
5	3	5	2	3	3	16
6	4	8	5	7	8	32
7	5	6	4	4	4	23
8	6	7	8	8	7	36
9	7	3	9	9	9	37
10	2	9	7	5	5	28

Table 12. Overall aperture performance, best to worst, based upon relative scoring from Table 11.

Ranking	Aperture configuration	Relative Score
1	1	5
2	5	16
3	4	19
4	7	23
5	10	28
6	6	32
7	8	36
8	9	37
9	3	37
10	2	42

The results of Table 12 are self explanatory. Aperture 1 (one large solitary collector) was the best all along, and naturally ends up in first place. The AFWL proposal, Aperture 5, comes second. It represents the best multiple aperture approximation to Aperture 1 (of all the arrangements tested). Aperture 4 comes third. The placement of Apertures 5 and 4 show the strength of tight symmetric arrangements in simulating a monolithic element. The Golay apertures came next, sticking together for the most part. Finally, all arrangements proved superior to Aperture 3, which in turn outperformed Aperture 2, a single small collector.

Design Considerations

Sub-Aperture Size. From a light gathering point of view, bigger is always better. The same is true for resolution. As predicted by Equation 1, a larger diameter offers better resolution. A comparison of the performances of Aperture 1 (one large circle) to Aperture 2 (one small circle) showed the former to be superior in every category.

Sub-Aperture Spacing. In almost every arrangement studied, the sub-aperture spacing was constant. No two elements were ever closer than the closest two of the AFWL proposal. With the Golay apertures, although the arrays are expanded, the position of each element was an even multiple of this original condition. This assisted the non-redundancy in the OTF. Technically therefore, the Golay apertures did not violate any spacing constraints; *either too close or too* far.

The one exception to the close packed arrays was Aperture 6, the large square. This aperture was identical to the AFWL proposal (Aperture 5), except the sub-aperture spacing was increased. The resulting performance speaks for itself. The PSF expanded, and the OTF developed nulls inside the pattern. Consequently, resolution deteriorated. Although this is in violation of Equation 1, a larger baseline does not guarantee better resolution for incoherent imaging when multiple apertures are used. Naturally, if the PSF widens, then any convolution of an edge with it will result in a

loss of definition. This analysis therefore concludes that closer is better.

Number of Elements. For light gathering power, more is always better, but how did increasing the number of elements affect resolution (assuming all elements are of the same size)? The single small sub-aperture was the worst performer. The two element system was better. Three elements arranged symmetrically about the middle were better still. But better yet was the four element system, when these elements were also arranged symmetrically about the middle. This analysis illustrates that more sub-apertures offer better resolution.

Array Shape. The strong performances by the three element triangle and the four element square show a dominance for array symmetry. The non-symmetric Golay apertures, when held to the other constraints of size and spacing, did not meet the standards of the symmetric arrays. The Golay PSFs were very good, but the proportion of irradiance in the side lobes to the central spike, when compared to Apertures 4 and 5, was too high. This resulted in slightly degraded resolution.

The Golay apertures also suffered from high instabilities due to orientation sensitivity. In real life, it is not possible to control the orientation of an object, particularly when viewed from space, so these apertures would be at a disadvantage. This is all above and beyond the

added technical challenge that engineers would face in trying to couple the asymmetric inputs into one image. For these reasons, the Golays, although they performed well, are not the best arrangements for incoherent imaging.

The array shape of choice is deduced to be a tight symmetric pattern, all elements spaced equidistant from the center of the array. This analysis has shown this to be true for arrangements of up to four apertures.

IX. Laboratory Experimental Procedure

Experimental Apparatus

The laboratory portion of this thesis was conducted in the Optics Lab in building 194 of Area B at WPAFB. The apparatus used is illustrated in Figure 24. On the far left is located an incoherent light source. This was a projector bulb with a variable power source, thus allowing the output intensity to be varied as required. In front of the bulb, two short focal length lenses were used to collect and then project the light forward. The first lens focused the bulb filament into the second lens, and the second lens was positioned one focal length away from the first. The result was a fairly uniform column of light propagating to the right.

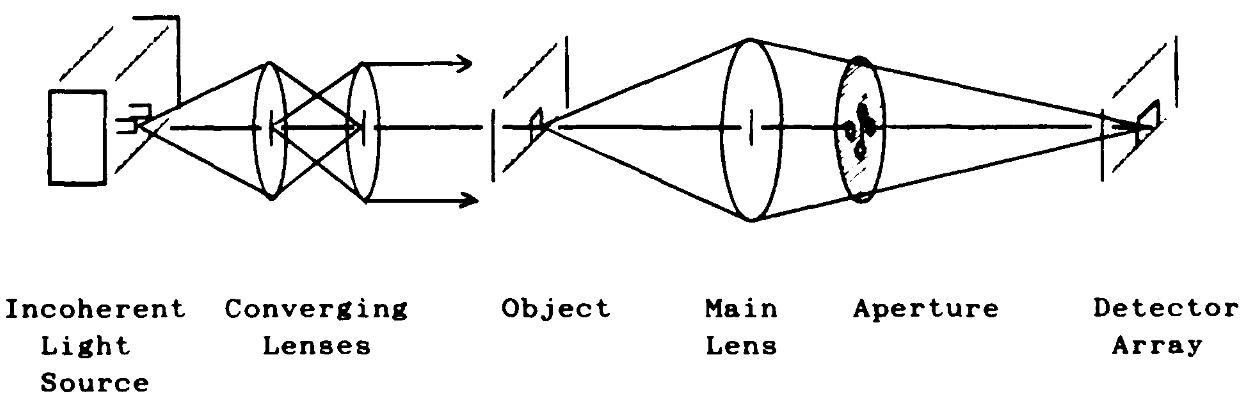

Figure 24. Laboratory Experimental Apparatus

The column of light next illuminated the object, which was a razor blade edge, supported vertically. In this way, the object light irradiance pattern was established as being "on" beyond the edge of the object, and "off" behind the boundaries where the incident light was blocked.

The system main lens was positioned beyond the object. A relatively large lens was used for this, the imaging lens. The larger diameter enabled fewer aberrations to be a factor, as the experiment could be conducted on or near the central axis, well away from the perimeter effects of the lens. This lens was positioned with the illuminated object in the object plane, and a detector array was located in the image plane.

The multiple aperture effect was created by placing the designed multiple aperture discs as close to the main lens as possible. These discs blocked all incident light except for the light passing through the sub-apertures themselves. In the case of a four element multiple aperture, this effectively simulated four separate collectors, and the effect of the main lens would be to recombine their four separate images into just one.

The final image was projected onto a detector array at the far right. This array was a Charge Coupled Device (CCD) consisting of 256 detectors arranged in a straight line. The detector array was oriented to be perpendicular to the edge of the image. The output of the detectors was fed to an

oscilloscope where the light transition from dark to light (across an edge) could be easily studied and photographed.

General Procedure

Each aperture was studied one at a time. Particular attention was devoted to the edge analysis since this was the base case for all further analysis. For each test, the resulting detector output was photographed on the oscilloscope.

The item of interest was image resolution, and not image intensity. With each aperture, intensity would vary. This was due to the different collecting radius of some apertures, but also due to the different effective resolution radius. The further spread out the elements were, in general, the less light would get through to the image because most of the intensity was transmitting on or near the optical axis. As the effective resolution radius increases, more of this central component is lost.

Because the intensity varied, it was necessary to normalize the experimental image intensity just as the output had been normalized during the computer simulation. This normalization was accomplished by varying the bulb intensity to compensate for aperture losses. Additionally, the oscilloscope output could be scaled using its controls so that each aperture's image started and ended at the same intensity levels. From that point on, it was only necessary to compare the different slopes of the graphs for each

aperture to compare performance. Steeper slopes represented more rapid transition from dark to light, and hence better resolution. Also, the speed with which the edge image "curved" at top and at bottom was another indicator of performance. The sharper the curve, the less overall distortion or blurring.

Results

The experimental portion of this thesis verified the computer simulation. Photographs of the oscilloscope display were taken for each two-dimensional slice through the image of an edge. These could be compared directly to the computer two-dimensional theoretical views of the same thing. The photographic results of this are found in Appendix J. Figure 25 shows an example (in this case for Aperture 1) of the comparison between simulation and experimental results . Note that the oscilloscope photo doesn't have the finite detail of the simulation graph, but the general shape is similar enough to confirm the results. Also note that although both plots are normalized, the X-axis scales are not the same.

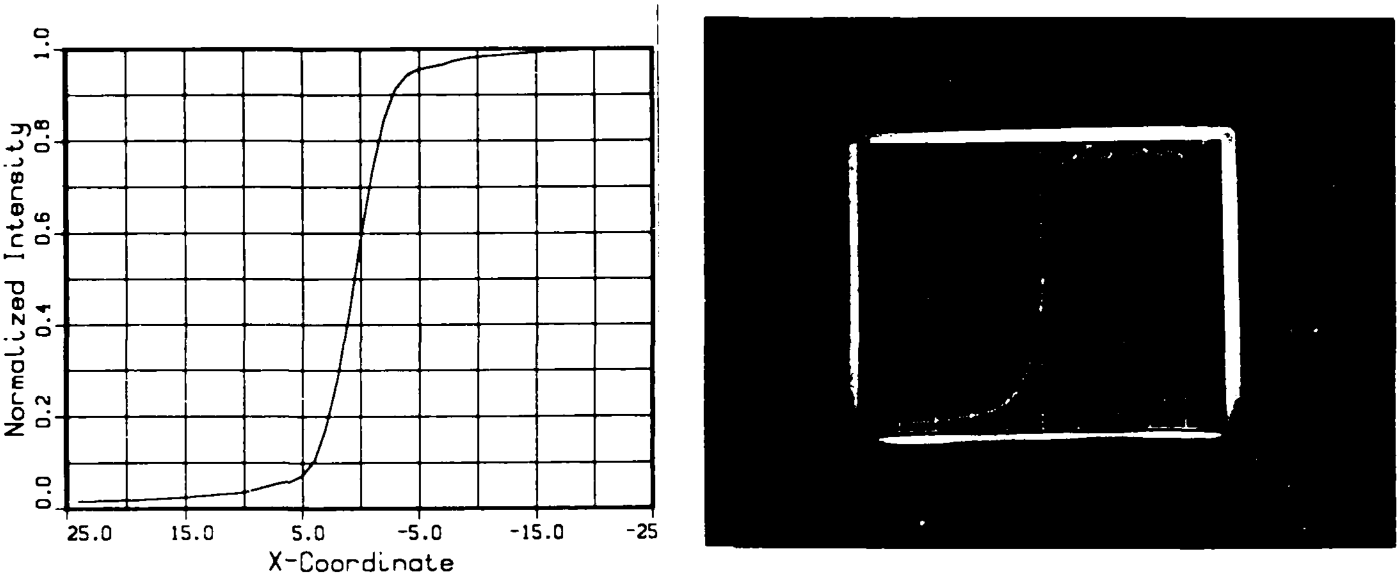

Figure 25. Theoretical Edge compared to Experimental Edge.

X. Conclusions

Summary

The purpose of this thesis was to evaluate and compare the resolution capability of various multiple aperture systems. Their performance was to be assessed while they imaged objects using incoherent light. A total of ten configurations was selected for study. These ranged in size from one single element to a maximum of four per arrangement. Each aperture was studied to reveal its Point Spread Function and Optical Transfer Function. A computer program was written to simulate the imaging of edges, slits, rectangles and circles by each of these apertures. The detailed results of each of these are found in the Appendices. The validity of the computer program was verified through actual experimentation in the Optics Laboratory.

A two-dimensional slice was cut through each edge image to produce a set of data for analysis. This data was studied to reveal the optical performance of each aperture. Based on numerical scores for performance in a series of resolution criteria, a relative ranking of the apertures was achieved.

The Air Force Weapons Lab is proposing the construction of a four element optical sensor. This design was included in the analysis as Aperture Number 5. It was one of the goals of this thesis to determine whether there might be a better arrangement for the AFWL proposal.

Specific Conclusions

This thesis drew conclusions subject to the conditions of incoherent imaging, and to the resolution criteria derived by the author. These criteria concerned the analysis of each aperture's edge image. Apertures were ranked based on their characteristic irradiance slopes at a series of test points, as well as on their integrated area values for specific regions under each curve.

Given the choice between a single element aperture and a multiple aperture system (whose total collecting area is equal to that of the single element aperture), the single element offers better resolution. In other words, Aperture 1 is the best performer. Using multiple aperture optics, the best approximation to the ideal performance of Number 1 is found in Aperture 5, the AFWL proposal.

In assessing the parameters of a multiple aperture design, the following was found. The sub-aperture size should be as large as possible. Fewer large elements can outperform many small ones. As far as sub-aperture spacing is concerned, the closer the better. A tight array offers better resolution. When deciding upon the number of sub-apertures to use, this thesis determined more is better, not only for light gathering power, but also for better resolution. Finally, in selecting the multiple aperture pattern, it is concluded that symmetric arrangements provide the best overall performance.

All the above design goals are embodied in the AFWL proposal. This thesis proves that for up to a four aperture system of a predetermined sub-aperture size, you can do no better than a tight square array. Such is the AFWL design.

General Conclusions

This thesis can draw some conclusions about multiple aperture arrays in general; not only for those of four apertures or less. The first is that increasing the sub-aperture size is always beneficial in terms of improving resolution. A larger sub-aperture yields a narrower PSF. The PSF's exterior envelope is only a function of the sub-aperture size, and not of how many sub-apertures are used. The use of additional sub-apertures forces a narrower central spike and the introduction of side lobes, but these are still limited to the area outlined by the original sub-aperture. Therefore, the way to drive down the confines of the PSF is to increase the sub-aperture size. A narrower PSF, when convolved with an edge, will produce a sharper image.

A second general conclusion is that sub-aperture spacing should always be kept to a minimum. The tighter the pattern, the more compact the side lobes become. This forces a greater fraction of the total irradiance into the central spike. A convolution with such a PSF will give the sharpest possible image.

The third general conclusion is that the more sub-apertures you use, the better your resolution becomes (providing all the other design goals are also fulfilled). An increase in light gathering power is the most basic advantage, but the PSF also changes. The central spike narrows, and the side lobes are driven down in magnitude. The PSF becomes tighter, so this results in crisper images.

A last general conclusion is that symmetric arrays are preferable to non-symmetric arrays. The more symmetric the array, the more symmetric is the PSF. A perfectly symmetric PSF has the advantage of being convolved with an edge from any direction, and the result is always the same. This allows maximum stability in the quality of the image despite the orientation between object and aperture. The logical extrapolation of this thesis' analysis is that an infinite number of elements, if arranged in a symmetric pattern, would produce the most symmetric PSF, and would therefore afford maximum orientation stability.

Suggestions and Recommendations

This thesis opens the way to additional research in the area of multiple aperture incoherent imaging. Future projects could involve studying larger arrays to see whether the above design conditions hold true. Also, attention could be devoted to the complex engineering problem of actually combining the multiple aperture inputs into one image, as would have to be performed in the real world.

APPENDIX A - Aperture Computer Representations

The following three-dimensional graphs are computer representations of each aperture. Each graph represents the transmittance of light at the aperture plane. The "xy" coordinate system is representative of the aperture plane, and the "z" axis records the transmittance at each "xy" coordinate.

The scale of the image plane is 1 to 1 with the computer array that stored the pattern: the base area is 96 by 96, corresponding to the central 96 by 96 area of the original aperture array in the program (256 by 256).

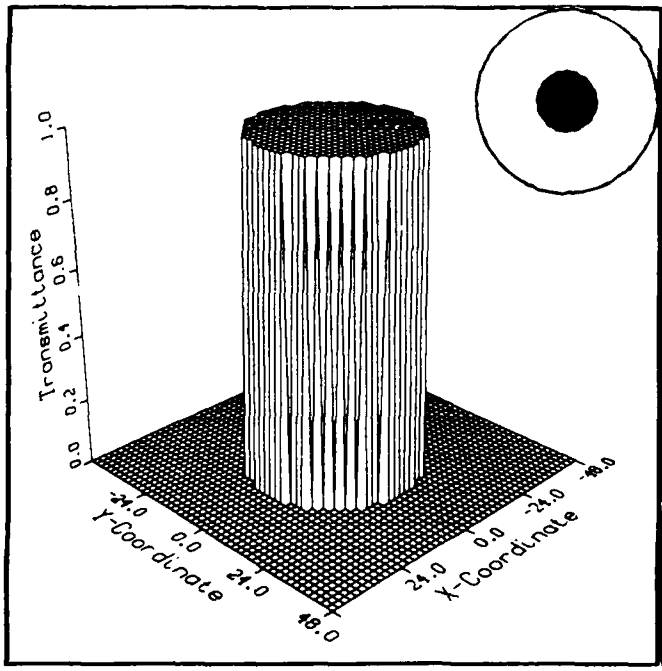

Fig. A-1. Aperture 1.

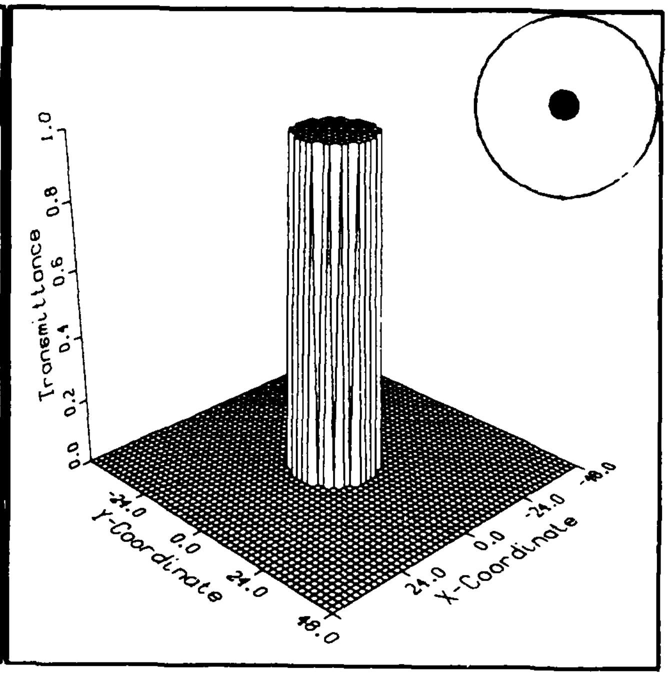

Fig. A-2. Aperture 2.

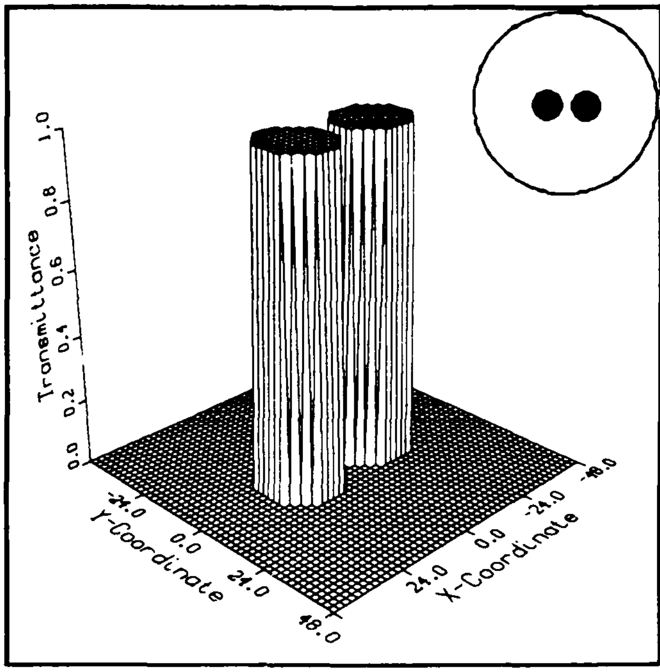

Fig. A-3. Aperture 3.

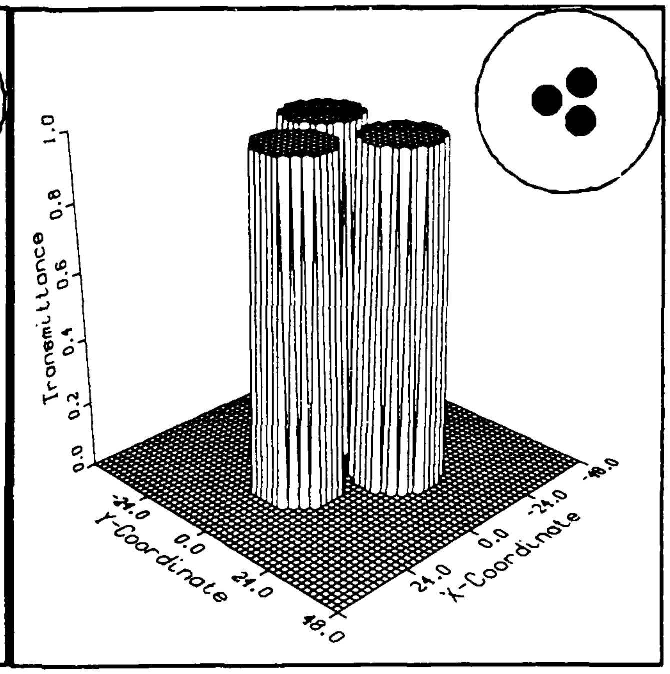

Fig. A-4. Aperture 4.

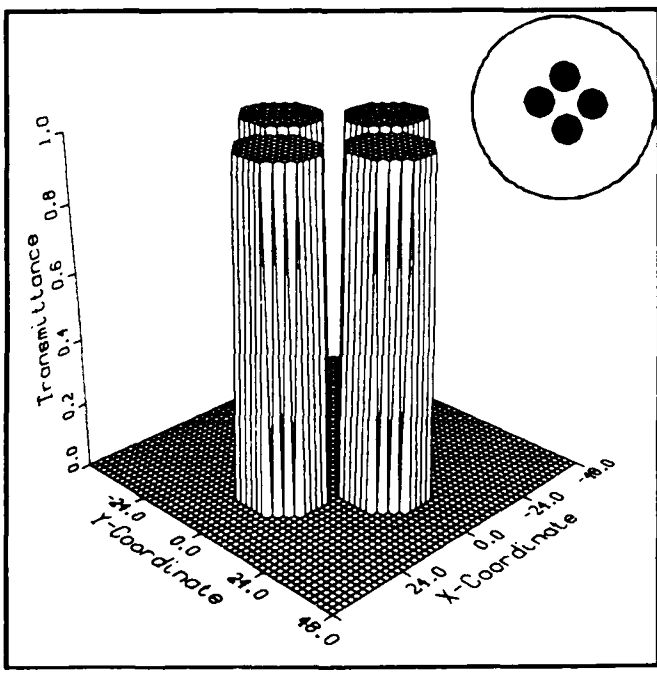

Fig. A-5. Aperture 5.

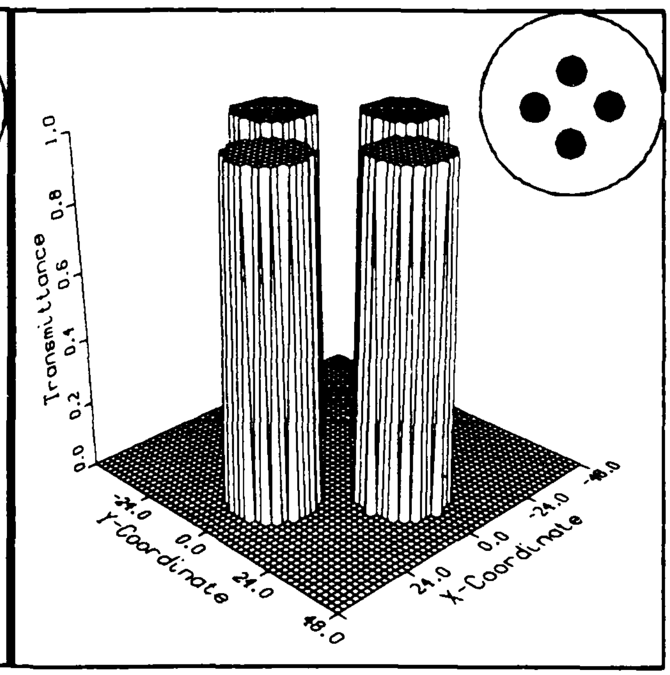

Fig. A-6. Aperture 6.

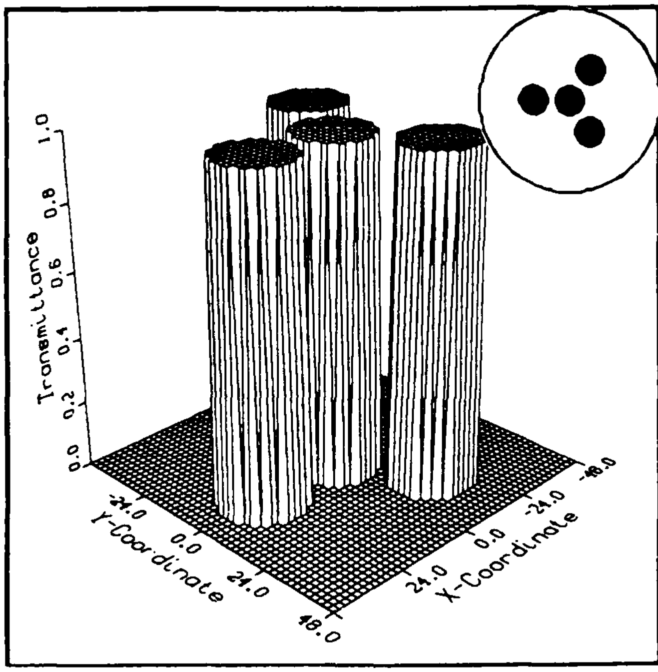

Fig. A-7. Aperture 7.

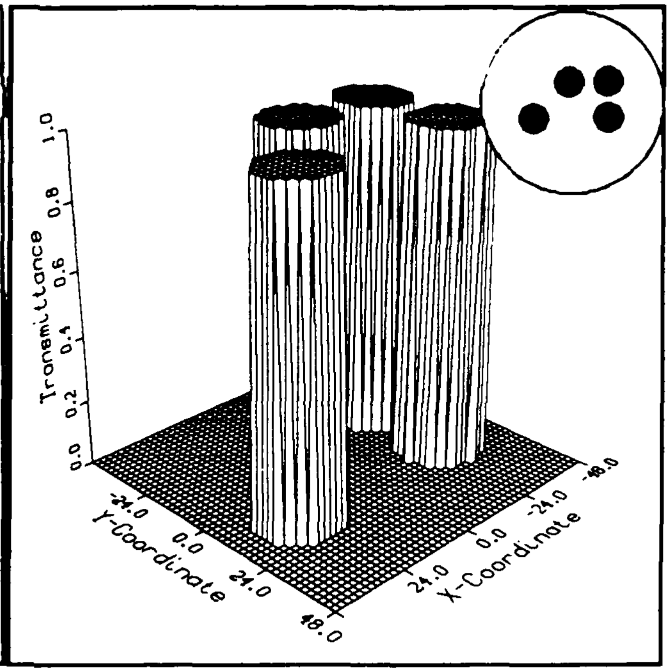

Fig. A-8. Aperture 8.

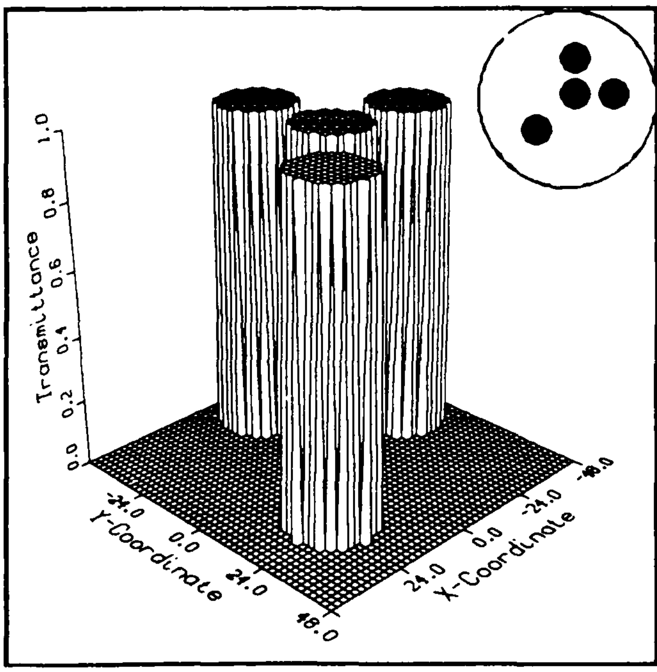

Fig. A-9. Aperture 9.

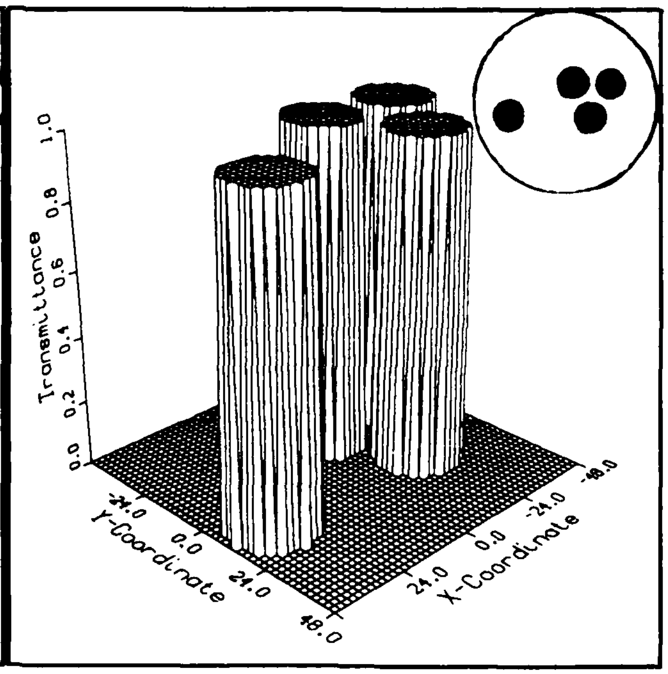

Fig. A-10. Aperture 10.

APPENDIX B - Aperture Point Spread Functions

The following three-dimensional graphs are computer representations of each aperture's theoretical Point Spread Function (PSF). Each graph represents the intensity of the irradiance of light in the image plane. The "xy" coordinate system is representative of that same image plane, and the "z" axis records the normalized intensity of the irradiance at each "xy" coordinate.

The scale of the image plane is 1 to 1 with the computer array that stored the pattern: the base area is 48 by 48, corresponding to the central 48 by 48 area of the original target array in the program (256 by 256).

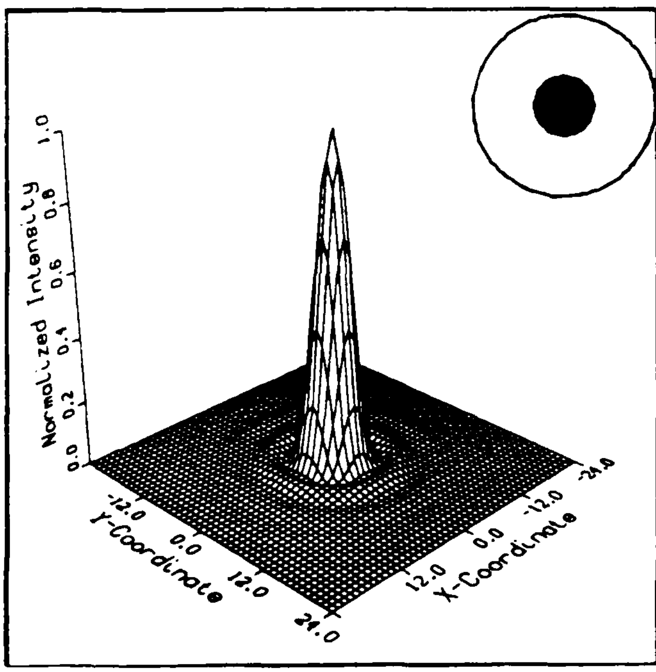

Fig. B-1. Aperture 1 PSF.

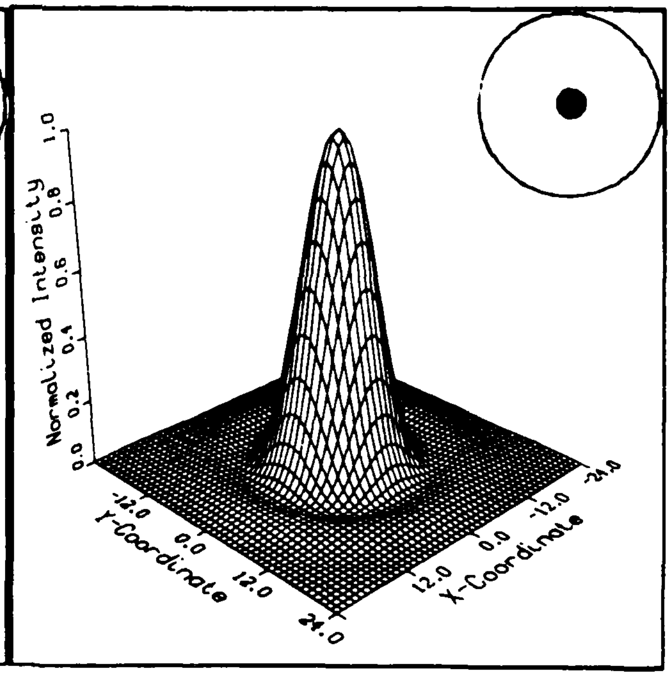

Fig. B-2. Aperture 2 PSF.

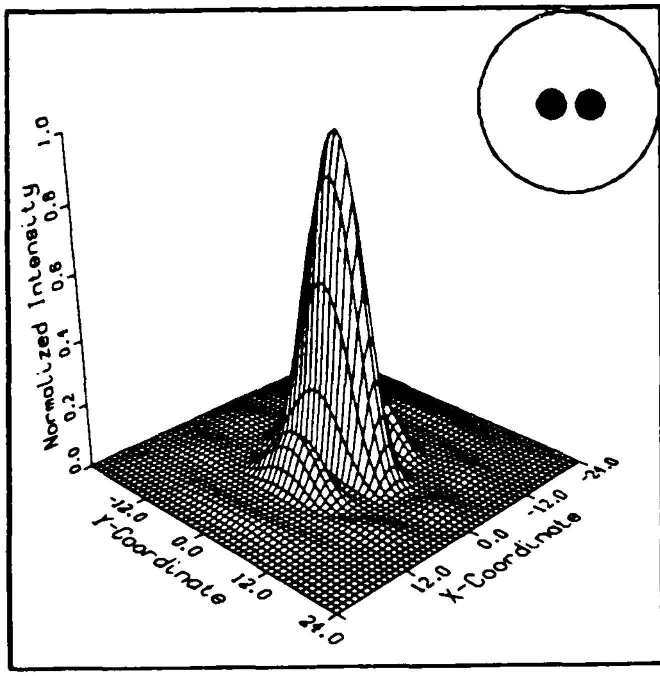

Fig. B-3. Aperture 3 PSF.

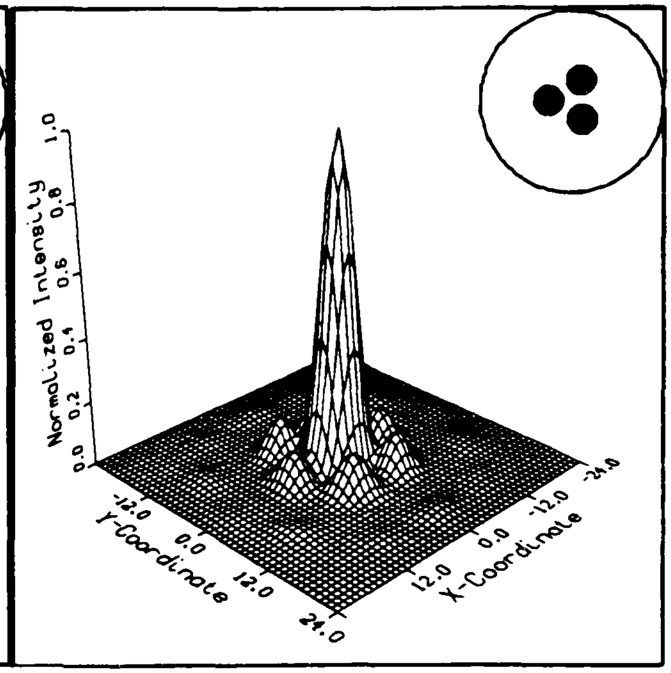

Fig. B-4. Aperture 4 PSF.

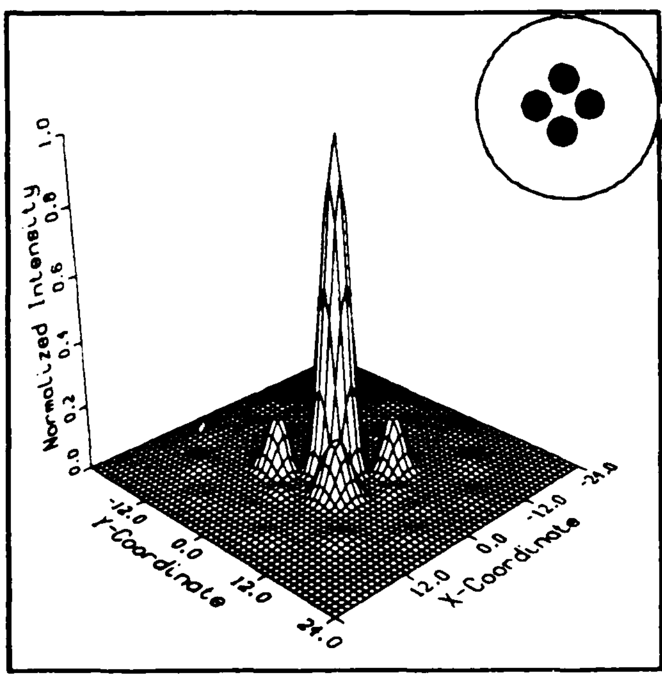

Fig. B-5. Aperture 5 PSF.

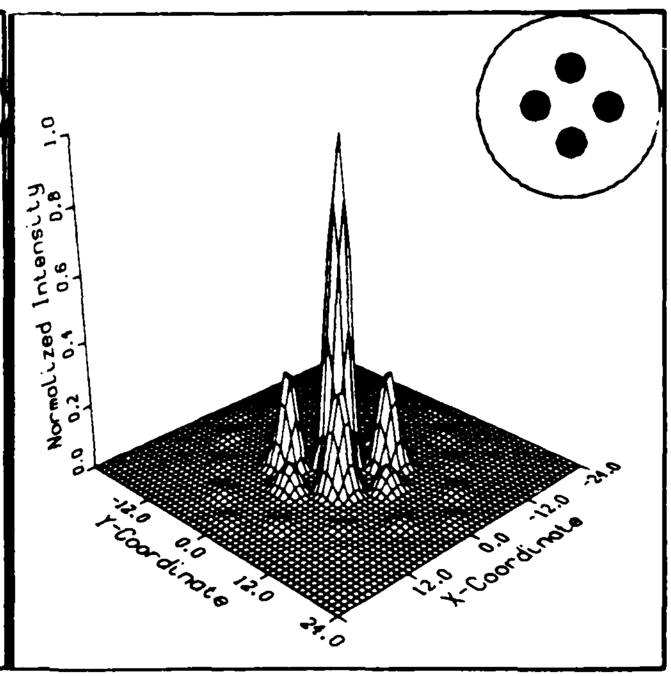

Fig. B-6. Aperture 6 PSF.

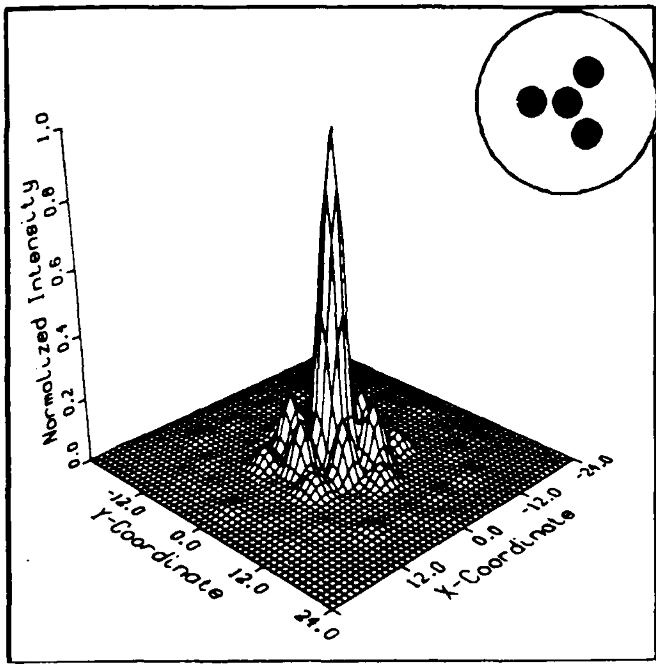

Fig. B-7. Aperture 7 PSF.

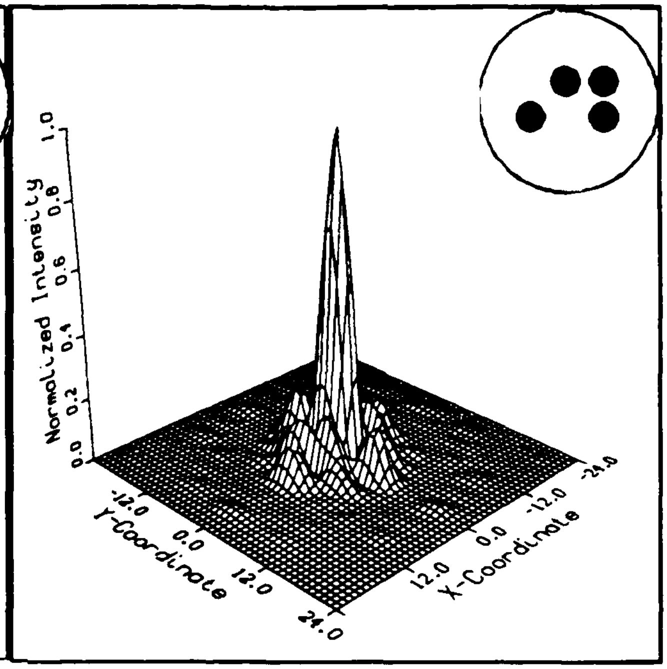

Fig. B-8. Aperture 8 PSF.

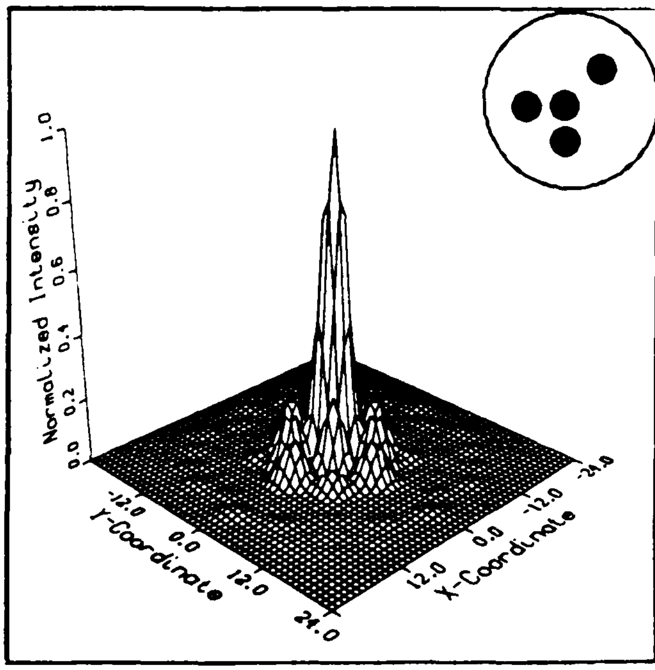

Fig. B-9. Aperture 9 PSF.

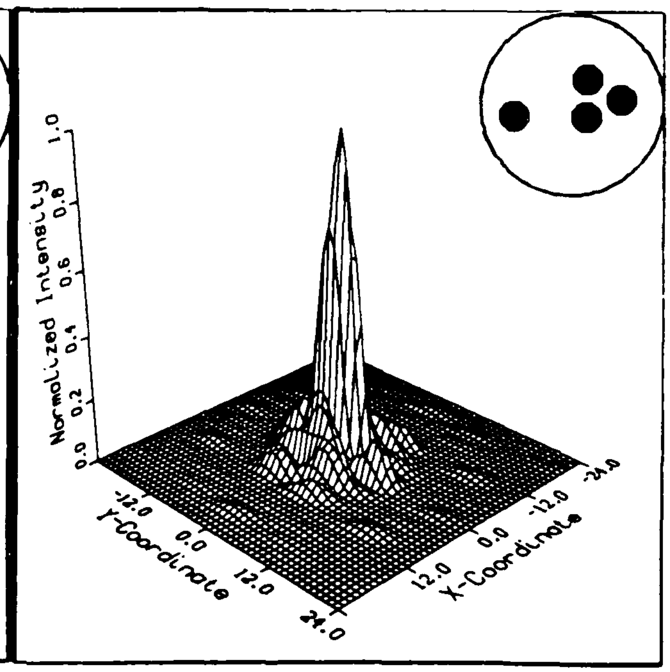

Fig. B-10. Aperture 10 PSF.

APPENDIX C - Aperture Optical Transfer Functions

The following three-dimensional graphs are computer representations of each aperture's theoretical Optical Transfer Function (OTF). Each graph represents the weighting function for transmittance of spatial frequencies. The "xy" coordinate system is representative of the aperture plane, and the "z" axis records the normalized transmittance the spatial frequency at each "xy" coordinate.

The scale of the image plane is 1 to 1 with the computer array that stored the pattern: the base area is 192 by 192, corresponding to the central 192 by 192 area of the original target array in the program (256 by 256).

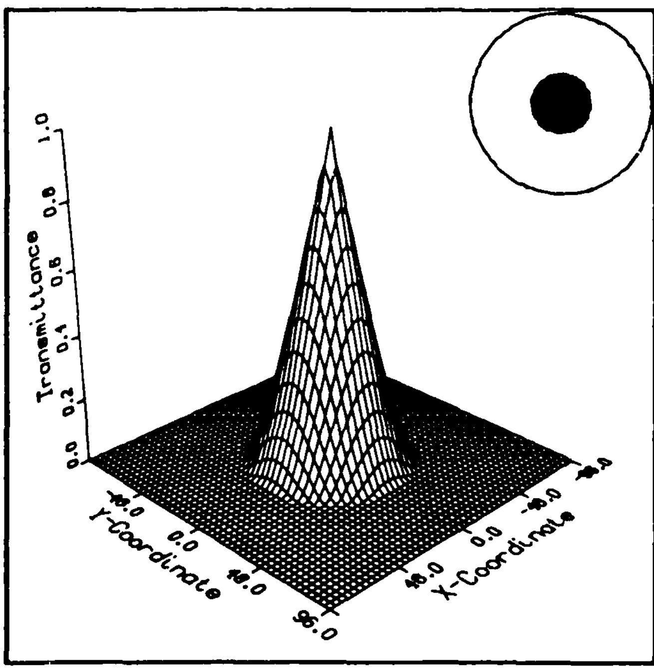

Fig. C-1. Aperture 1 OTF.

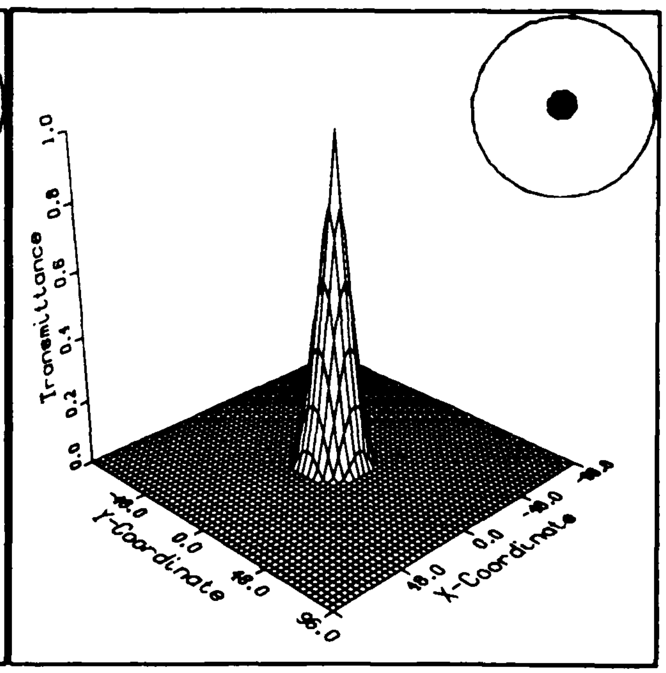

Fig. C-2. Aperture 2 OTF.

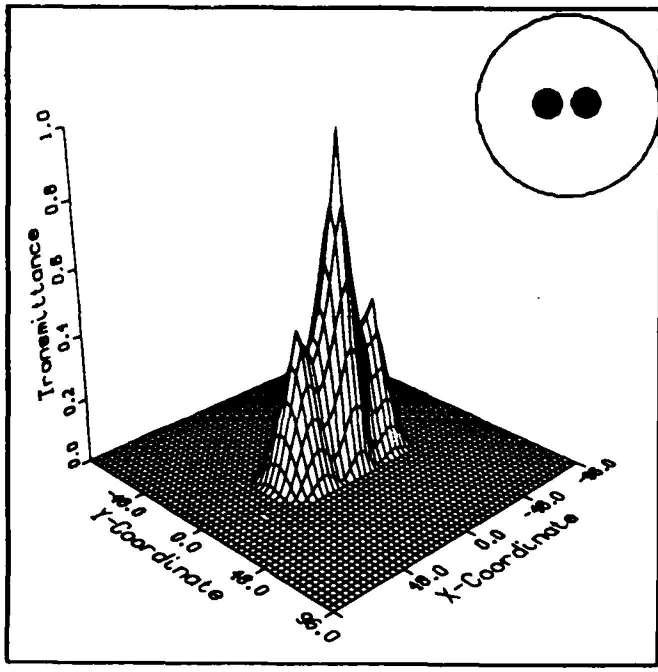

Fig. C-3. Aperture 3 OTF.

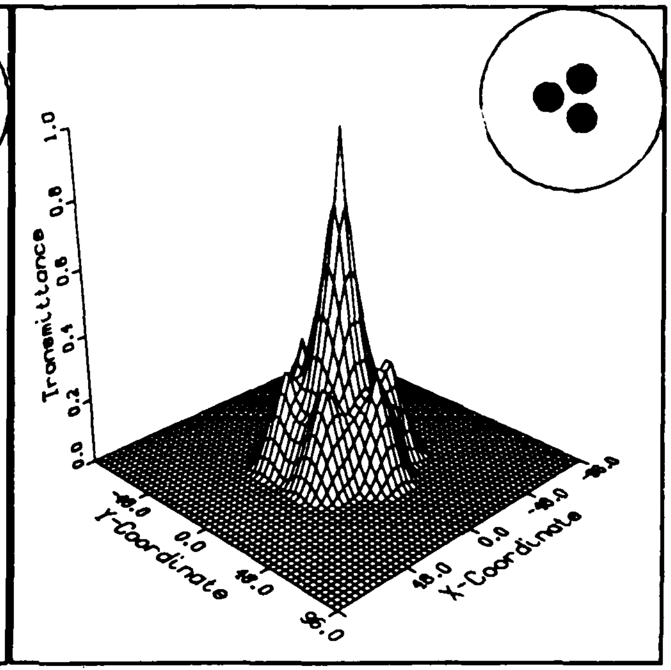

Fig. C-4. Aperture 4 OTF.

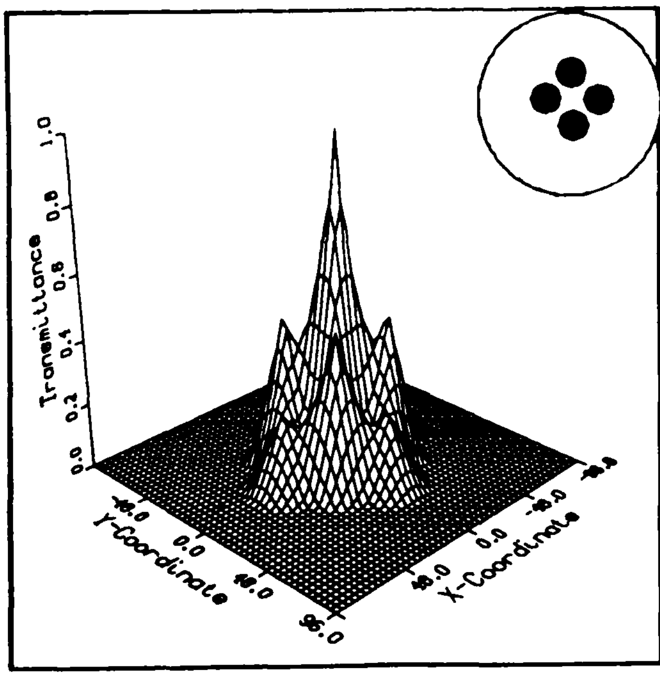

Fig. C-5. Aperture 5 OTF.

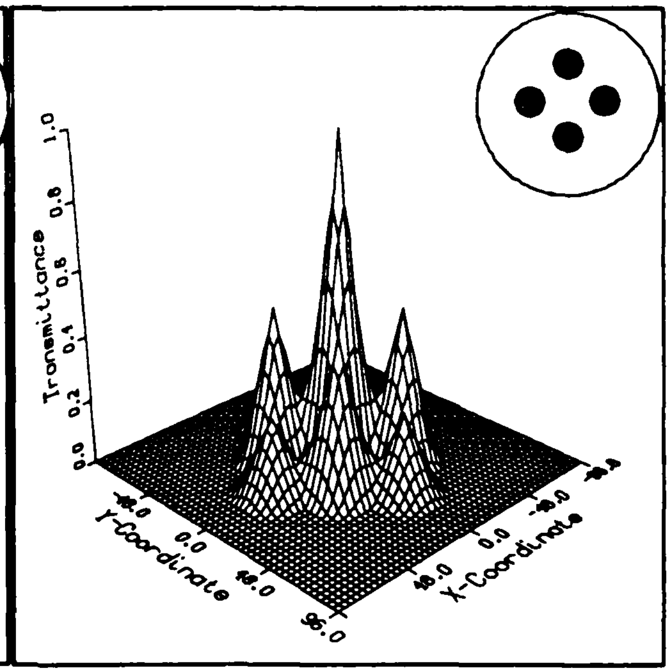

Fig. C-6. Aperture 6 OTF.

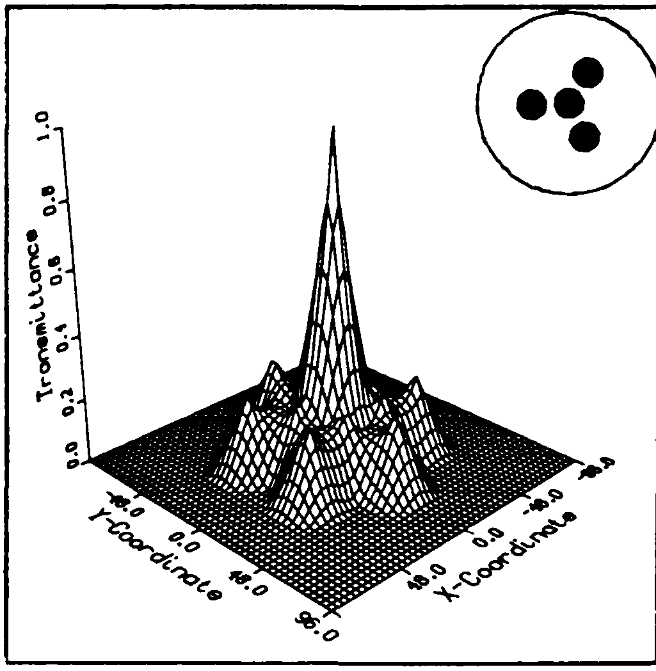

Fig. C-7. Aperture 7 OTF.

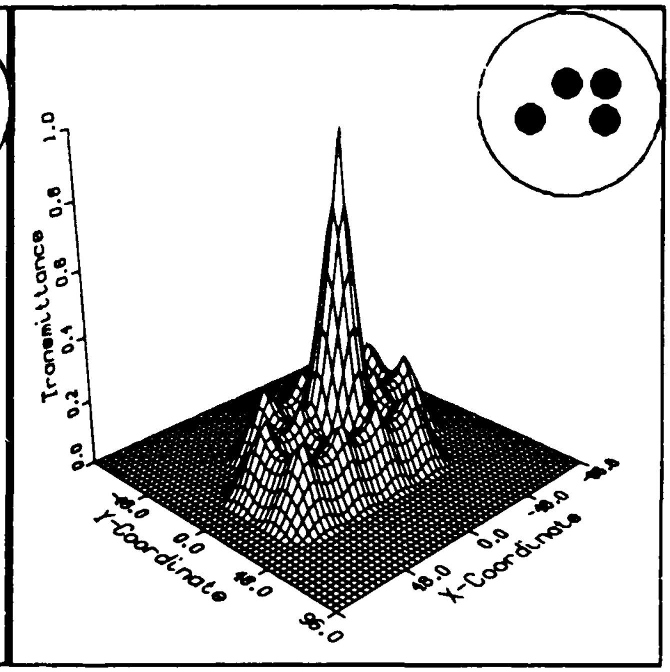

Fig. C-8. Aperture 8 OTF.

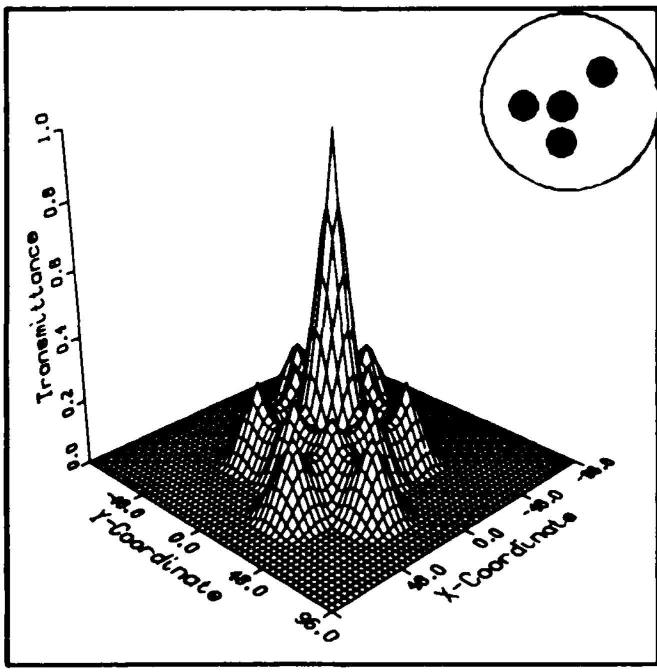

Fig. C-9. Aperture 9 OTF.

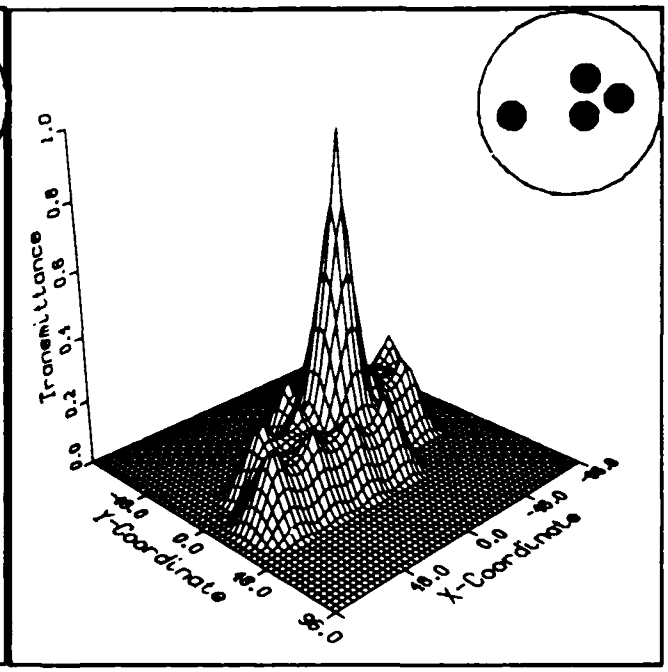

Fig. C-10. Aperture 10 OTF.

APPENDIX D - Three Dimensional Computer Predictions of Images of Edges for each Aperture

The following three-dimensional graphs are computer representations of the image of an edge as seen through each aperture. Each graph represents the intensity of the irradiance of light in the image plane. The "xy" coordinate system is representative of that same image plane, and the "z" axis records the normalized intensity of the irradiance at each "xy" coordinate.

The scale of the image plane is 1 to 1 with the computer array that stored the pattern: the base area is 48 by 48, corresponding to the central 48 by 48 area of the original target array in the program (256 by 256).

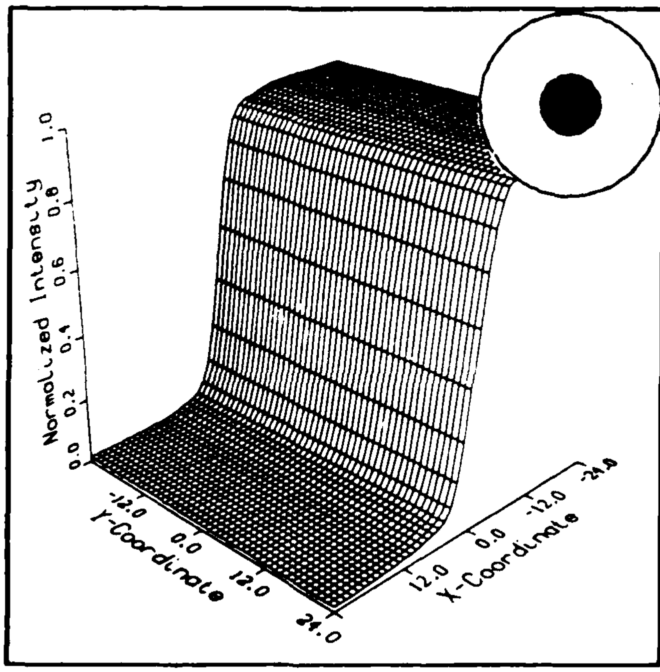

Fig. D-1. Aperture 1 Edge.

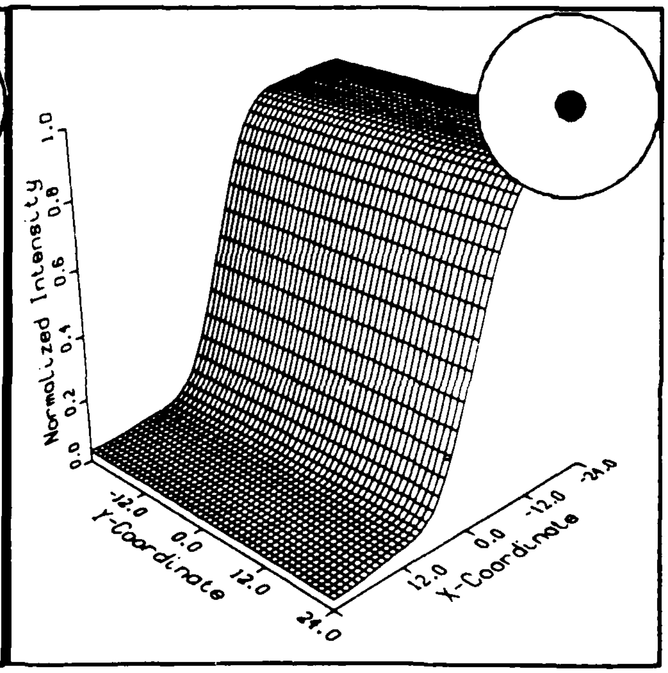

Fig. D-2. Aperture 2 Edge.

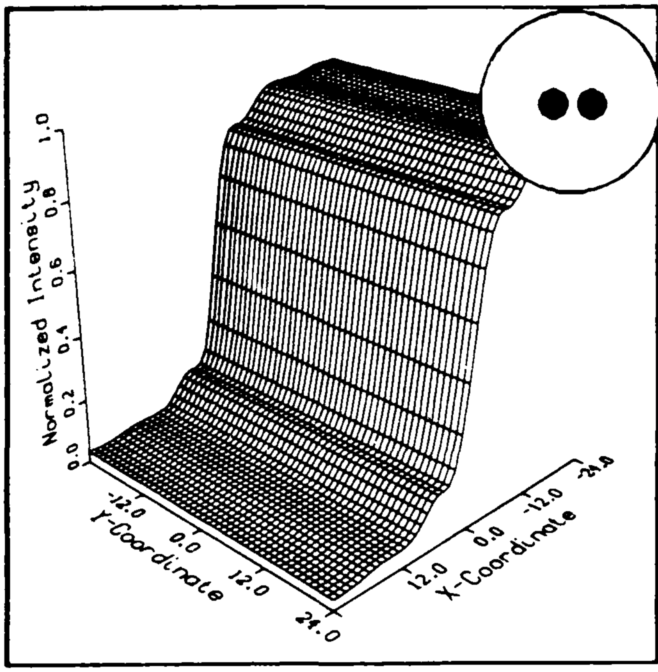

Fig. D-3. Aperture 3 Edge.

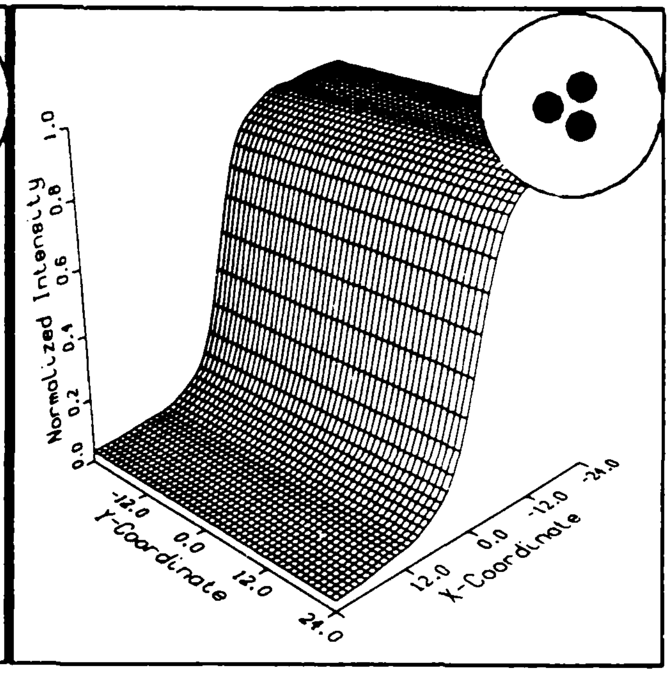

Fig. D-4. Aperture 4 Edge.

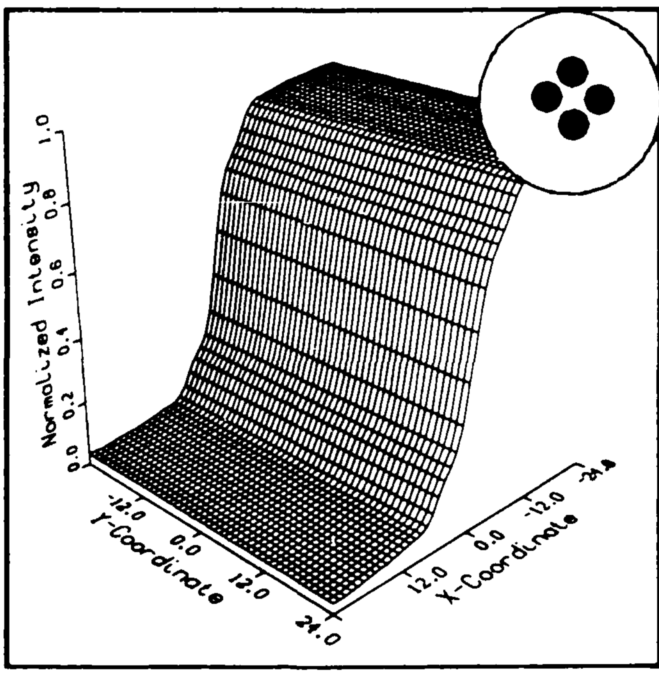

Fig. D-5. Aperture 5 Edge.

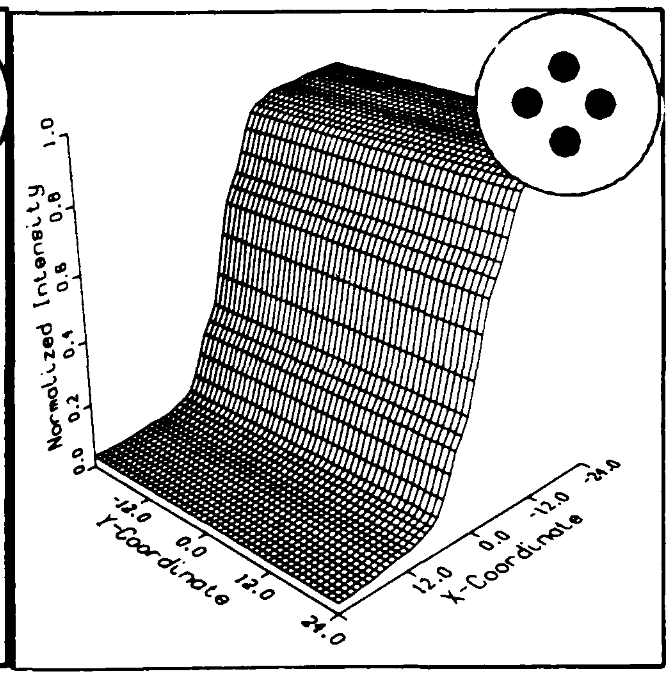

Fig. D-6. Aperture 6 Edge.

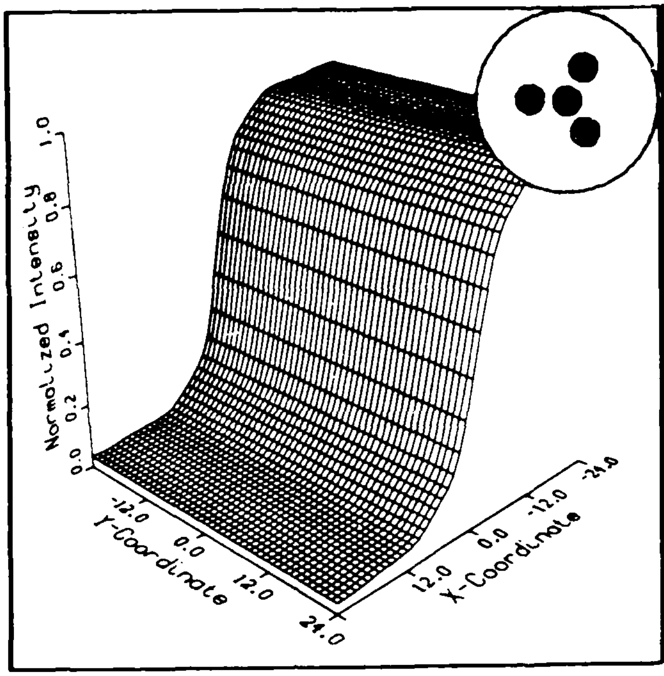

Fig. D-7. Aperture 7 Edge.

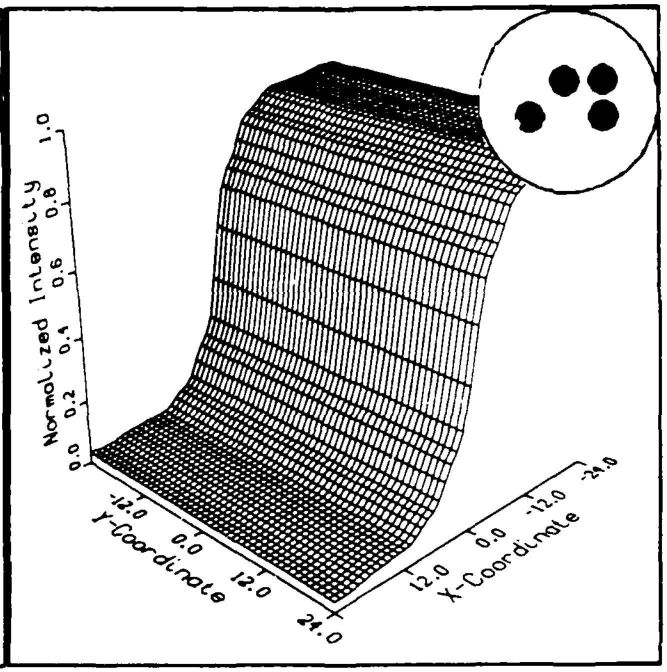

Fig. D-8. Aperture 8 Edge.

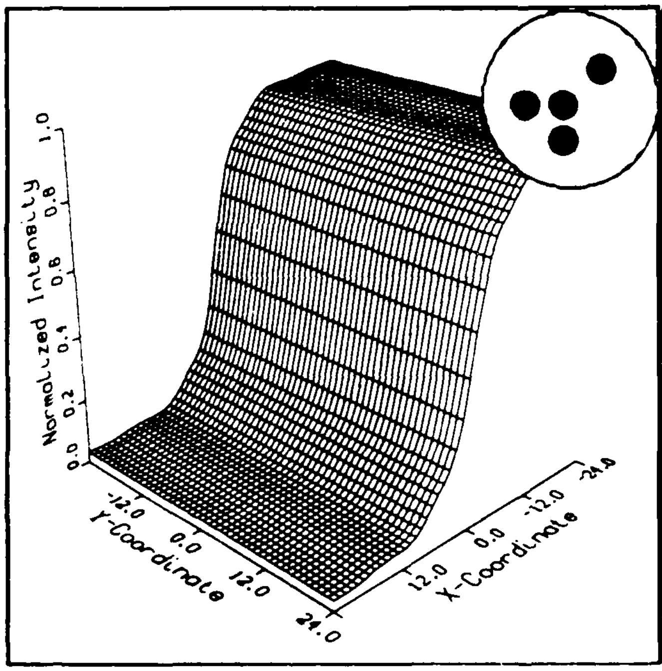

Fig. D-9. Aperture 9 Edge.

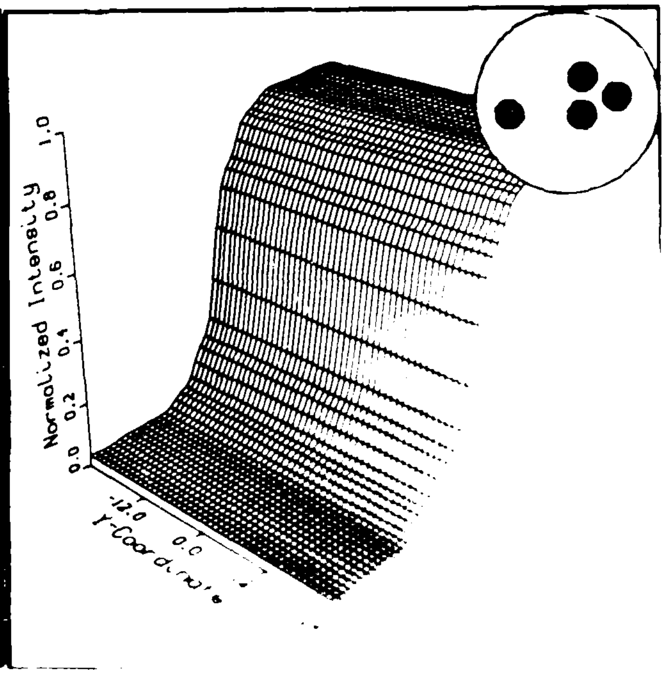

Fig

AD-A189 706 INCOHERENT MULTIPLE APERTURE OPTICAL IMAGING SYSTEMS: ANALYSIS AND DESIGN(U) AIR FORCE INST OF TECH WRIGHT-PATTERSON AFB OH SCHOOL OF ENGI.. R T REILANDER 2/2

UNCLASSIFIED DEC 87 AFIT/GSO/ENP/87D-2 F/G 17/5 NL

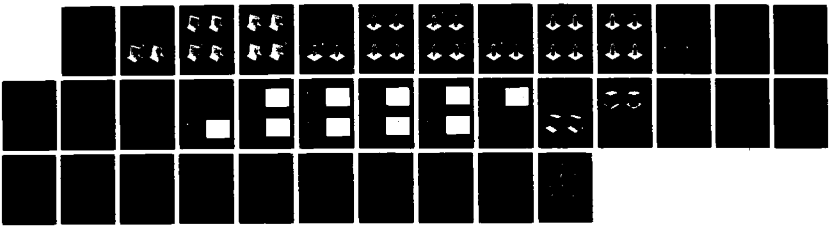

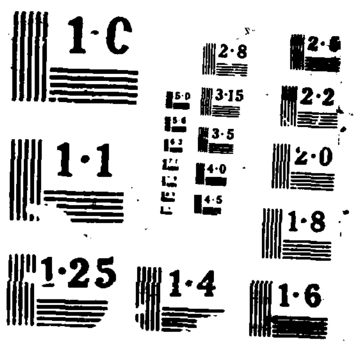
1·0
2·8
2·5
3·15
2·2
3·5
4·0
2·0
4·5
1·8
1·1
1·25
1·4
1·6

APPENDIX E - Three Dimensional Computer Predictions of Images of Slits for each Aperture

The following three-dimensional graphs are computer representations of the image of a slit as seen through each aperture. Each graph represents the intensity of the irradiance of light in the image plane. The "xy" coordinate system is representative of that same image plane, and the "z" axis records the normalized intensity of the irradiance at each "xy" coordinate.

The scale of the image plane is 1 to 1 with the computer array that stored the pattern: the base area is 48 by 48, corresponding to the central 48 by 48 area of the original target array in the program (256 by 256).

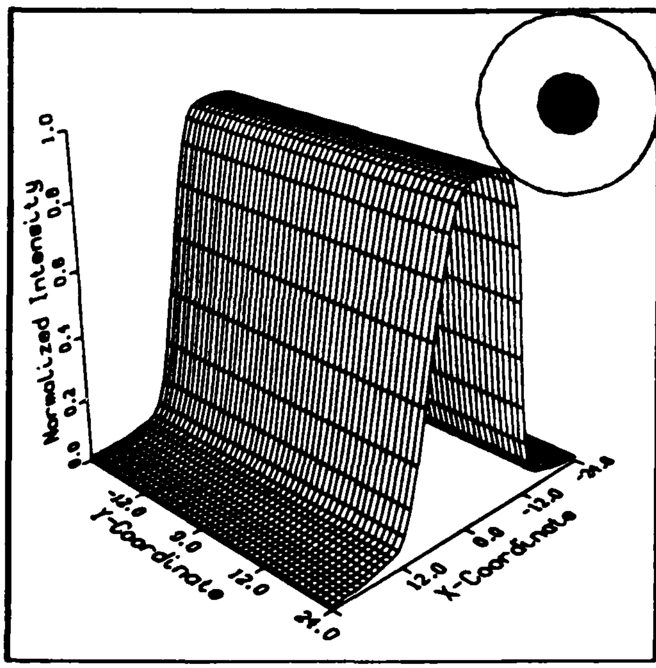

Fig. E-1. Aperture 1 Slit.

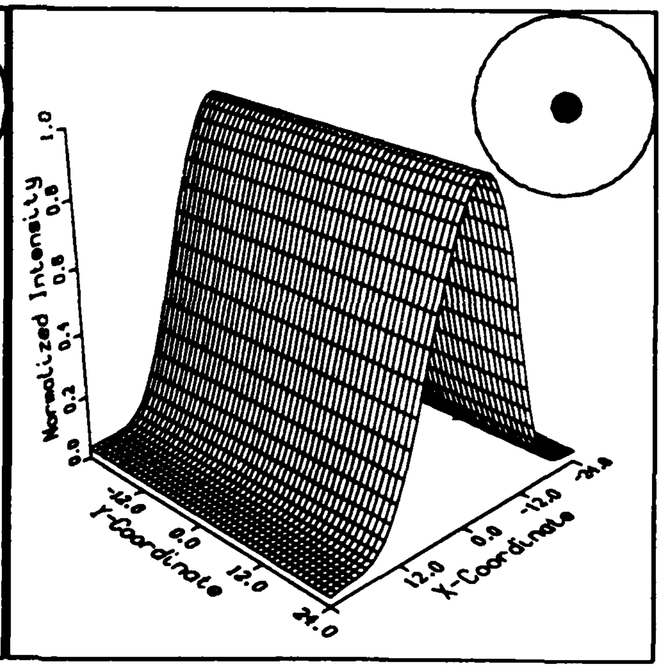

Fig. E-2. Aperture 2 Slit.

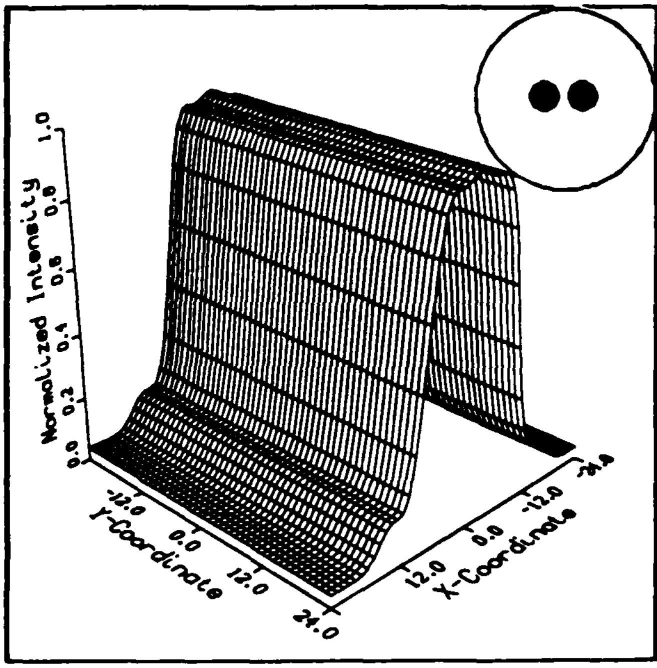

Fig. E-3. Aperture 3 Slit.

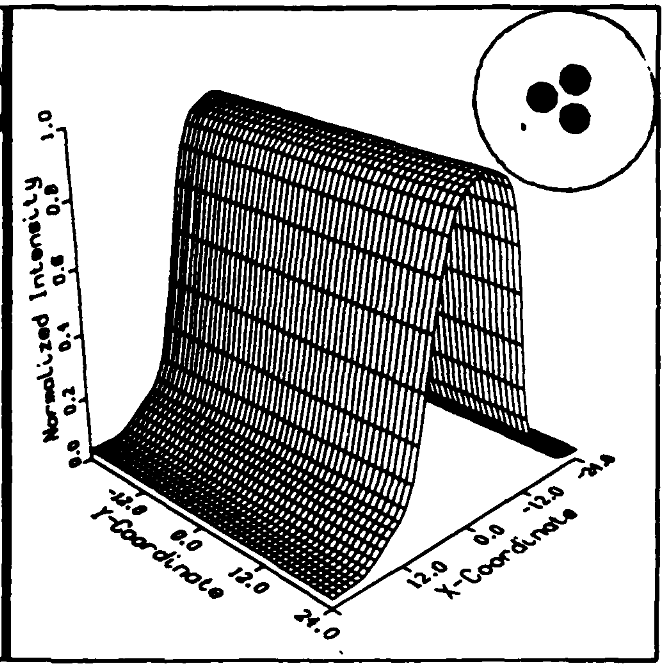

Fig. E-4. Aperture 4 Slit.

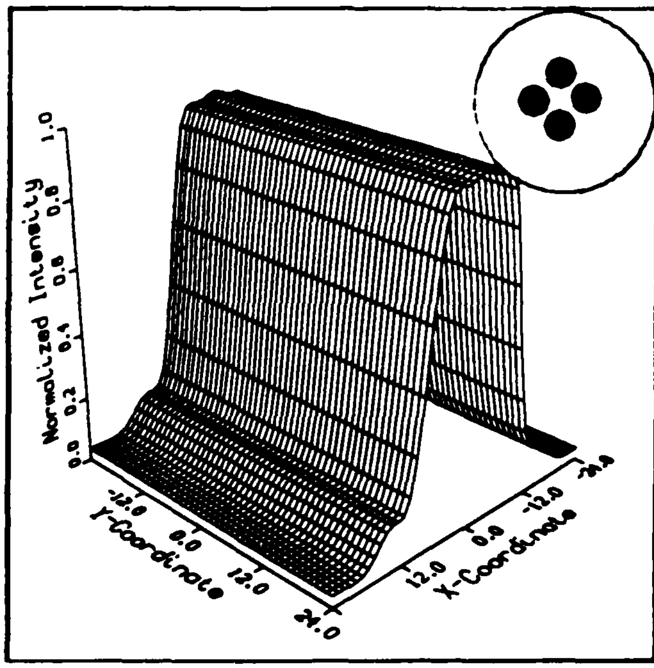

Fig. E-5. Aperture 5 Slit.

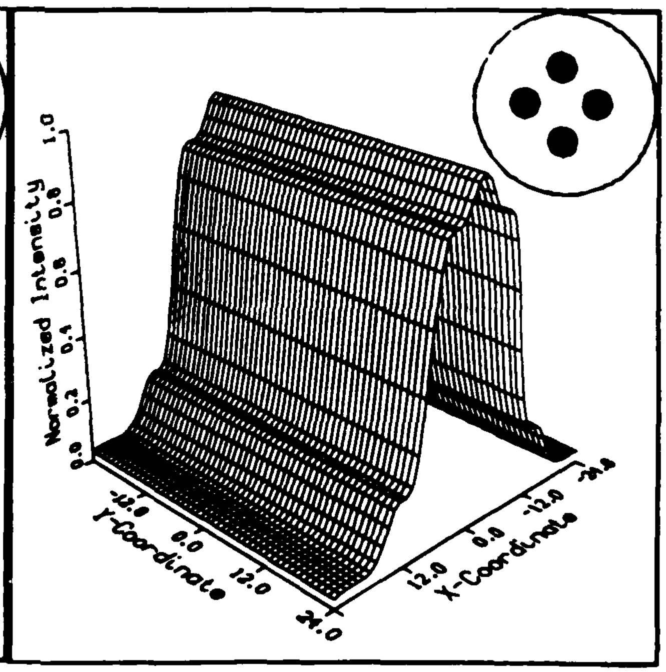

Fig. E-6. Aperture 6 Slit.

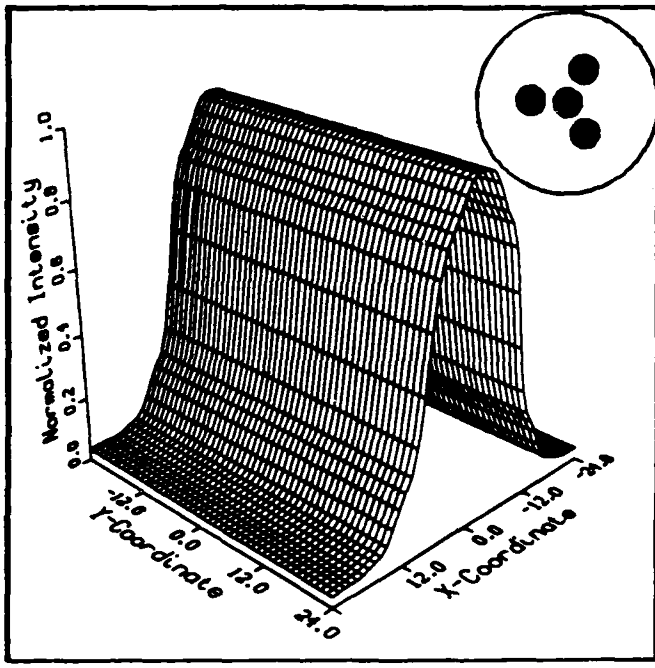

Fig. E-7. Aperture 7 Slit.

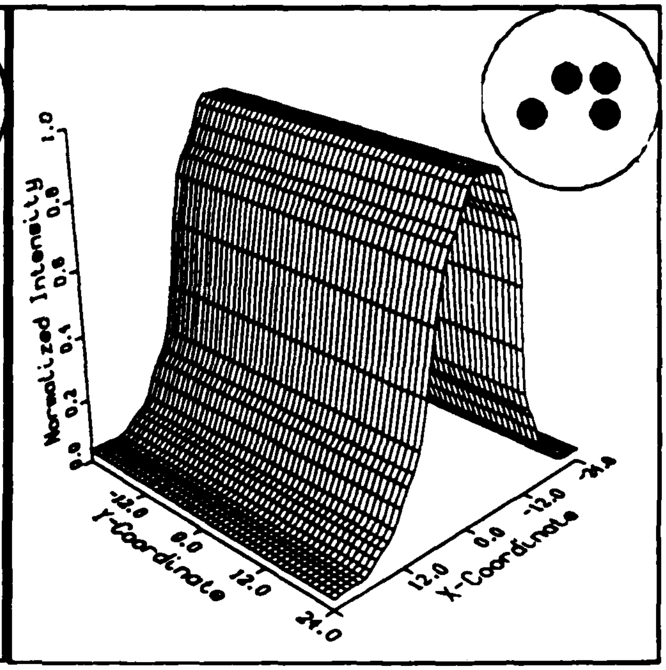

Fig. E-8. Aperture 8 Slit.

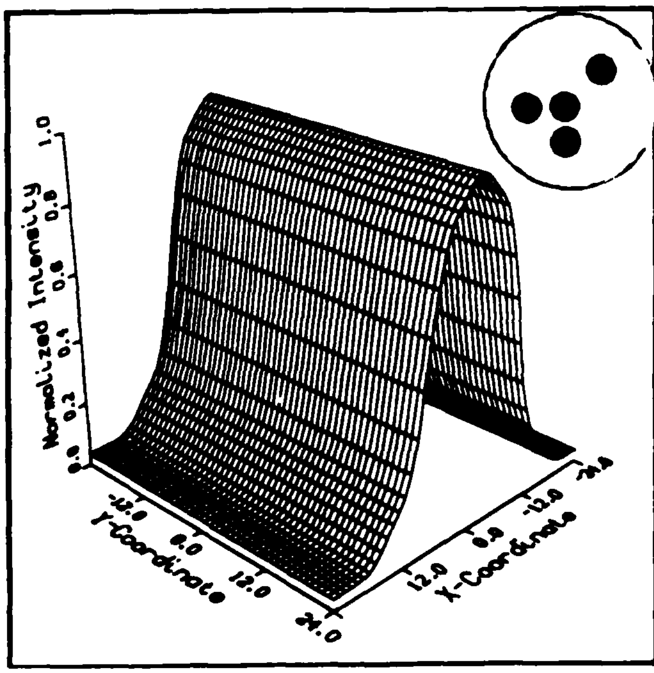

Fig. E-9. Aperture 9 Slit.

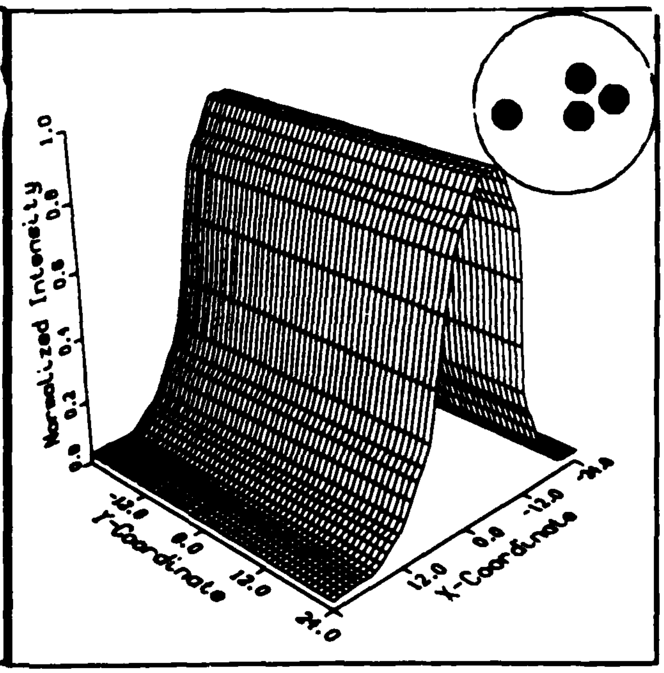

Fig. E-10. Aperture 10 Slit.

APPENDIX F - Three Dimensional Computer Predictions of Images of Rectangles for each Aperture

The following three-dimensional graphs are computer representations of the image of a rectangle as seen through each aperture. Each graph represents the intensity of the irradiance of light in the image plane. The "xy" coordinate system is representative of that same image plane, and the "z" axis records the normalized intensity of the irradiance at each "xy" coordinate.

The scale of the image plane is 1 to 1 with the computer array that stored the pattern: the base area is 96 by 96, corresponding to the central 96 by 96 area of the original target array in the program (256 by 256).

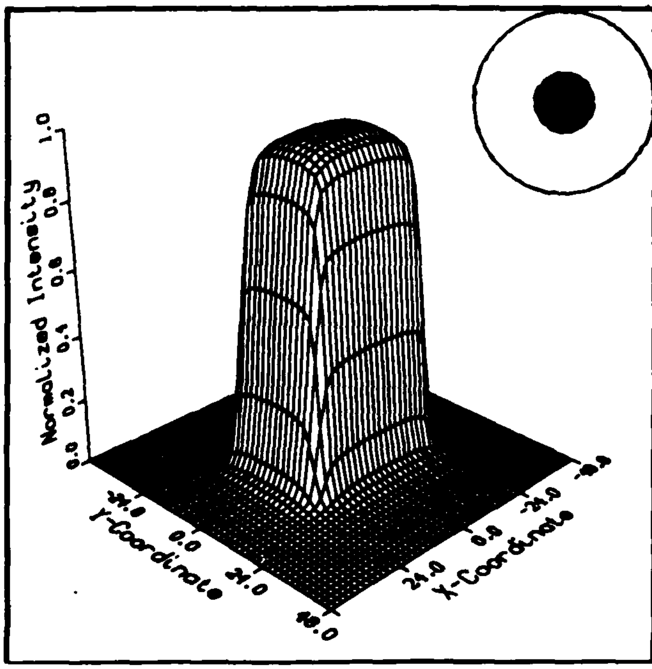

Fig. F-1. Aperture 1 Rect.

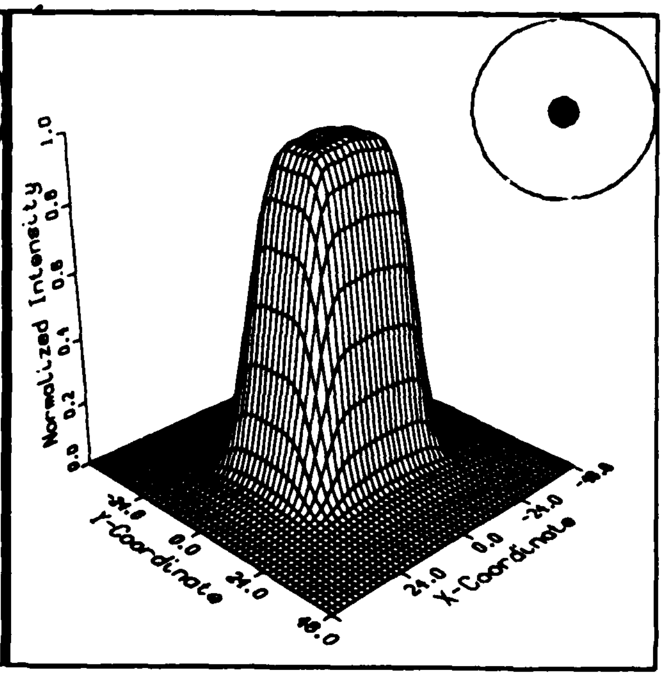

Fig. F-2. Aperture 2 Rect.

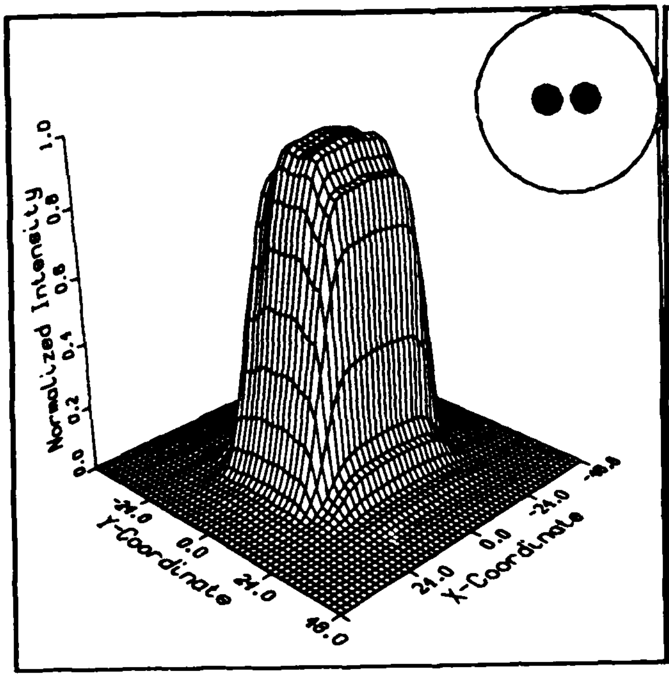

Fig. F-3. Aperture 3 Rect.

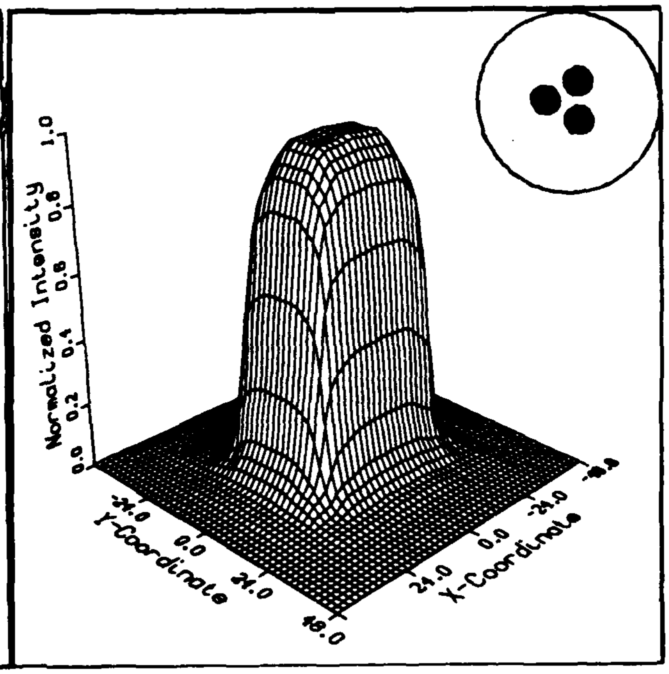

Fig. F-4. Aperture 4 Rect.

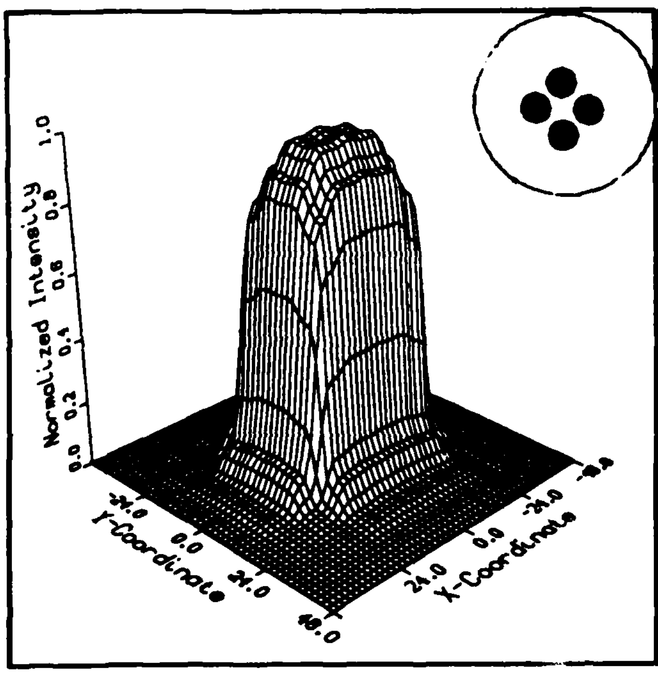

Fig. F-5. Aperture 5 Rect.

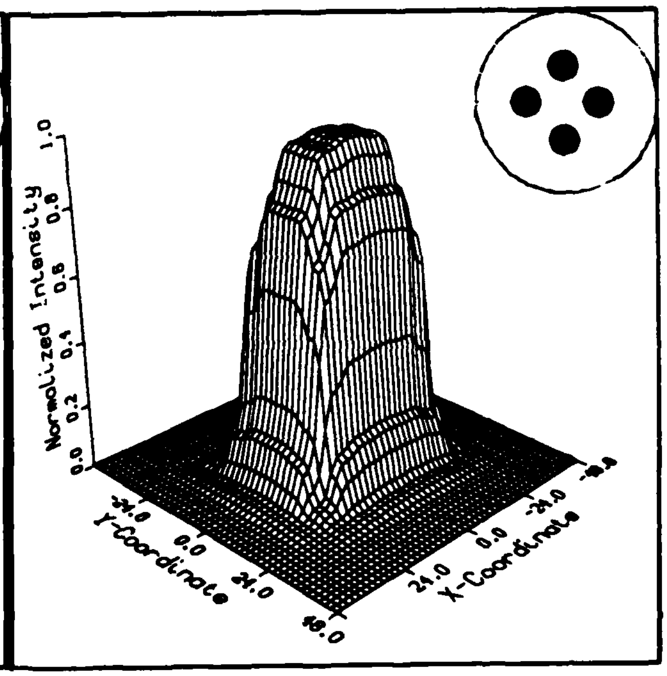

Fig. F-6. Aperture 6 Rect.

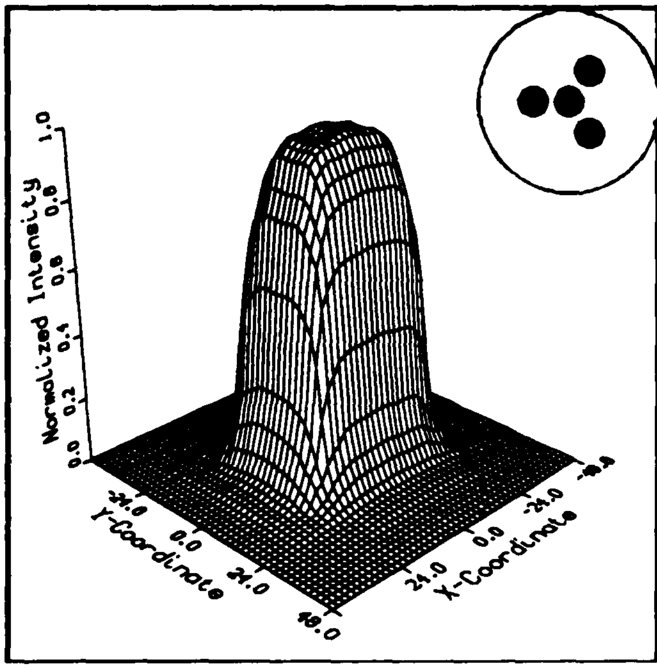

Fig. F-7. Aperture 7 Rect.

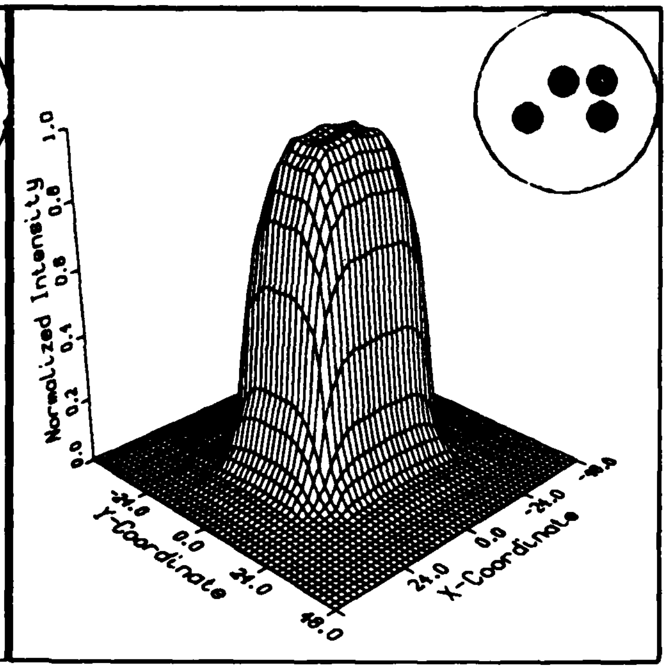

Fig. F-8. Aperture 8 Rect.

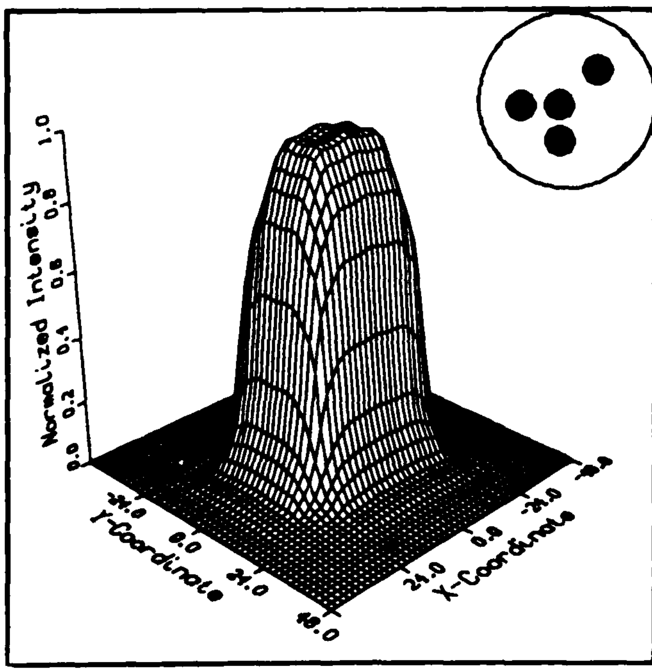

Fig. F-9. Aperture 9 Rect.

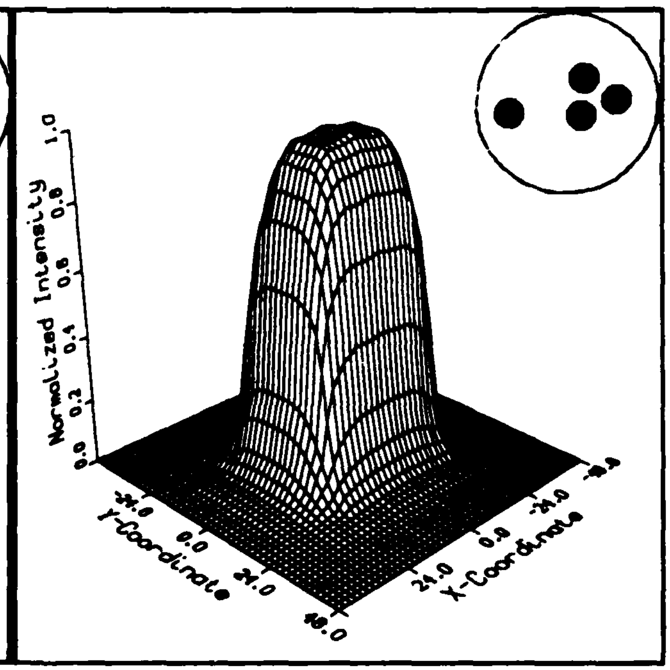

Fig. F-10. Aperture 10 Rect.

APPENDIX G - Three Dimensional Computer Predictions of Images of Circles for each Aperture

The following three-dimensional graphs are computer representations of the image of a circle as seen through each aperture. Each graph represents the intensity of the irradiance of light in the image plane. The "xy" coordinate system is representative of that same image plane, and the "z" axis records the normalized intensity of the irradiance at each "xy" coordinate.

The scale of the image plane is 1 to 1 with the computer array that stored the pattern: the base area is 96 by 96, corresponding to the central 96 by 96 area of the original target array in the program (256 by 256).

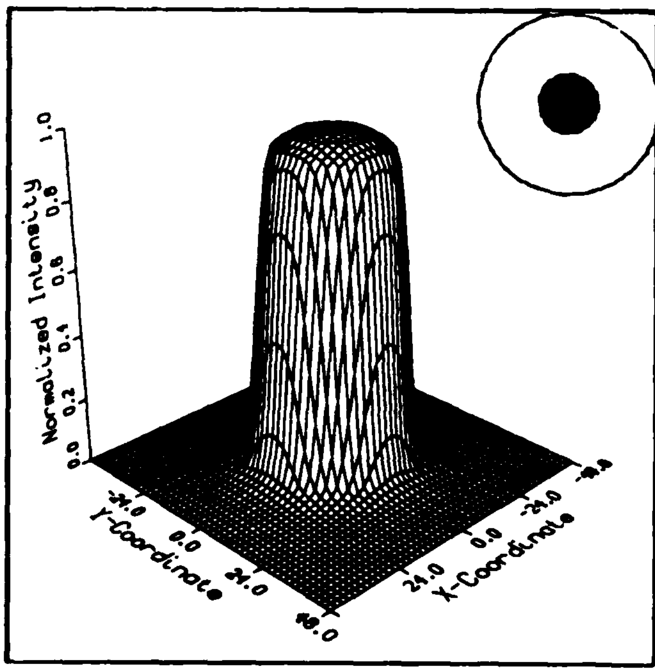

Fig. G-1. Aperture 1 Circ.

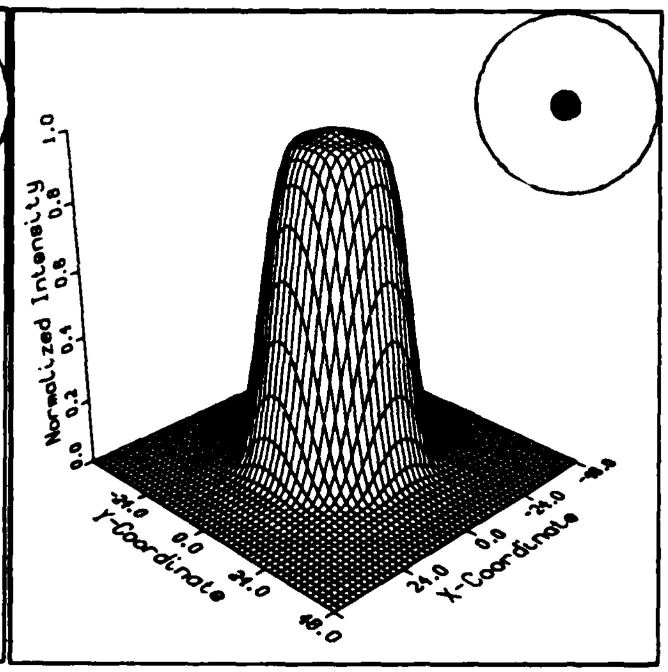

Fig. G-2. Aperture 2 Circ.

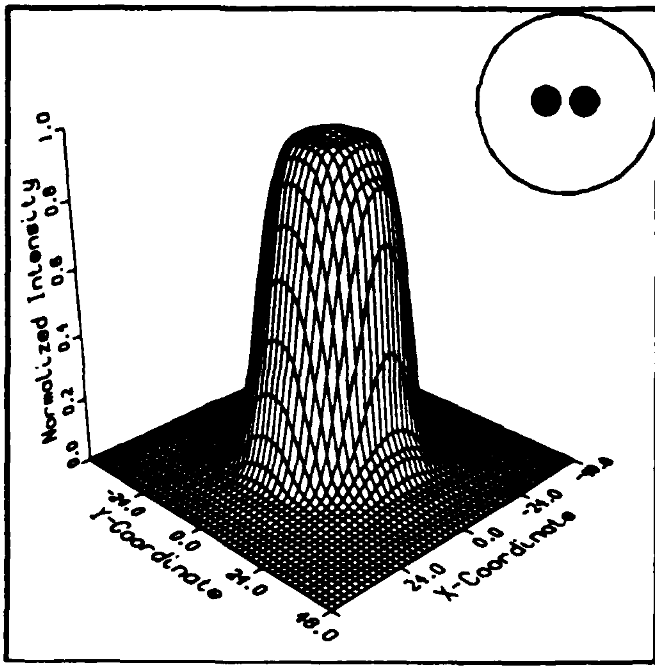

Fig. G-3. Aperture 3 Circ.

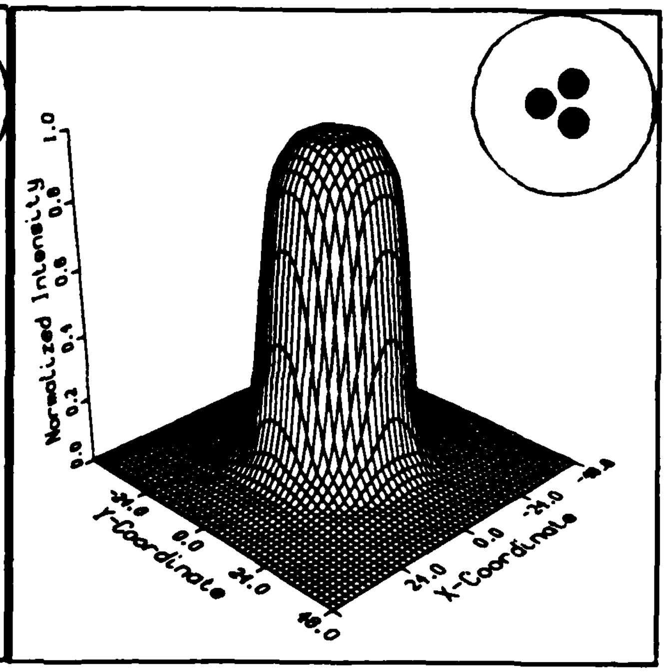

Fig. G-4. Aperture 4 Circ.

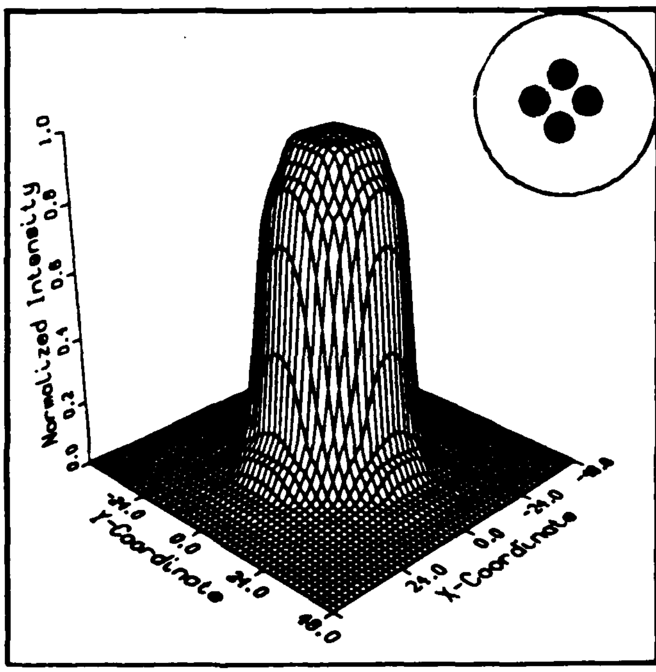

Fig. G-5. Aperture 5 Circ.

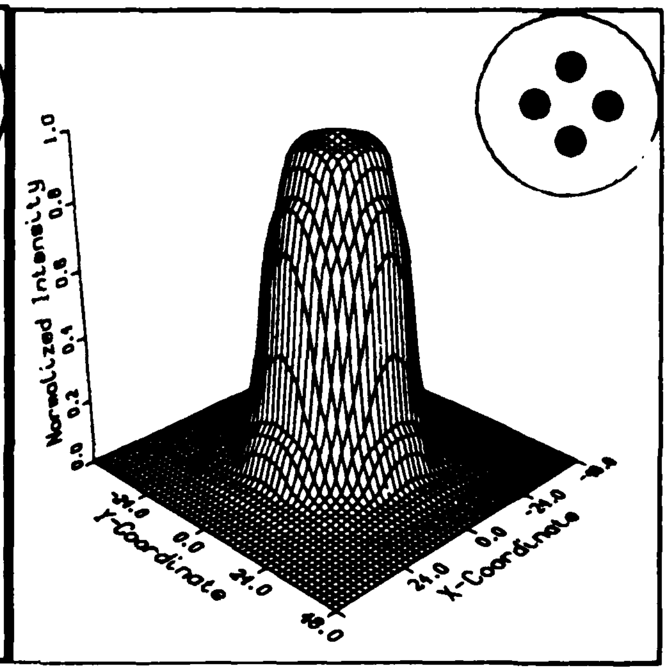

Fig. G-6. Aperture 6 Circ.

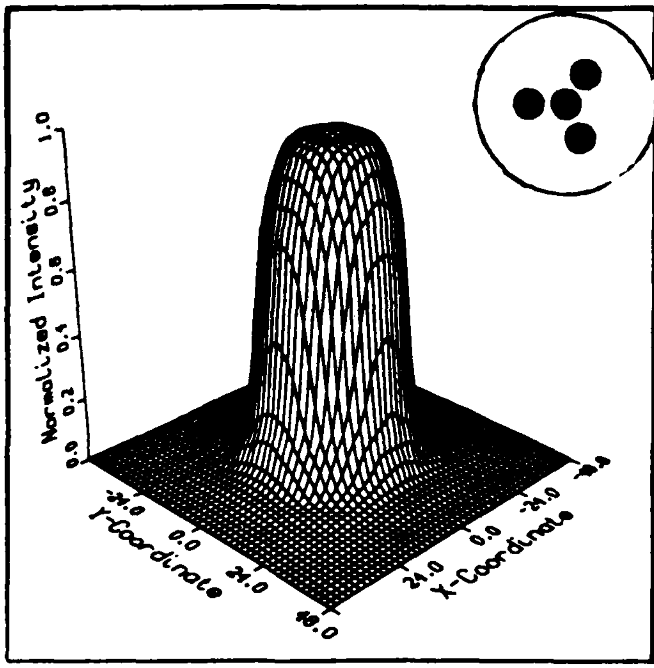

Fig. G-7. Aperture 7 Circ.

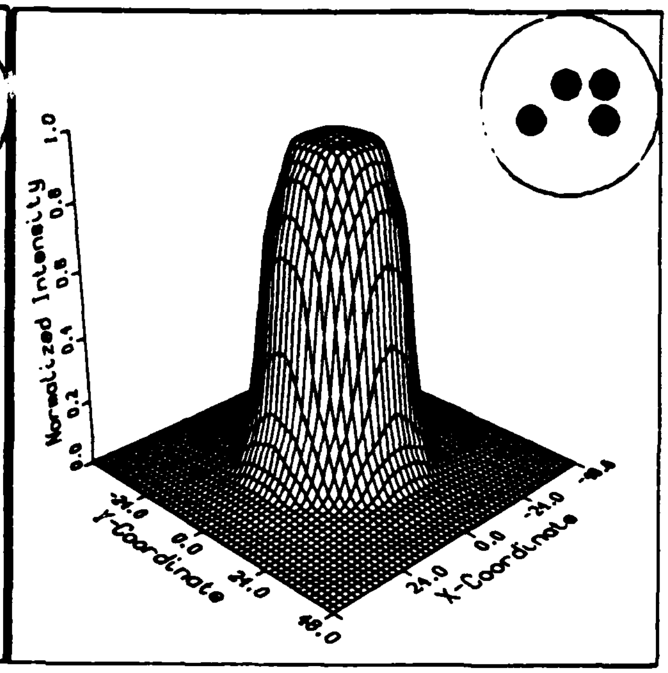

Fig. G-8. Aperture 8 Circ.

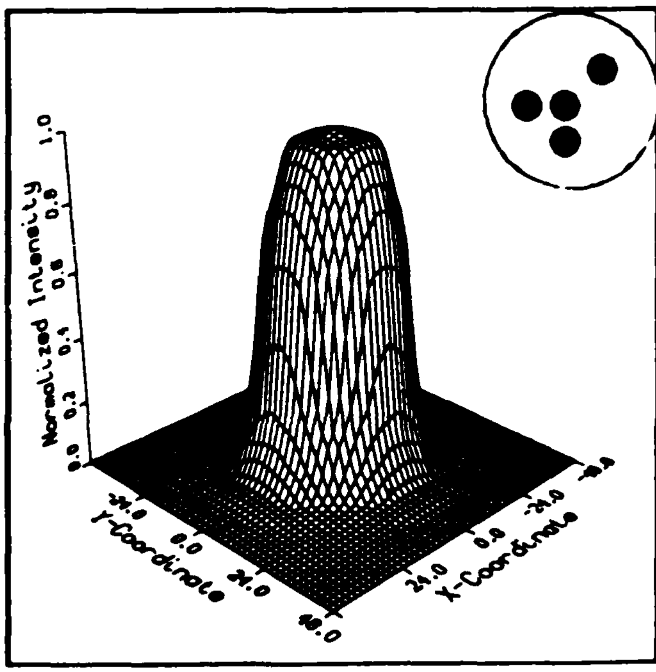

Fig. G-9. Aperture 9 Circ.

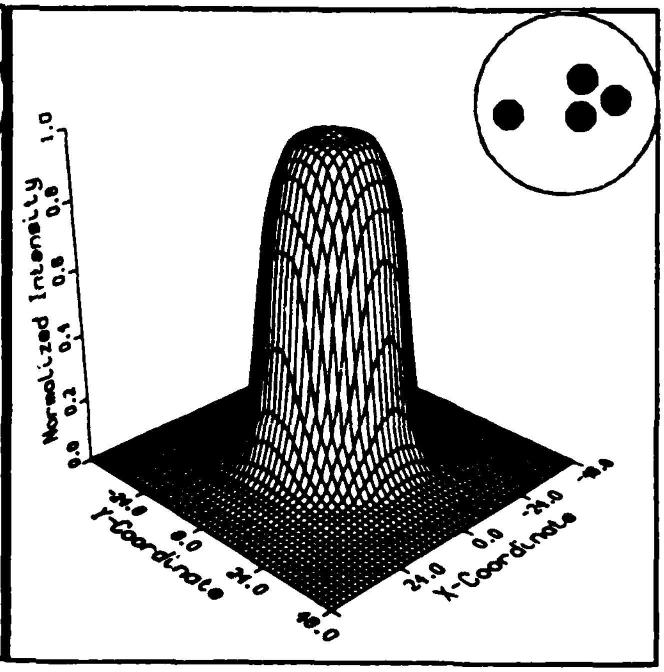

Fig. G-10. Aperture 10 Circ.

APPENDIX H - Two Dimensional Computer Predictions of Images of Edges for each Aperture Based Upon Aperture Orientation

The following two-dimensional graphs are computer representations of the image of an edge as seen through each aperture. Each graph represents the intensity of the irradiance of light in the image plane. The "x" coordinate marks position relative to the geometric location of the edge. The "z" axis records the normalized intensity of the irradiance at each "x" coordinate. There are two graphs for each aperture, showing the two extremes of resolution based on aperture orientation with the object. The apertures are oriented as shown, while the edge they image is oriented parallel to the right edge of this page.

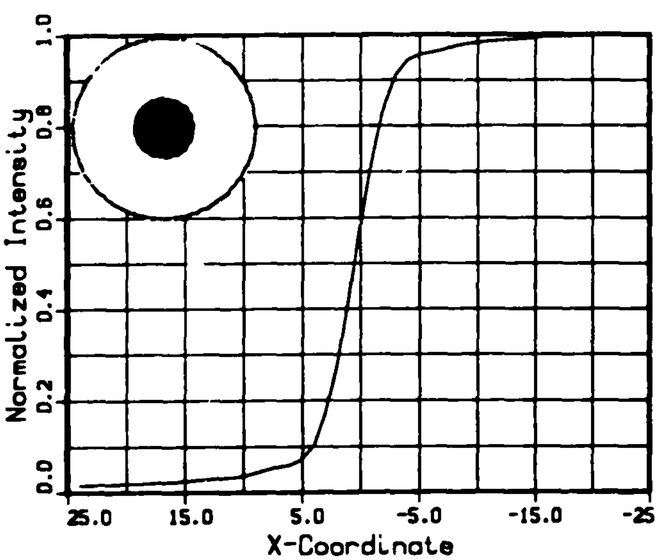

Fig. H-1. Aper.1 best Edge.

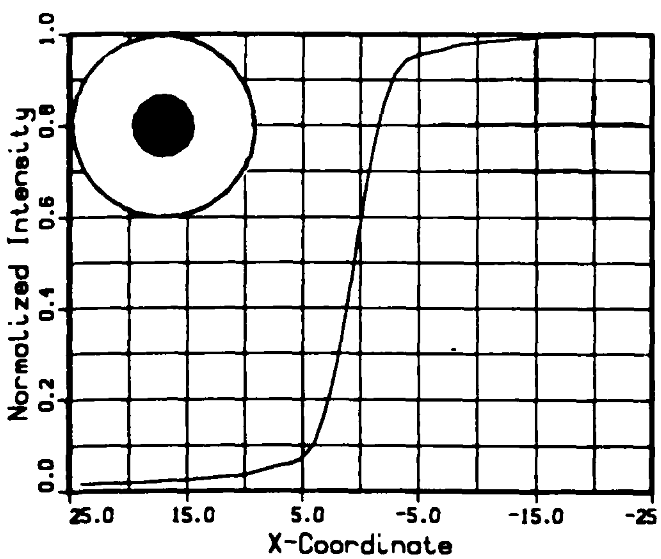

Fig. H-2. Aper.1 worst Edge.

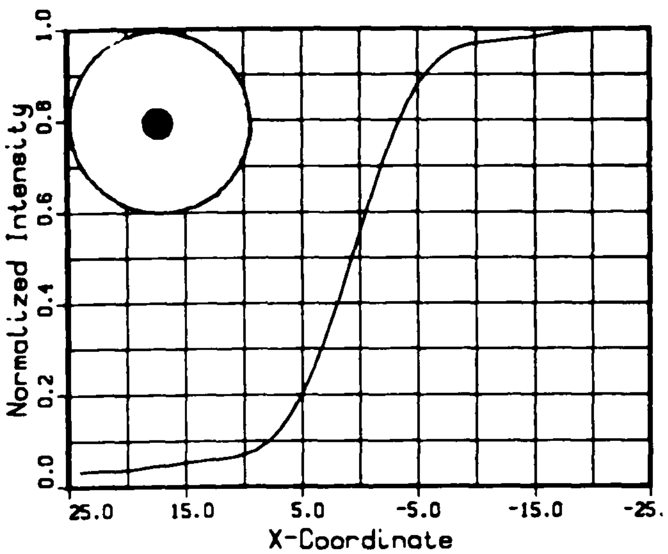

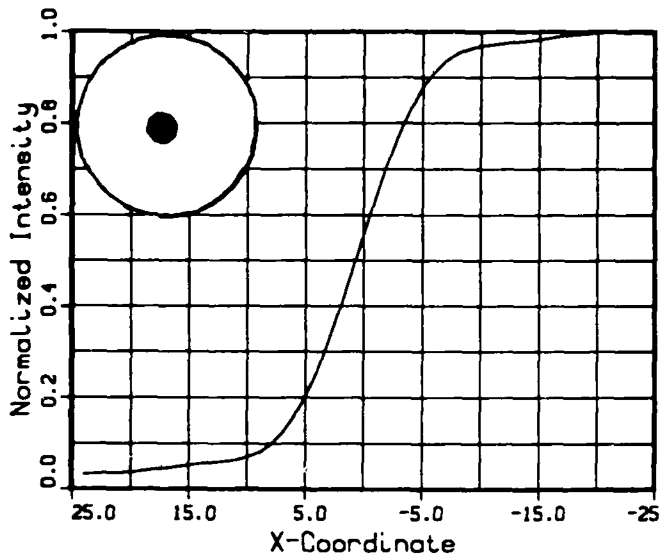

Fig. H-3. Aper.2 best Edge.

Fig. H-4. Aper.2 worst Edge.

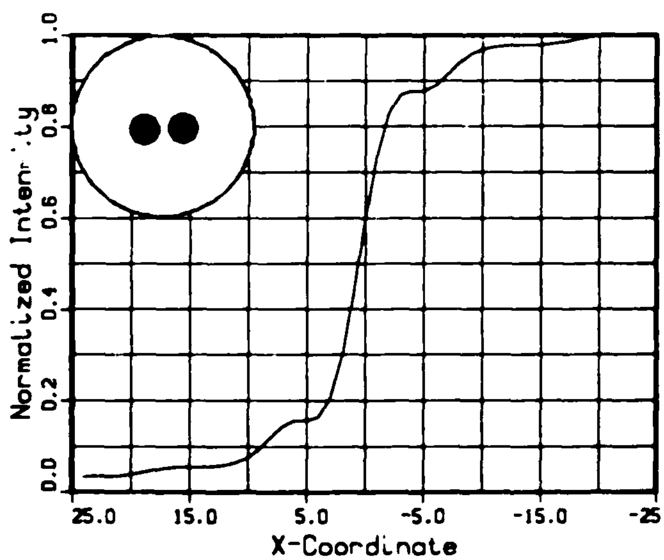

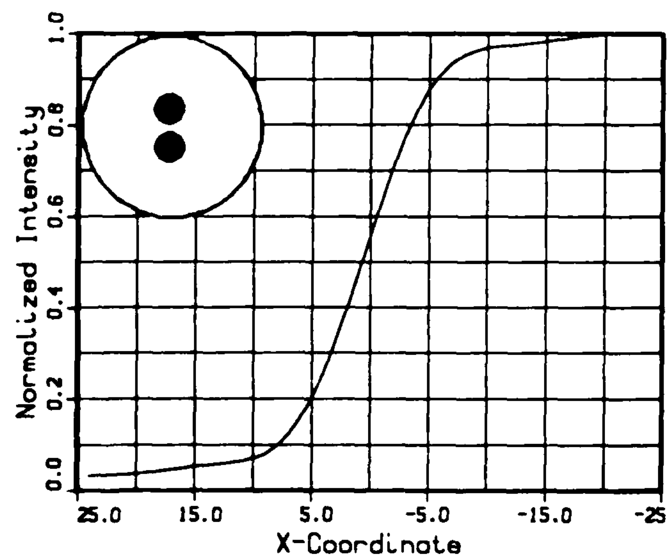

Fig. H-5. Aper.3 best Edge.

Fig. H-6. Aper.3 worst Edge.

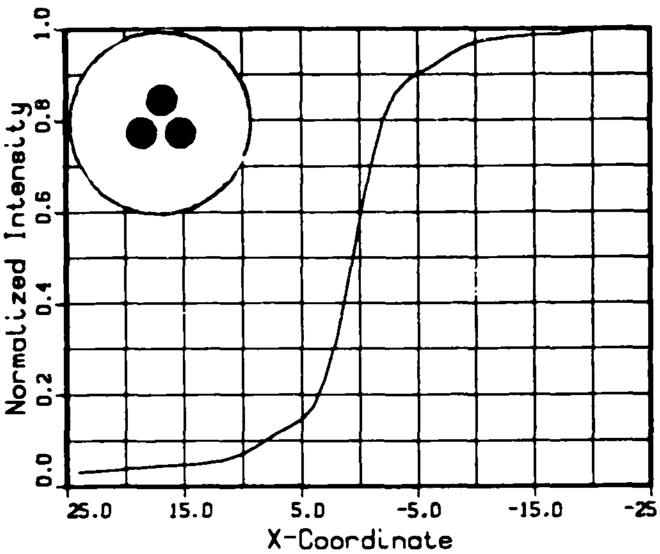

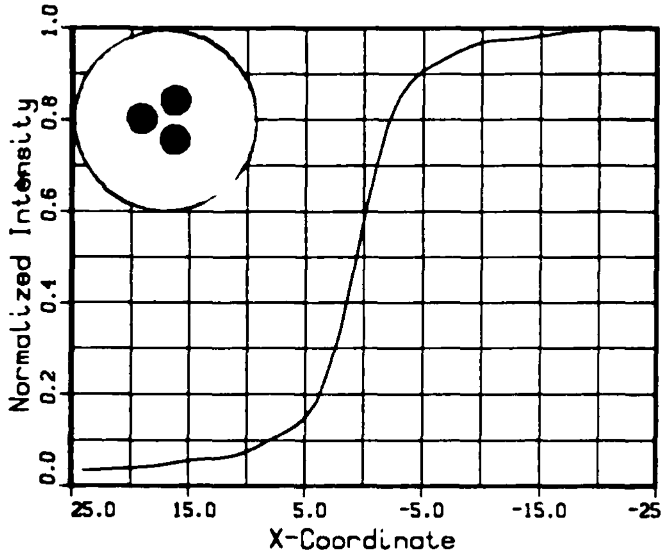

Fig. H-7. Aper.4 best Edge.

Fig. H-8. Aper.4 worst Edge.

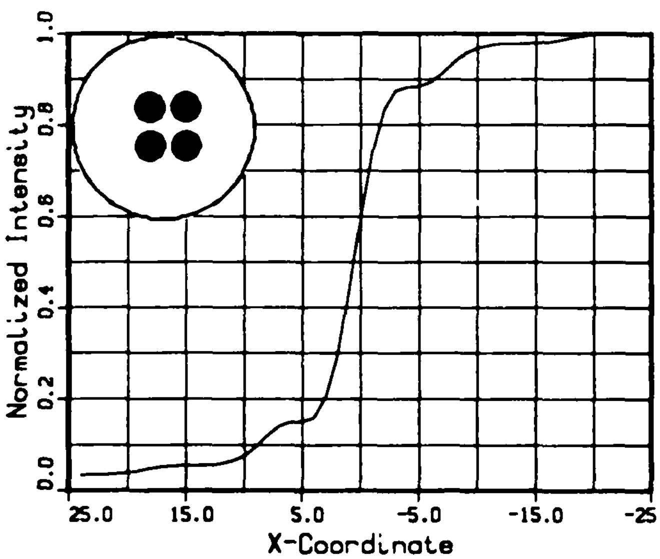

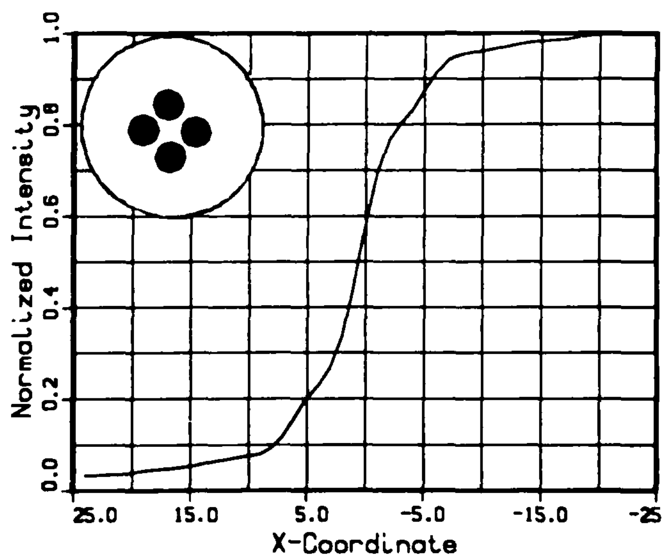

Fig. H-9. Aper.5 best Edge.

Fig. H-10. Aper.5 worst Edge.

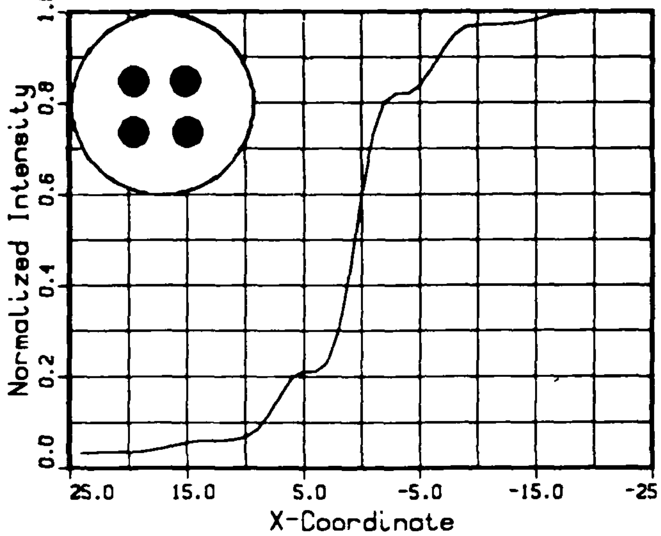

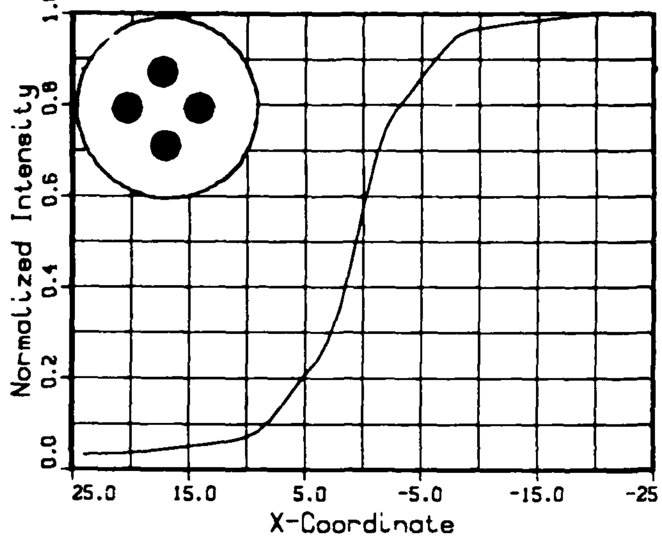

Fig. H-11. Aper.6 best Edge. Fig. H-12. Aper.6 worst Edge.

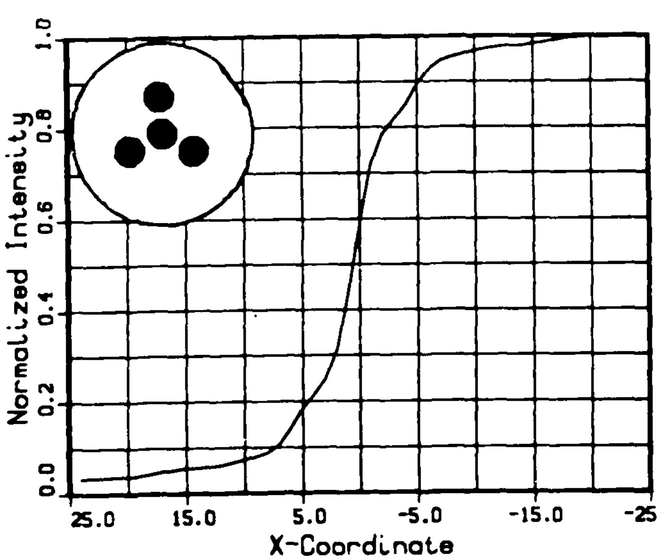

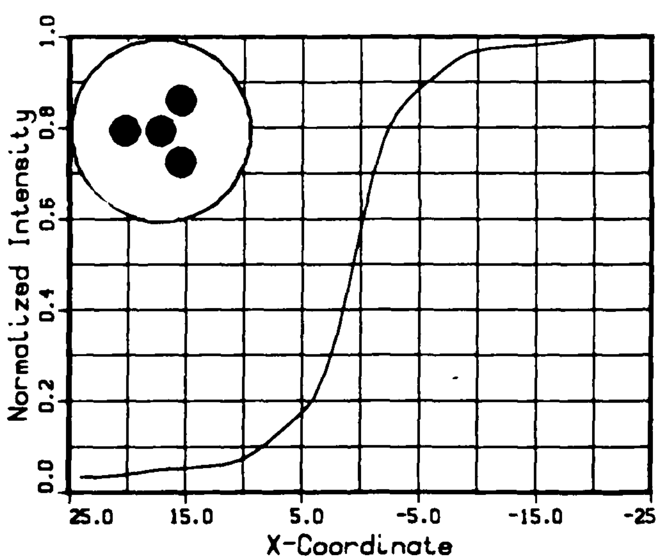

Fig. H-13. Aper.7 best Edge. Fig. H-14. Aper.7 worst Edge.

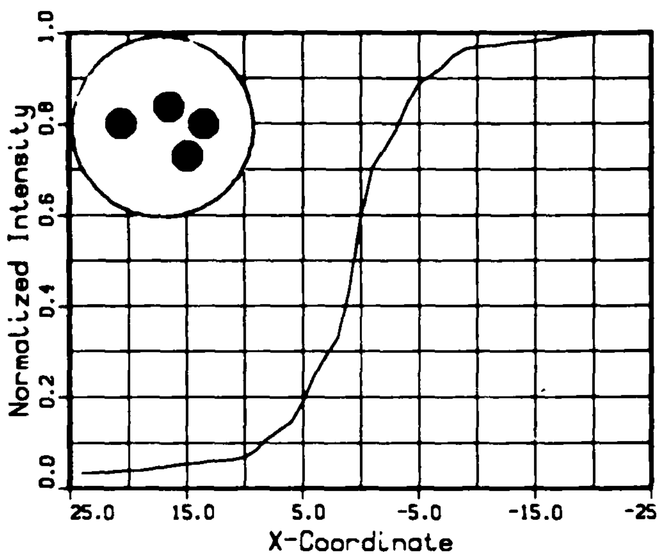

Fig. H-15. Aper.8 best Edge.

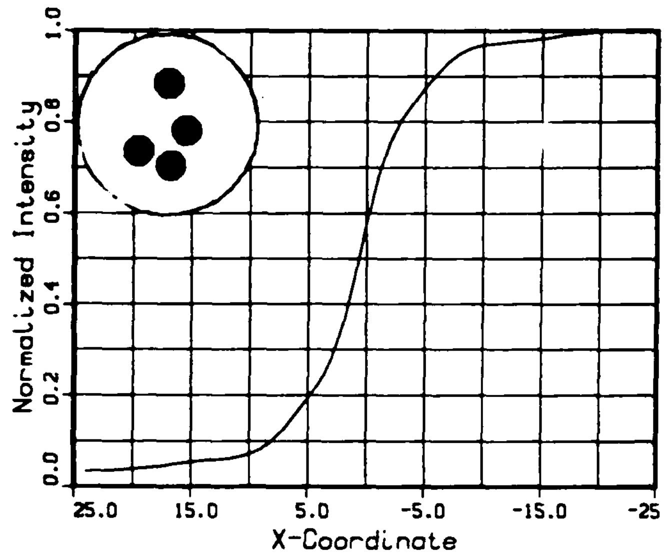

Fig. H-16. Aper.8 worst Edge.

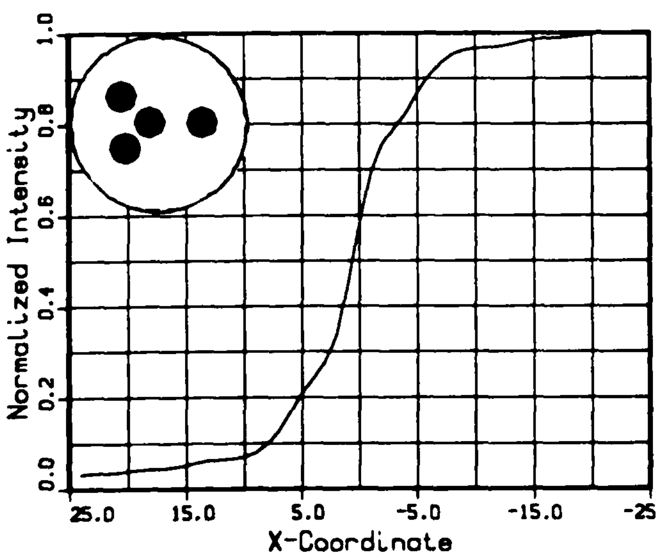

Fig. H-17. Aper.9 best Edge.

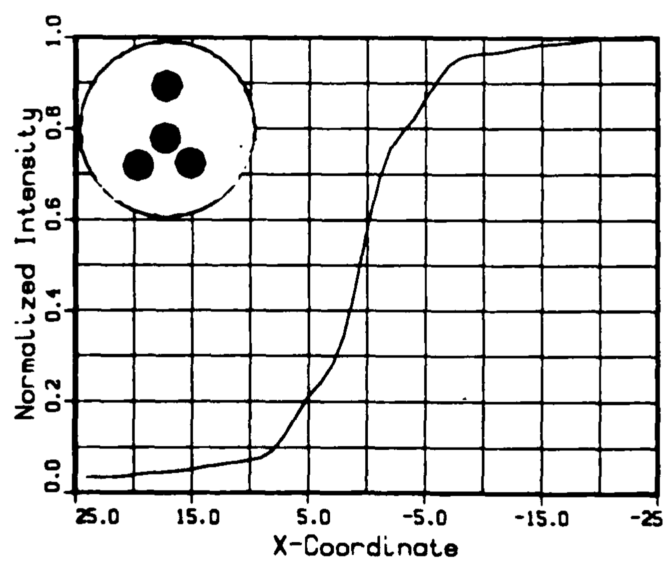

Fig. H-18. Aper.9 worst Edge.

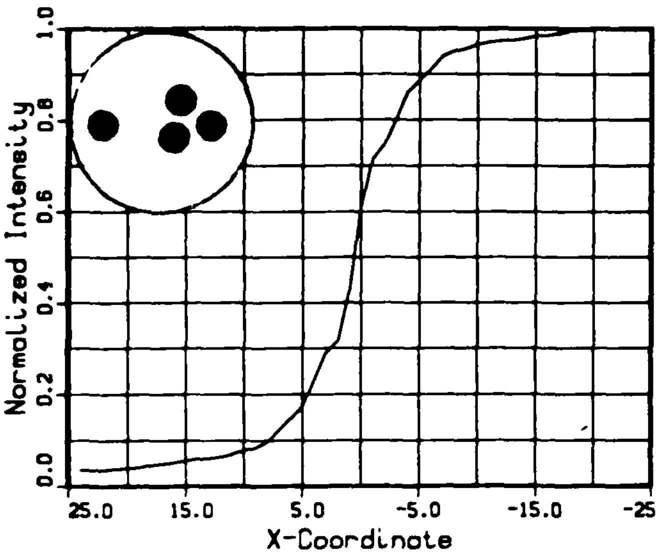

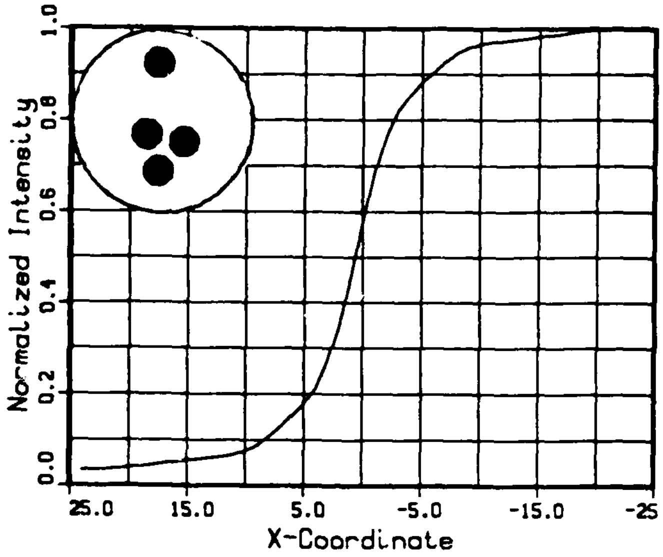

Fig. H-19. Aper.10 best Edge. **Fig. H-20. Aper.10 worst Edge.**

APPENDIX J - Two Dimensional Computer Prediction of Image of Edge Compared to Experimental Result for each Aperture

The following two-dimensional pairs of graphs are the image of an edge, computer predicted and experimentally photographed, respectively, as seen through each aperture. Each graph represents the intensity of the irradiance of light in the image plane. The "x" coordinate marks position relative to the geometric location of the edge. The "z" axis records the normalized intensity of the irradiance at each "x" coordinate. Both the theoretical and experimental graphs are normalized, but the "x" coordinate values are not to scale. All computer graphs are in scale with each other, and all photos are in scale with each other, but the computer graphs and the photos are not exactly in scale with one other. Still, the curve similarities are noteworthy.

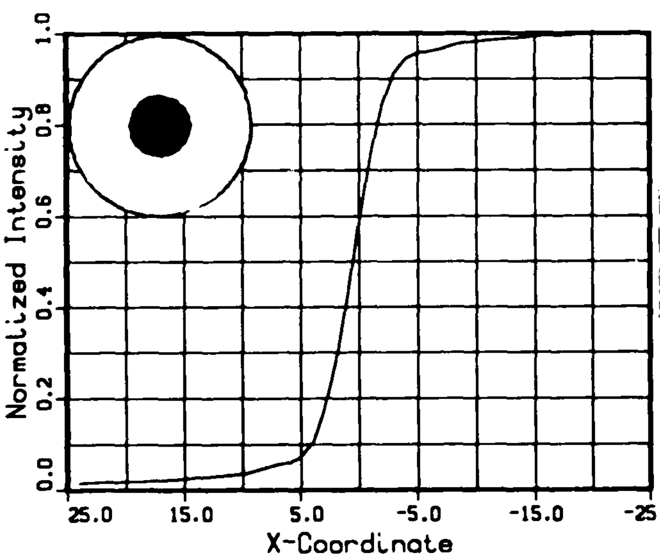

Fig. J-1. No.1 edge theory.

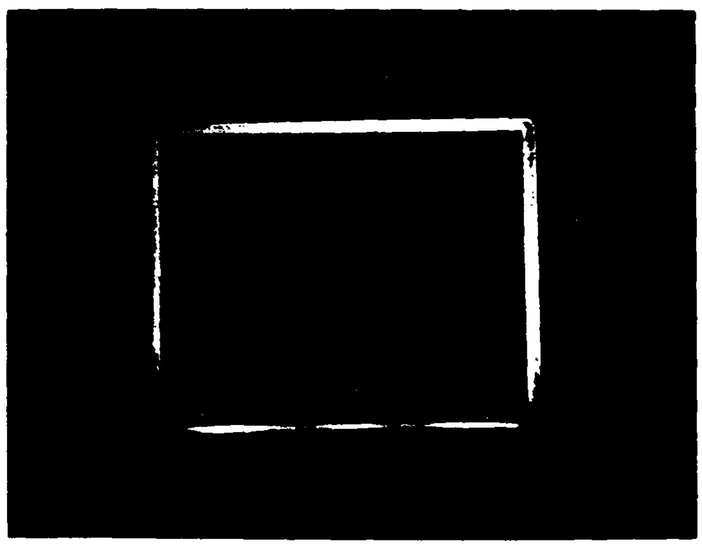

Fig. J-2. No.1 edge actual.

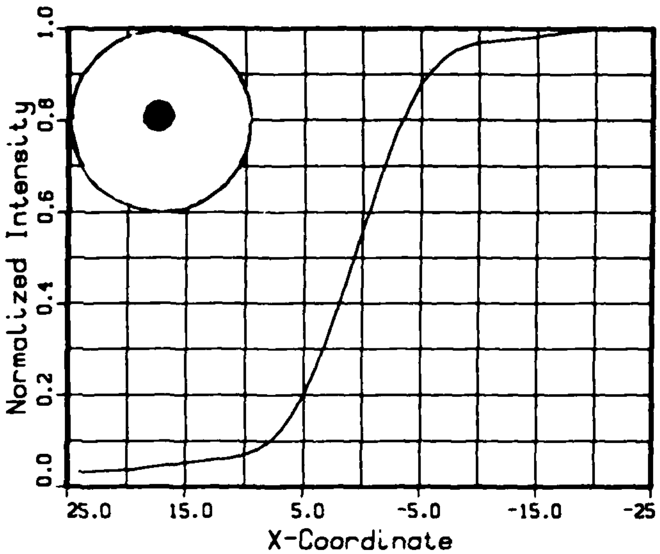

Fig. J-3. No.2 edge theory.

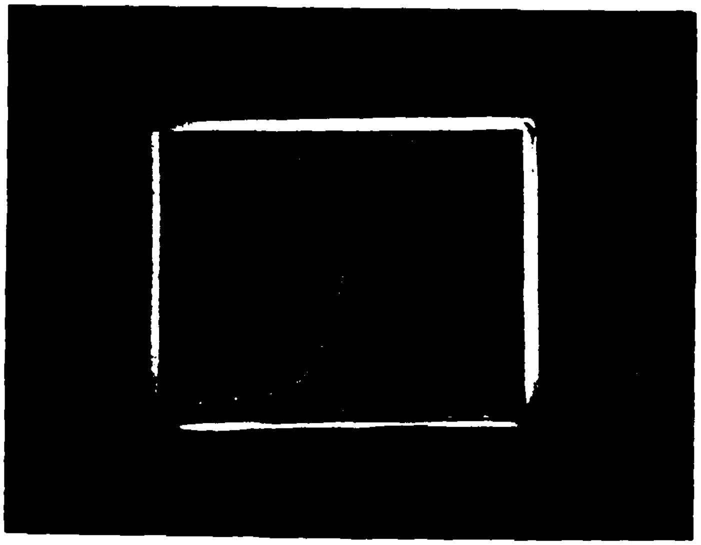

Fig. J-4. No.2 edge actual.

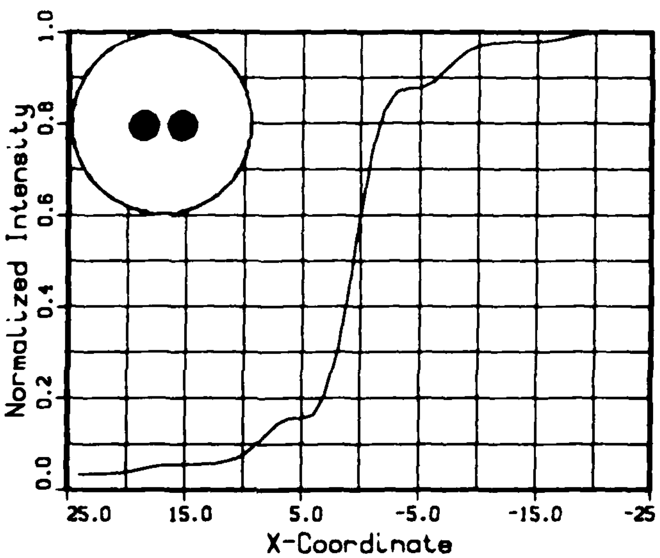

Fig. J-5. No.3 edge theory.

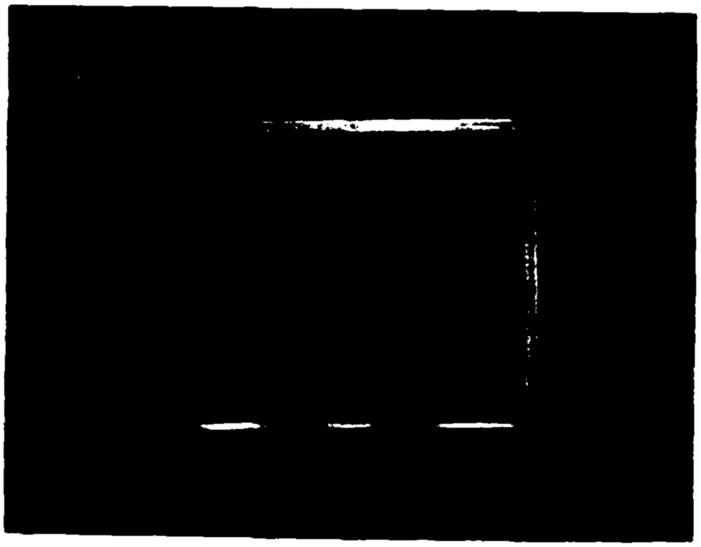

Fig. J-6. No.3 edge actual.

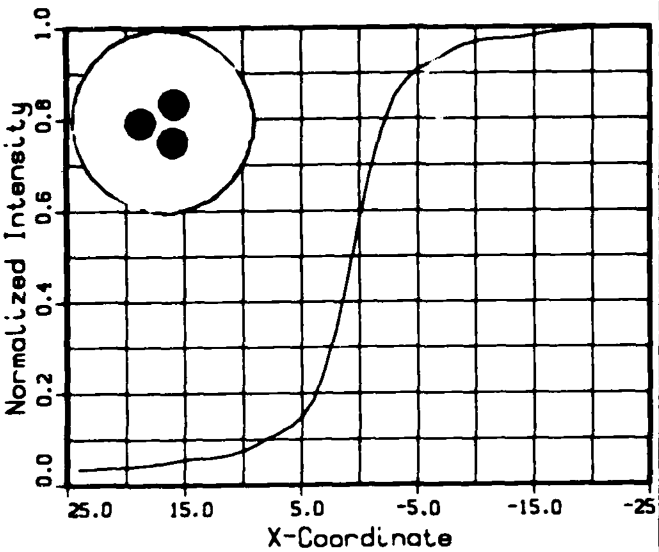

Fig. J-7. No.4 edge theory.

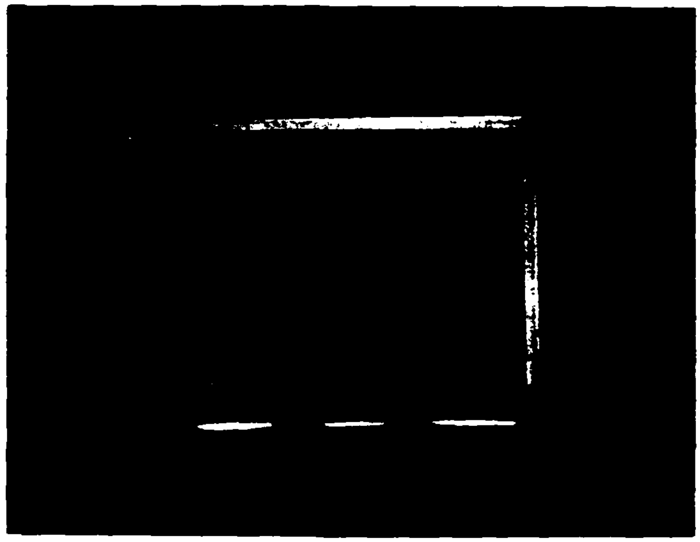

Fig. J-8. No.4 edge actual.

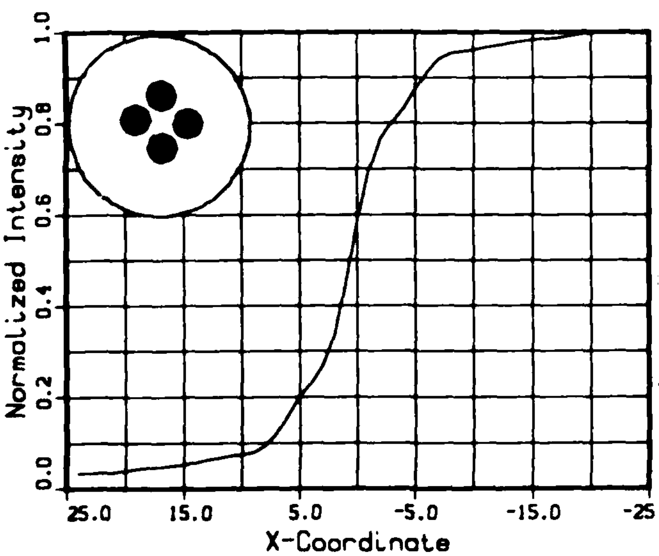

Fig. J-9. No.5 edge theory.

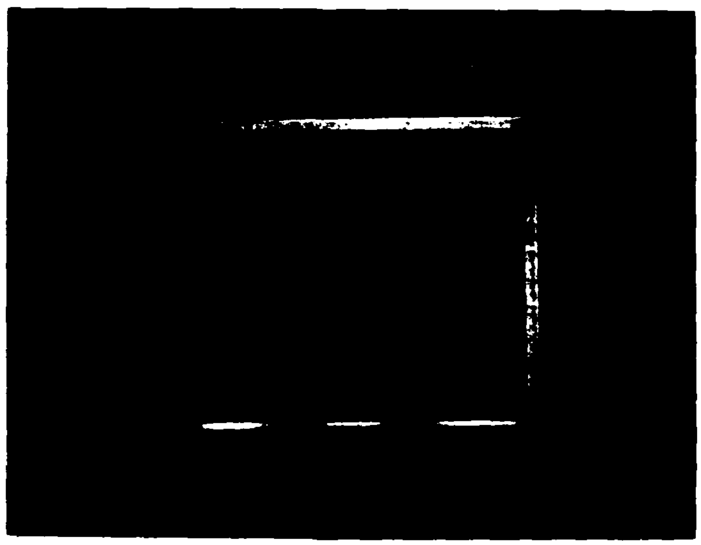

Fig. J-10. No.5 edge actual.

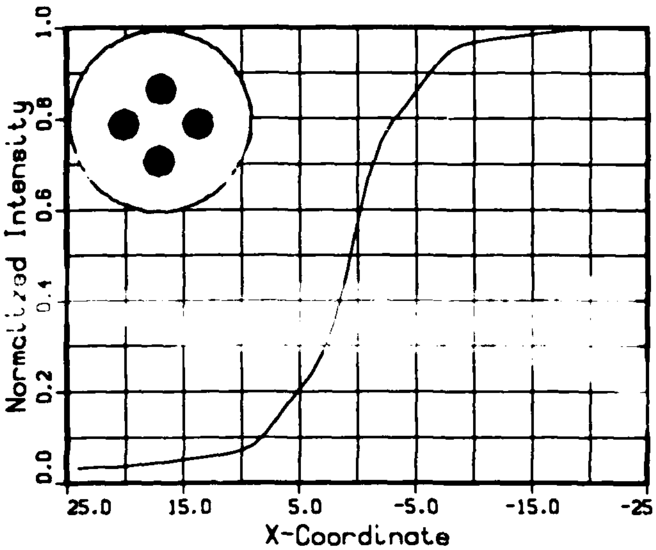

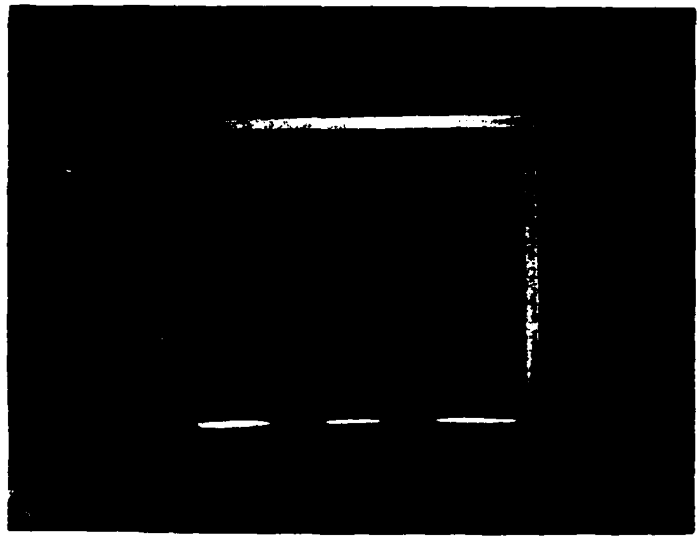

Fig. J-11. No.6 edge theory. Fig. J-12. No.6 edge actual.

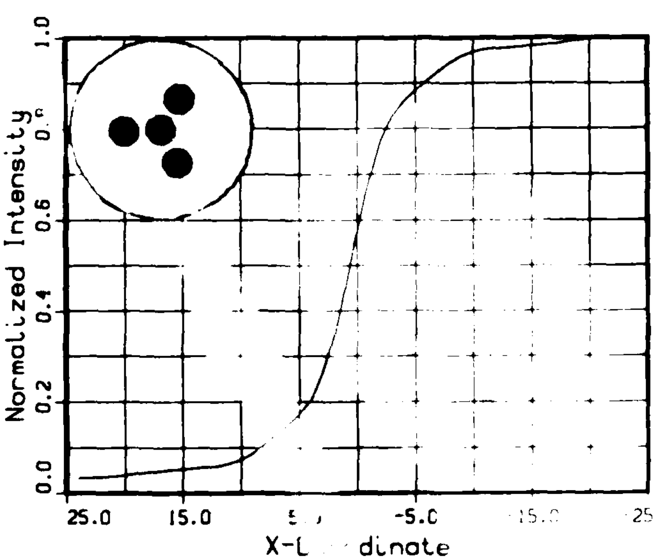

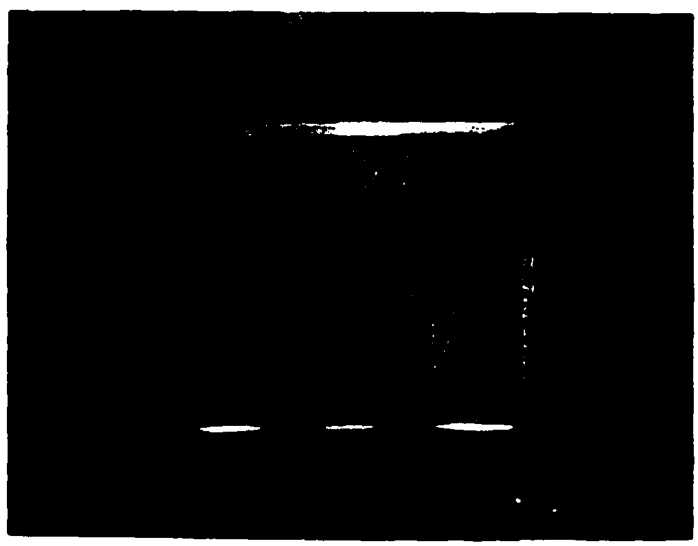

Fig. J-13. No.7 edge theory. Fig. J-14. No.7 edge actual.

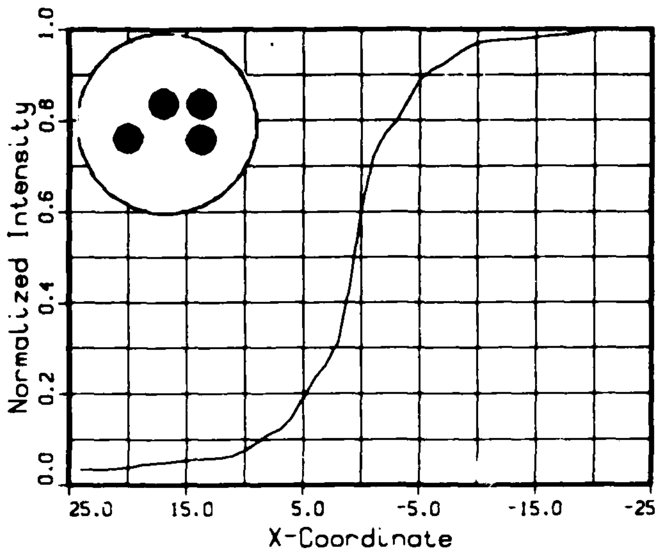

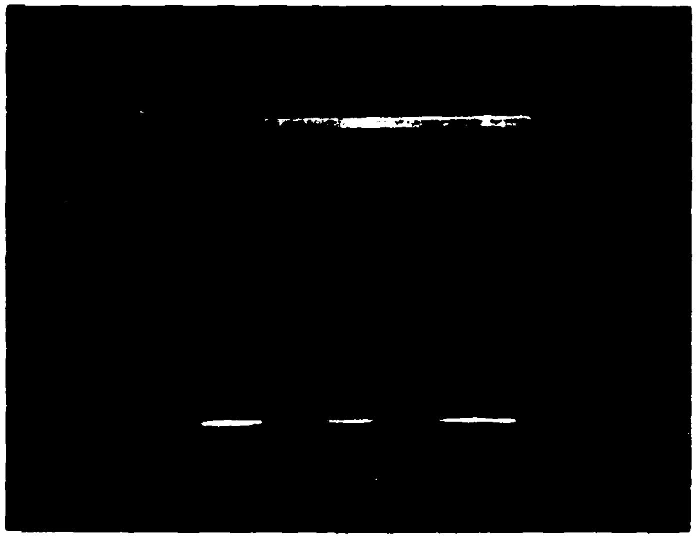

Fig. J-15. No.8 edge theory.

Fig. J-16. No.8 edge actual.

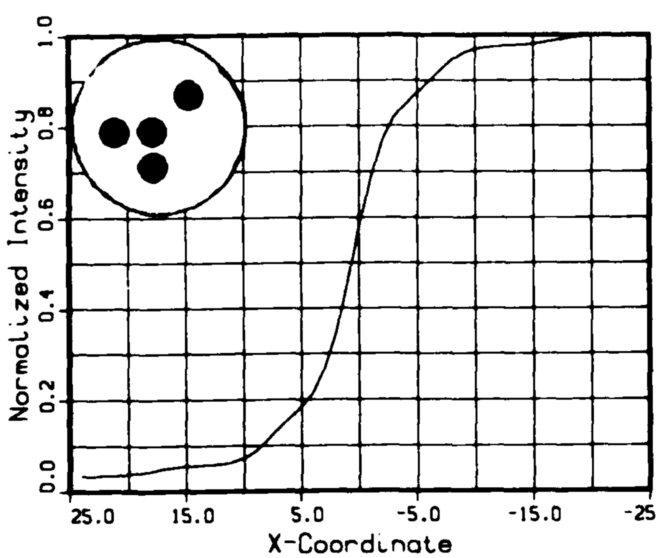

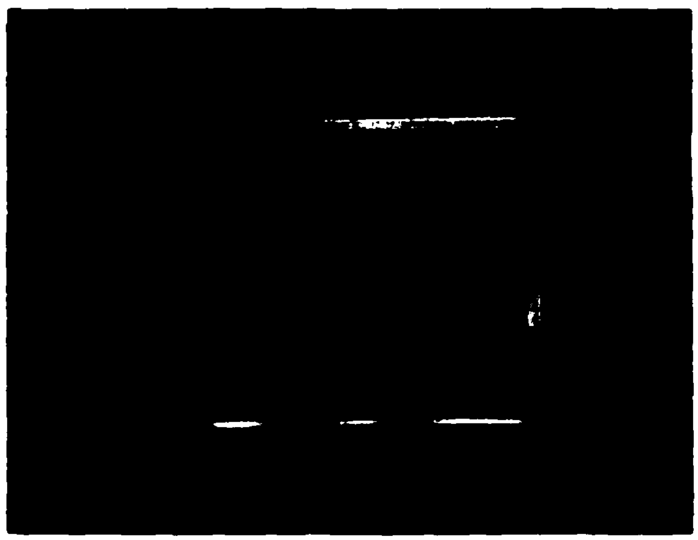

Fig. J-17. No.9 edge theory.

Fig. J-18. No.9 edge actual.

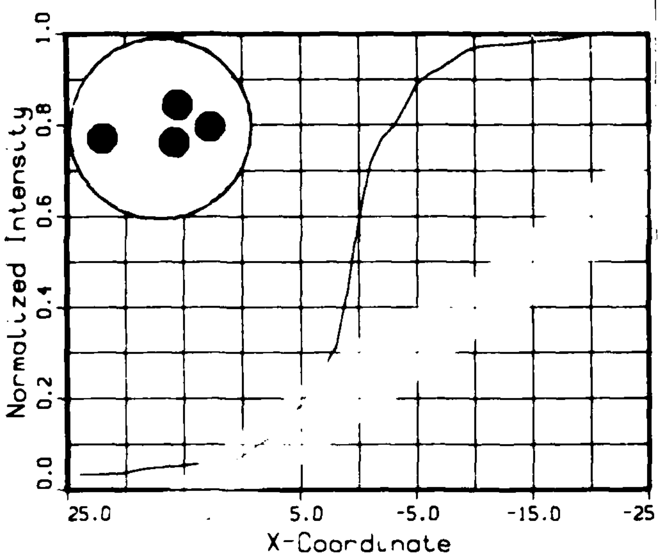

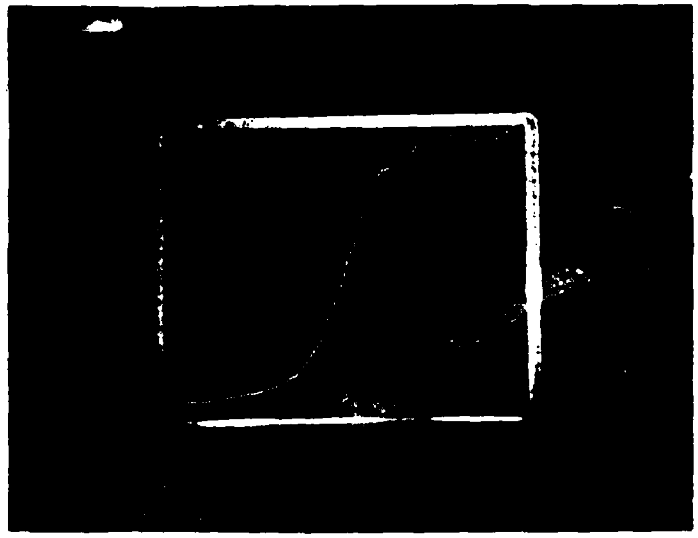

Fig. J-19. No.10 edge theory. **Fig. J-20. No.10 edge actual.**

APPENDIX K - Object Computer Representations

The following three-dimensional graphs are computer representations of each input object. Each graph represents the transmittance of light at the object plane. The "xy" coordinate system is representative of the object plane, and the "z" axis records the transmittance at each "xy" coordinate.

The scale of the image plane is 1 to 1 with the computer array that stored the pattern: the base area is 48 by 48, corresponding to the central 48 by 48 area of the original aperture array in the program (256 by 256).

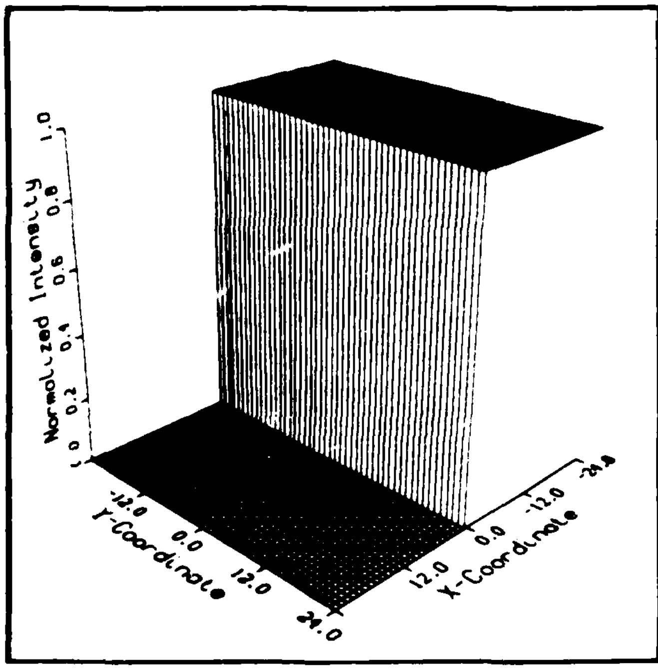

Fig. K-1. An Edge.

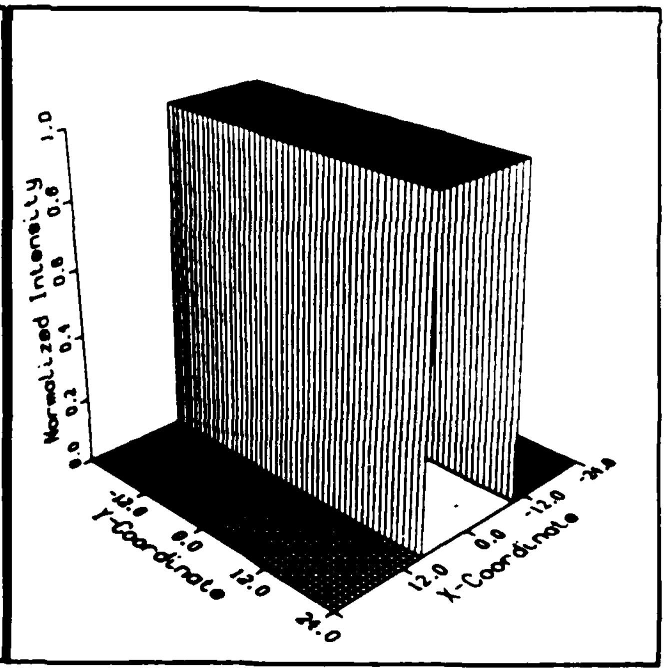

Fig. K-2. A Slit.

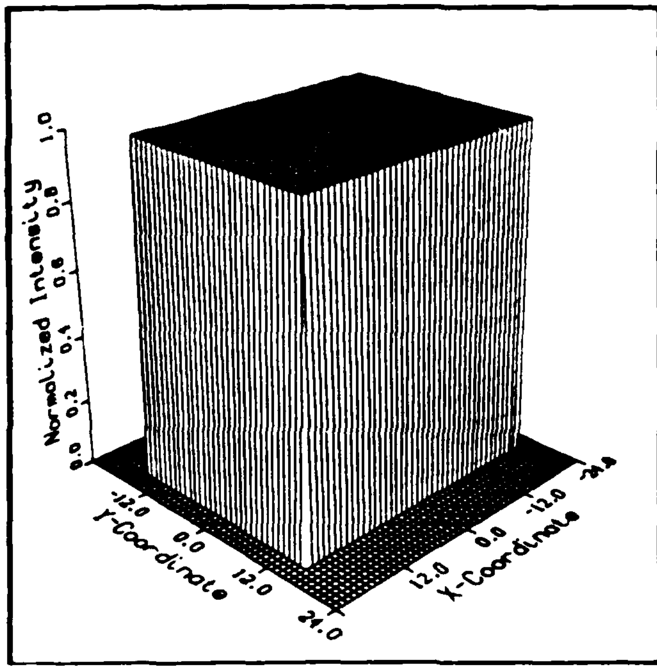

Fig. K-3. A Rectangle.

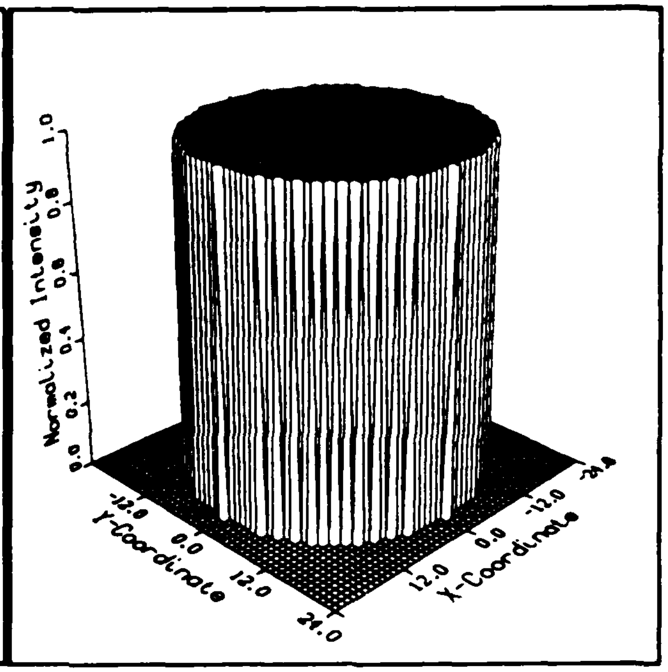

Fig. K-4. A Circle.

APPENDIX L: COMPUTER CODE USED FOR SIMULATION

```
C
C     ***************************************************
C     *                                                 *
C     *              PROGRAM INTENSITY                  *
C     *                                                 *
C     ***************************************************
C
C         THIS PROGRAM CALCULATES THE INTENSITY
C         OF AN IMAGE OF AN OBJECT AS SEEN THROUGH A
C         MULTIPLE APERTURE OPTICAL SYSTEM.
C
C
      INTEGER L,N,NN,APE,SFACTOR,PLOT,ASYM,XCEN,YCEN
      INTEGER RECTS,ICOOR,JCOOR,ISIZE,JSIZE,SHAPE,CIRCRAD
      INTEGER IWK(2000),IA1,IA2,N1,N2,N3,IJOB,CNTR,SLICE
      REAL BUFF(48),RWK(4000),ROT,NV,NV2
      REAL M(48,48),INT(48,48)
      COMPLEX A(256,256),CWK(256),B(256,256),F(256,256)
C
      OPEN(UNIT=24,STATUS='NEW',FILE='INT.DAT')
      OPEN(UNIT=25,STATUS='NEW',FILE='OTF.DAT')
      OPEN(UNIT=26,STATUS='NEW',FILE='INT2.DAT')
      OPEN(UNIT=27,STATUS='NEW',FILE='APER.DAT')
      OPEN(UNIT=28,STATUS='NEW',FILE='OBJ.DAT')
      OPEN(UNIT=29,STATUS='NEW',FILE='PSF.DAT')
C
C  READ PARAMETER VALUES FROM COM FILE
C
      READ(5,20)N
      READ(5,20)PLOT
      READ(5,20)SLICE
      READ(5,40)SRADIUS
      READ(5,40)RADIUS
      READ(5,40)APER
      READ(5,20)ASYM
      READ(5,40)ROT
      READ(5,20)CNTR
      READ(5,20)RECTS
      READ(5,20)SHAPE
      READ(5,20)CIRCRAD
C
20        FORMAT(I3)
40        FORMAT(F15.4)
45        FORMAT(' Z = [')
46        FORMAT(F15.4,' ...')
47        FORMAT(F15.4)
48        FORMAT(' ];')
49        FORMAT(I3,X,I3)
C
C    1  - N=NUMBER OF SAMPLE POINTS IN ONE DIMENSION
C    2  - PLOT=TYPE OF OUTPUT (1 = 2-D, ELSE 2-D AND 3-D)
C    3  - SLICE= Y COORDINATE FOR 2-D SLICE OF 3-D IMAGE
```

```
C     4  - SRADIUS=RADIUS OF INDIVIDUAL SUB-APERTURES
C     5  - RADIUS=OUTER RADIUS OF SYNTHESIZED APERTURE
C             (EXPRESSED AS MULTIPLE OF SUB-APERTURE RADIUS)
C     6  - APER=NUMBER OF SUB-APERTURES IN THE ARRAY
C     7  - ROT=ROTATION OF ARRAY (DEGREES)
C     8  - CNTR=CENTER APERTURE (1=YES, 0=NO)
C     9  - RECTS=NUMBER OF OBJECT RECTANGLES
C    10  - ICOOR=I COORDINATE FOR BOTTOM LEFT OF RECT
C    11  - JCOOR=J COORDINATE FOR BOTTOM LEFT OF RECT
C    12  - ISIZE=I COORDINATE FOR WIDTH OF RECTANGLE
C    13  - JSIZE=J COORDINATE FOR HEIGHT OF RECTANGLE
C    14  - SHAPE=OBJECT SHAPE (2=CIRCLE AND RECT,
C                   1=CIRCLE ONLY, 0=RECT ONLY)
C    15  - CIRCRAD=RADIUS OF OBJECT CIRCLE
C
      APE=APER-1.
      IRAD=RADIUS*SRADIUS
      ORAD=IRAD
      IDIAM=2*IRAD
      SDIAM=2*SRADIUS
      PI=3.1415927
      Q1=3.*PI/4.
      DL=3.*PI/2.
      NN=N/2
      ROT=2.*PI/360.*ROT
C
C     CLEAR MAIN ARRAYS
C
      DO 101 I=1,N
      DO 100 J=1,N
        A(I,J)=CMPLX(0.,0.)
        B(I,J)=CMPLX(0.,0.)
        F(I,J)=CMPLX(0.,0.)
100   CONTINUE
101   CONTINUE
C
C***************************************************************
C
C     CREATE OBJECT FUNCTION
C
C***************************************************************
C
C IF OBJECT CONTAINS A CIRCLE...
C
      IF (SHAPE.GT.0) THEN
        IARG=128-CIRCRAD
        JARG=128-CIRCRAD
        ISIZE=128+CIRCRAD
        JSIZE=128+CIRCRAD
        DO 190 I=IARG,ISIZE
        DO 180 J=JARG,JSIZE
        RAD=SQRT((128.-I)**2+(128.-J)**2)
        IF (RAD.LE.CIRCRAD) THEN
          B(I,J)=CMPLX(1.,0.)
        END IF
180     CONTINUE
190     CONTINUE
        IF (SHAPE.EQ.2)THEN
```

```
            GO TO 195
           ELSE
            GO TO 202
          END IF
        END IF
C
C IF OBJECT CONTAINS A RECTANGLE OF SERIES OF RECTANGLES
C
195     DO 202,L=1,RECTS
          READ(5,20)ICOOR
          READ(5,20)JCOOR
          READ(5,20)ISIZE
          READ(5,20)JSIZE
          DO 201 I=ICOOR,ISIZE
            DO 200 J=JCOOR,JSIZE
            B(I,J)=CMPLX(1.,0.)
200         CONTINUE
201       CONTINUE
202     CONTINUE
C
C WRITE OBJECT FUNCTION TO DATA FILE
C
C         WRITE(28,45)
          DO 206 I=1,48
            DO 205 J=1,48
            IF (J.EQ.48) THEN
              WRITE(28,47)CABS(B(104+I,104+J))
             ELSE
              WRITE(28,46)CABS(B(104+I,104+J))
            ENDIF
205         CONTINUE
206       CONTINUE
C
C**********************************************************
C
C   CREATE CIRCULAR APERTURE WITH VARIABLE TRANSMITTANCE
C
C**********************************************************
          IARG=NN-SRADIUS+(ORAD-SRADIUS)*COS(ROT)
          JARG=NN-SRADIUS+(ORAD-SRADIUS)*SIN(ROT)
          DO 390 I=1,SDIAM
            DO 380 J=1,SDIAM
            RAD=SQRT((I-SRADIUS)**2+(J-SRADIUS)**2)
            IF(RAD.LE.SRADIUS)THEN
              A(I+IARG,J+JARG)=CMPLX(1.,0.)
            END IF
380         CONTINUE
390       CONTINUE
C
C  CREATE REMAINING SUB-APERTURES
C
          DO 402 I=1,APE
          IF(ASYM.EQ.1) THEN
            READ(5,49)XCEN,YCEN
            XP=XCEN-SRADIUS
            YP=YCEN-SRADIUS
            GO TO 399
          ENDIF
```

```
          L=(ORAD-SRADIUS)*COS(I*2.*PI/APER+ROT)
          U=L
          L=(ORAD-SRADIUS)*SIN(I*2.*PI/APER+ROT)
          V=L
          XP=(NN-1)-SRADIUS+U
          YP=(NN-1)-SRADIUS+V
399       DO 401 J=1,SDIAM
            DO 400 K=1,SDIAM
            RR=SQRT(((SRADIUS-J)**2)+((SRADIUS-K)**2))
            IF(RR.GT.SRADIUS) GO TO 400
            A(XP+J,YP+K)=A(XP+J,YP+K)+A(J+IARG,K+JARG)
            CZ=CABS(A(XP+J,YP+K))
            IF(CZ.GT.1.) THEN
              A(XP+J,YP+K)=CMPLX(1.,0.)
            END IF
400         CONTINUE
401       CONTINUE
402       CONTINUE
C
C     CREATE CENTER APERTURE IF DESIRED
C
          IF (CNTR.EQ.1) THEN
            XP=NN-1-SRADIUS
            YP=NN-1-SRADIUS
            DO 501 J=1,SDIAM
              DO 500 K=1,SDIAM
              A(XP+J,YP+K)=A(XP+J,YP+K)+A(J+IARG,K+JARG)
              CZ=CABS(A(XP+J,YP+K))
              IF(CZ.GT.1.) THEN
                A(XP+J,YP+K)=CMPLX(1.,0.)
              END IF
500           CONTINUE
501         CONTINUE
          END IF
C
C WRITE APERTURE FUNCTION
C
C         WRITE(27,45)
          DO 506 I=1,48
            DO 505 J=1,48
            IF (J.EQ.48) THEN
              WRITE(27,47)CABS(A(79+I*2,79+J*2))
             ELSE
              WRITE(27,46)CABS(A(79+I*2,79+J*2))
            ENDIF
505       CONTINUE
506       CONTINUE
C
C***********************************************************
C
C  PERFORM FAST FOURIER TRANSFORM USING IMSL
C  TO FIND IMPULSE RESPONSE 'h'
C
C***********************************************************
C
          IA1=N
          IA2=N
          N1=N
```

```
      N2=N
      N3=1
      IJOB=1
      CALL FFT3D (A,IA1,IA2,N1,N2,N3,IJOB,IWK,RWK,CWK)
C
C
C  SHIFT ZERO FREQUENCY TO ARRAY CENTER
C
      DO 620 I=1,N
        DO 610 J=1,NN
        F(I,J)=A(I,NN+1-J)
        F(I,NN+J)=A(I,N+1-J)
610     CONTINUE
620   CONTINUE
      DO 640 I=1,NN
        DO 630 J=1,N
        A(I,J)=F(NN+1-I,J)
        A(NN+I,J)=F(N+1-I,J)
630     CONTINUE
640   CONTINUE
C
C  FIND INTENSITY OF ARRAY; SQUARE 'h'
C
      DO 660 I=1,N
        DO 650 J=1,N
        A(I,J)=CABS(A(I,J))**2.
650     CONTINUE
660   CONTINUE
C
C  WRITE POINT SPREAD FUNCTION
C
C     WRITE(29,45)
      DO 680 I=1,48
      DO 670 J=1,48
      IF (J.EQ.48) THEN
        WRITE(29,47)CABS(A(I+104,J+104))/CABS(A(128,128))
       ELSE
        WRITE(29,46)CABS(A(I+104,J+104))/CABS(A(128,128))
      ENDIF
670   CONTINUE
680   CONTINUE
C       WRITE(29,48)
C
C***************************************************************
C
C  PERFORM FAST FOURIER TRANSFORM USING IMSL
C  TO FIND FOURIER OF 'h' SQUARED
C
C***************************************************************
C
      IA1=N
      IA2=N
      N1=N
      N2=N
      N3=1
      IJOB=1
      CALL FFT3D (A,IA1,IA2,N1,N2,N3,IJOB,IWK,RWK,CWK)
C
```

```
C***************************************************************
C
C  PERFORM FAST FOURIER TRANSFORM USING IMSL
C  TO FIND FOURIER OF OBJECT IRRADIANCE
C
C***************************************************************
C
       IA1=N
       IA2=N
       N1=N
       N2=N
       N3=1
       IJOB=1
       CALL FFT3D (B,IA1,IA2,N1,N2,N3,IJOB,IWK,RWK,CWK)
C
C***************************************************************
C
C   CALCULATE PRODUCT OF ARRAY A*B
C
C***************************************************************
C
C
       DO 910 I=1,N
         DO 900 J=1,N
         B(I,J)=CABS(A(I,J))*B(I,J)
900      CONTINUE
910    CONTINUE
C
C
C***************************************************************
C
C  PERFORM INVERSE FAST FOURIER TRANSFORM USING IMSL
C  TO FIND ACTUAL IRRADIANCE
C
C***************************************************************
C
       IA1=N
       IA2=N
       N1=N
       N2=N
       N3=1
       IJOB=-1
       CALL FFT3D (B,IA1,IA2,N1,N2,N3,IJOB,IWK,RWK,CWK)
C
C
C***************************************************************
C
C    WRITE RESULTS
C
C***************************************************************
C
C        WRITE(24,45)
C        WRITE(25,45)
C        WRITE(26,45)
       NV=1.0
       NV2=1.0
       DO 1210 I=1,48
         DO 1200 J=1,48
```

```
               INT(I,J)=CABS(B(I*2+NN-48,J*2+NN-48))
               IF (INT(I,J).GT.NV) THEN
                 NV=INT(I,J)
               END IF
1200           CONTINUE
1210         CONTINUE
             DO 1250 I=1,48
               DO 1240 J=1,48
               INT(I,J)=INT(I,J)/NV
C *******************************************
C PREPARE "SIDE" FILE FOR 2-DIMENSION VIEW
C *******************************************
               IF (J .EQ. SLICE) THEN
                 BUFF(I)=INT(I,J)
               END IF
               IF (PLOT .EQ. 1) GO TO 1255
C *******************************************
C WRITE "INT" FILE FOR 3-DIMENSION VIEW
C *******************************************
               IF (J .EQ. 48) THEN
                 WRITE(24,47)INT(I,J)
                ELSE
                 WRITE(24,46)INT(I,J)
               END IF
1240           CONTINUE
1250         CONTINUE
C *******************************************
C WRITE "INT2" FILE FOR 2-DIMENSION VIEW
C *******************************************
1255         DO 1270 I=1,48
             IF (I .EQ. 48)THEN
               WRITE(26,47)BUFF(49-I)
              ELSE
               WRITE(26,46)BUFF(49-I)
             END IF
1270         CONTINUE
C
C *******************************************
C WRITE OFT FUNCTION FOR 3-DIMENSIONAL VIEW.
C FIRST, SHIFT ZERO FREQUENCY TO ARRAY CENTER.
C *******************************************
C
             IF (PLOT .EQ. 1) GO TO 1400
             DO 1290 I=1,N
               DO 1280 J=1,NN
               F(I,J)=A(I,NN+1-J)
               F(I,NN+J)=A(I,N+1-J)
1280           CONTINUE
1290         CONTINUE
             DO 1292 I=1,NN
               DO 1291 J=1,N
               A(I,J)=F(NN+1-I,J)
               A(NN+I,J)=F(N+1-I,J)
1291           CONTINUE
1292         CONTINUE
             DO 1294 I=1,48
               DO 1293 J=1,48
               INT(I,J)=CABS(A(I*4+NN-96,J*4+NN-96))
```

```
          IF (INT(I,J).GT.NV2) THEN
          NV2=INT(I,J)
          END IF
1293    CONTINUE
1294    CONTINUE
        DO 1301 I=1,48
          DO 1300 J=1,48
          IF (J .EQ. 48) THEN
            WRITE(25,47)INT(I,J)/NV2
          ELSE
            WRITE(25,46)INT(I,J)/NV2
          END IF
1300      CONTINUE
1301    CONTINUE
C
C ********************************************
C CLOSE ALL FILES AND TERMINATE
C ********************************************
C
1400    CONTINUE
C         WRITE(24,48)
C         WRITE(25,48)
C         WRITE(26,48)
C         WRITE(27,48)
C         WRITE(28,48)
        CLOSE(UNIT=24)
        CLOSE(UNIT=25)
        CLOSE(UNIT=26)
        CLOSE(UNIT=27)
        CLOSE(UNIT=28)
        CLOSE(UNIT=29)
        STOP
        END
C
C***********************************************************
C
C  END MAIN PROGRAM
C
C***********************************************************
C
```

Bibliography

1. Beckers, J. M., Hege, E.K. and Strittmatter, P.A. "Optical Interferometry With The MMT," Proceedings of SPIE- The International Society For Optical Engineering. 85-92. Bellingham, Washington: SPIE Press, 1984.

2. Bergey, Dana J. Coherent Multiple Aperture Optical Imaging Systems: Analysis And Design. MS Thesis, GEE-87M. School of Engineering, Air Force Institute of Technology (AU), Wright -Patterson AFB OH, March 1987.

3. Carleton, Nathaniel P. and William F. Hoffman. "The Multiple-Mirror Telescope," Physics Today, 31: 30-37 (September 1978).

4. Cornell, James. "On a mountaintop in Arizona, things are starting to look up," Smithsonian, 10: 42-51 (May 1979)

5. -----. "Six New Eyes Peer from Mount Hopkins," Sky and Telescope, 58: 23-24 (July 1979)

6. Fender, Janet S. "Synthetic Apertures: An Overview," Proceedings of SPIE- The International Society For Optical Engineering. 2-8. Bellingham, Washington: SPIE Press, 1983.

7. Gaskill, Jack D. Linear Systems, Fourier Transforms, and Optics. New York: John Wiley and Sons, 1978.

8. Golay, Marcel J.E. "Point Arrays Having Compact, Nonredundant Autocorrelations," Journal Of The Optical Society of America, 61: 272-273 (February 1971).

9. Goodman, Joseph W. Introduction To Fourier Optics. New York: McGraw-Hill Book Company, 1968.

10. Jacchia, Luigi. "Forefathers of the MMT," Sky and Telescope, 55: 100-103 (February 1978)

11. Mills, James P. Assistant Professor ENP. Personal interview. AFIT, Wright-Patterson AFB OH, 25 March 1987.

12. -----. Class handout distributed in PHYS 544, Fundamentals of Optics III. School of Engineering, AFIT, Wright-Patterson AFB OH, April 1987.

13. O'Shea, Donald C. Elements Of Modern Optical Design. New York: John Wiley and Sons, 1985.

14. Robinson, Leif J. "Update: Telescopes of the Future," Sky and Telescope, 72: 23-24 (July 1986)

15. Schwartzchild, Bertram M. "Large New-Technology Optical Telescopes Proposed," Physics Today, 34: 17-20 (August 1981).

16. Sears, Francis W. and Mark W. Zemansky. University Physics (Fourth Edition). Reading Massachusetts: Addison-Wesley Publishing Company, 1970.

17. Thomsen, Dietrick E. "NNTT's next generation: Harmonizing a quartet of large telescopes," Science News, 129: 55-56 (January 1986)

18. Waldrop, Mitchell M. "The New Technology Telescopes," Science, 216: 280-281 (April 1982).

19. Woolf, Henry B. Webster's New Collegiate Dictionary. Springfield, Mass: Merriam-Webster, 1979.

VITA

Major Robert T. Reilander was born in Winnipeg, Manitoba, on 13 January 1956. He graduated from Silver Heights Collegiate in Winnipeg in 1974, and then attended the Royal Military College of Canada in Kingston, Ontario. He graduated in 1978 with a Bachelor of Mechanical Engineering. As a participant of the Regular Officer Training Plan, he was awarded a Commission in the Canadian Armed Forces as a Lieutenant in the Communications and Electronics Branch. After subsequent tours as a staff officer in a communication squadron, radar squadron, and training squadron, he was employed as a computer programmer for NATO AWACS. He was selected for post graduate training in the fall of 1985, and in May 1986, reported to the School of Engineering at the Air Force Institute of Technology as a student of the Graduate Space Operations Program.

UNCLASSIFIED

SECURITY CLASSIFICATION OF THIS PAGE

REPORT DOCUMENTATION PAGE

Form Approved OMB No. 0704-0188

1a. REPORT SECURITY CLASSIFICATION: UNCLASSIFIED

1b. RESTRICTIVE MARKINGS:

2a. SECURITY CLASSIFICATION AUTHORITY:

2b. DECLASSIFICATION / DOWNGRADING SCHEDULE:

3. DISTRIBUTION / AVAILABILITY OF REPORT: Approved for public release; distribution unlimited

4. PERFORMING ORGANIZATION REPORT NUMBER(S): AFIT/GSO/ENP/87D-2

5. MONITORING ORGANIZATION REPORT NUMBER(S):

6a. NAME OF PERFORMING ORGANIZATION: School of Engineering

6b. OFFICE SYMBOL (If applicable): AFIT/ENP

7a. NAME OF MONITORING ORGANIZATION:

6c. ADDRESS (City, State, and ZIP Code): Air Force Institute of Technology, Wright-Patterson AFB, OH 45433

7b. ADDRESS (City, State, and ZIP Code):

8a. NAME OF FUNDING / SPONSORING ORGANIZATION:

8b. OFFICE SYMBOL (If applicable):

9. PROCUREMENT INSTRUMENT IDENTIFICATION NUMBER:

8c. ADDRESS (City, State, and ZIP Code):

10. SOURCE OF FUNDING NUMBERS

PROGRAM ELEMENT NO.	PROJECT NO.	TASK NO.	WORK UNIT ACCESSION NO.

11. TITLE (Include Security Classification): INCOHERENT MULTIPLE APERTURE OPTICAL IMAGING SYSTEMS: ANALYSIS AND DESIGN (UNCLASSIFIED)

12. PERSONAL AUTHOR(S): ROBERT T. REILANDER, MAJOR, CANADIAN ARMED FORCES

13a. TYPE OF REPORT: MS THESIS

13b. TIME COVERED: FROM ______ TO ______

14. DATE OF REPORT (Year, Month, Day): 1987 DECEMBER

15. PAGE COUNT: 130

16. SUPPLEMENTARY NOTATION:

Approved for public release: IAW AFR 190-1

24 Feb 88

E. WOLAVER

17. COSATI CODES

FIELD	GROUP	SUB-GROUP
20	6	

18. SUBJECT TERMS (Continue on reverse if necessary and identify by block number): multiaperture, synthetic aperture, incoherent imaging

19. ABSTRACT (Continue on reverse if necessary and identify by block number)

Various multiple aperture optical arrays were compared while imaging objects illuminated with incoherent light. The aperture arrays contained from one to four sub-apertures. The objects were edges, slits, rectangles and circles. An emphasis was placed on edge resolution, and the author derived his own set of resolution criteria. Based on this analysis, a tight square four-element array was the best performer.

The study concluded with an analysis of design criteria for optimum incoherent imaging resolution. Max sub-aperture size, min sub-aperture spacing, max number of sub-aperture elements, and a symmetric pattern were all determined to be desireable in order to obtain the best performance.

Thesis Advisor: James P. Mills, Lt Col, USAF

20. DISTRIBUTION / AVAILABILITY OF ABSTRACT: ☒ UNCLASSIFIED/UNLIMITED ☐ SAME AS RPT. ☐ DTIC USERS

21. ABSTRACT SECURITY CLASSIFICATION: UNCLASSIFIED

22a. NAME OF RESPONSIBLE INDIVIDUAL: James P. Mills, Lt Col, USAF

22b. TELEPHONE (Include Area Code): 513-255-2012

22c. OFFICE SYMBOL: AFIT/ENP

DD Form 1473, JUN 86 — Previous editions are obsolete.

SECURITY CLASSIFICATION OF THIS PAGE

UNCLASSIFIED

END
DATE
FILMED
APRIL
1988
DTIC